HYGROTHERMALLY STABLE LAMINATED COMPOSITES

WITH OPTIMAL COUPLING

A Dissertation
Presented to
The Academic Faculty

by

Robert Andrew Haynes

In Partial Fulfillment
of the Requirements for the Degree
Doctor of Philosophy in the
School of Aerospace Engineering

Georgia Institute of Technology
August 2010

HYGROTHERMALLY STABLE LAMINATED COMPOSITES

WITH OPTIMAL COUPLING

Approved by:

Dr. Erian Armanios, Advisor
School of Mechanical & Aerospace Engineering
University of Texas at Arlington

Dr. Andrew Makeev
School of Aerospace Engineering
Georgia Institute of Technology

Dr. Massimo Ruzzene, Co-advisor
School of Aerospace Engineering
Georgia Institute of Technology

Dr. Olivier Bauchau
School of Aerospace Engineering
Georgia Institute of Technology

Dr. D. Stefan Dancila
School of Mechanical & Aerospace Engineering
University of Texas at Arlington

Date Approved: June 11, 2010

FORWARD

It was in the Spring of 2005 that Robert Haynes proffered a solution that, in its elegance, heralded his unique journey of discovery. The solution was for one of the bonus problems I would often offer in my Structural Analysis class to challenge the most motivated and curious students to venture beyond the confines of textbook knowledge. Robert, then a sophomore, proposed an interesting derivation to the relationship between Young's and shear modulus for isotropic materials based on the stress and strain transformation introduced then as Mohr's circle.

His journey subsequently led him to find asymmetric stacking sequences that are hygrothermally stable—before ever taking a formal course on Mechanics of Composites. He was compelled to prove to himself that symmetric sequences are hygrothermally stable. The ultimate goal was to achieve extension-twist coupling, inherently asymmetric in flat composite laminates, while maintaining hygrothermal stability. A solution developed by Winckler at Rensselaer Polytechnic Institute capitalizing on the hygrothermal isotropy of $[0/90]_s$ sequences, with time, gained state-of-the-art benchmark status. A standing inquiry, however, begged for an answer: is this intuitive sequence unique? And if not, is it optimal?

Intuition had to be set aside, not substituted, for a theoretically based investigation. Its outcome affirmed that nothing is more practical than a good theory. Rather than following the impulse of seeking extension-twist coupling first and foremost, Robert ventured to find all stacking sequences that are hygrothermally stable. To this end, he had to determine the necessary and sufficient conditions for hygrothermal

stability. In the process, Richard Cross, the reigning Graduate Student Sudoku Champion at the ASC 21st Technical Conference ad hoc competition breaks, became intrigued by Robert's quest and joined the rising Senior in a mentoring role. The satisfaction of achieving this diabolical level challenge was documented in their first publication in the Journal of Composite Materials, in which they presented a rigorous proof of both necessary and sufficient conditions, demonstrating that the minimum number of plies to achieve hygrothermal stability in regular asymmetric laminates was determined to be five.

From within the newly found families of laminates, Robert systematically explored those exhibiting extension-twist, bend-twist, and other couplings. For extension-twist coupling, the eight-ply Winckler sequence was proved to be neither unique nor optimum, and the optimal families of five- to ten-ply laminates achieved in this dissertation, outperform it.

Should you be curious to learn if asymmetric hygrothermally stable layups outperform the bend-twist coupling of symmetric ones, I invite you to venture into this dissertation. Along the way, you will find out about other couplings, much like wandering in tributaries would be as interesting as navigating the mainstream, thanks to the path that Robert has blazed.

Erian Armanios
June 2010

ACKNOWLEDGMENTS

I wish to thank my advisor, Dr. Erian Armanios, for recognizing my potential during my undergraduate studies and encouraging that potential by providing me the opportunity to be a research assistant; for his unselfish assistance when I was deciding what to do after earning my bachelor's degree; for his continued advisement after his departure from the Georgia Institute of Technology; for his relentless support in my attending conferences; for his contagious enthusiasm toward discovery; and for his passionate interest in my success. I could not ask for a more attentive and generous advisor.

I wish to thank Dr. Massimo Ruzzene for being my co-advisor and for always being available when I needed assistance. I also want to thank the rest of my committee, Dr. D. Stefan Dancila, Dr. Andrew Makeev, and Dr. Olivier Bauchau, for the generous donation of their time and attention, allowing me to complete my dissertation. I want to give Dr. Marilyn Smith the credit she deserves for introducing me to Dr. Armanios, encouraging me to conduct undergraduate research, and supporting me through both my undergraduate and graduate careers; she truly was my conductor into the world of Aerospace Engineering. I also want to thank all of my professors and the Department of Aerospace Engineering staff who have been very supportive throughout my tenure at the Georgia Institute of Technology.

I wish to thank my family and friends, who have relentlessly insisted that I finish my thesis. Otherwise, I probably would have given in to the temptations of the working world by now. Specifically, I want to thank my parents, Mr. Andrew Haynes and Mrs.

Kay Haynes, for their encouragement and the time they spent professionally editing my thesis. I had a great deal of help in actually completing my thesis, not the least of which came from my former colleague, Dr. Yuan Tan, who taught me how to manufacture and test composites. Without her, I would not have this crucial piece of my thesis. Also, I want to thank my former colleagues, Dr. Richard Cross and Ms. Maria Chierichetti for their contributions to my thesis. Finally, I want to thank Mr. Ryan Carey and Dr. Samer Tawfik for supporting me in the lab.

TABLE OF CONTENTS

LIST OF TABLES

LIST OF FIGURES

SUMMARY

This work begins by establishing the necessary and sufficient conditions for hygrothermal stability of composite laminates. An investigation is performed into the range of coupling achievable from within all hygrothermally stable families. The minimum number of plies required to create an asymmetric hygrothermally stable stacking sequence is found to be five. Next, a rigorous and general approach for determining designs corresponding to optimal levels of coupling is established through the use of a constrained optimization procedure. Couplings investigated include extension-twist, bend-twist, extension-bend, shear-twist, and anticlastic. For extension-twist and bend-twist coupling, specimens from five- through ten-ply laminates are manufactured and tested to demonstrate hygrothermal stability and achievable levels of coupling. Nonlinear models and finite element analysis are developed, and predictions are verified through comparison with test results. Sensitivity analyses are performed to demonstrate the robustness of the hygrothermal stability and couplings to deviations in ply angle, typical of manufacturing tolerances. Comparisons are made with current state-of-the-art suboptimal layups, and significant increases in coupling over previously known levels are demonstrated.

CHAPTER 1

MOTIVATION

Composite laminates fabricated from the same specially orthotropic plies can be tailored through arrangement of each ply's fiber orientation angle to have certain couplings desirable to meet performance requirements. This work focuses on achievable extension-twist and bend-twist couplings. Extension-twist coupling has potential uses in rotor applications. For example, extension-twist-coupled wind turbine blades could passively adjust their twist distribution to achieve an angle of attack that maintains optimal generator speed. Also, extension-twist-coupled blades in a tilt-rotor aircraft could passively adjust their twist distribution, which in turn can achieve the angle of attack that optimizes efficiency in both the vertical and forward flight regimes. Bend-twist coupling has applications on swept-forward-wing aircraft to increase divergence speed and meet flutter requirements.

Designers often select symmetric stacking sequences to ensure hygrothermal curvature stability (henceforth, referred to as hygrothermal stability) whenever asymmetric stacking sequences were not required. Symmetric stacking sequences automatically satisfy hygrothermal stability, meaning they will not produce any out-of-plane deformation as a result of changes in temperature or moisture[1]. Asymmetric stacking sequences, however, are generally hygrothermally unstable. Hygrothermal stability is desirable because it ensures the geometry of the structure will not produce out-of-plane deformations through varying environmental conditions, including cooling after curing, while asymmetric stacking sequences enable beneficial couplings. This work

considers the entire range of possible stacking sequences for a laminate with a given number of plies, including both symmetric and asymmetric stacking sequences, and provides a rigorous, general methodology to producing hygrothermally stable laminates while still enabling out-of-plane mechanical coupling.

Bend-twist coupling is achievable using both symmetric and asymmetric layups. Unidirectional laminates with an off-axis fiber angle will have bend-twist coupling, although this design is prone to premature failure due to splitting. Extension-twist coupling in flat laminates, however, requires an asymmetric stacking sequence. Angle ply laminates are one such family that will have extension-twist coupling. Combining this family with the hygrothermally isotropic $[0°/90°]_s$ layup leads to a stacking sequence given by

$$\left[\theta/(\theta-90)_2/\theta/-\theta/(90-\theta)_2/-\theta\right] \tag{1}$$

which will be hygrothermally stable and have extension-twist coupling. This solution was developed previously by Winckler[2]. While intuitive, its uniqueness, and more significantly its optimality, have never been demonstrated.

In an attempt to answer the issue of optimality, this work begins by establishing the necessary and sufficient conditions for hygrothermal stability. Next, a survey of the range of available couplings from within these conditions is performed. This work culminates in the implementation of a constrained optimization routine to identify the stacking sequence that produces the highest level of a single coupling for a laminate with a given number of plies. Families that have significant increases in coupling over the current state-of-the-art are demonstrated through manufacture and testing, and nonlinear models and finite element analysis predict their response.

CHAPTER 2

LITERATURE SURVEY

A review of hygrothermal stability as it applies to asymmetric stacking sequences is provided with a focus on laminated strips. This is followed by an investigation of the past and current state of extension-twist coupling. Finally, an overview of past works involving bend-twist coupling with hygrothermal stability is provided.

2.1 Hygrothermal Stability

For most of the history of composites, symmetric layups have been used to ensure shape stability with changes in temperature or moisture,[3] referred to subsequently as hygrothermal stability. While this does not preclude bend-twist coupling, it does eliminate the possibility of extension-twist coupling, as well as out-of-plane warping with changes in temperature or moisture, such as thermally induced contractions that can result from cooling after curing. There have been some attempts in recent history to create laminates that are hygrothermally stable but have an asymmetric stacking sequence. One approach involves enforcing the coupling stiffness matrix to be zero, as will be proven later. Weaver[4] developed a class of laminates with at least seven plies that have an asymmetric stacking sequence but a coupling stiffness matrix equal to zero. These stacking sequences, while capable of having as few as two distinct ply angles, are not shown to be optimal.

The other approach to ensure hygrothermal stability with an asymmetric stacking sequence uses nested hygrothermally isotropic sublaminates, first proposed by Winckler[2].

Again, it combines the known couplings of a $[\pm\theta]$ laminate with the hygrothermal isotropy of a $[0°/90°]_s$ layup, as shown in Equation (1). Shortly thereafter in his doctoral dissertation[5], Winckler demonstrated that the $[\theta / \theta+90°]_s$ sublaminate could be used as many times as desired. Weaver arrived at similar results[4] by considering that the two axial non-mechanical stress resultants are equal and the remaining non-mechanical stress and moment resultants are zero, yielding zero non-mechanical curvatures. His formulation identified hygrothermally isotropic stacking sequences by $[\pm45°+\theta]_s$. Combinations of multiples of these sublaminates, such that each sublaminate is evenly spaced within another, creates an asymmetric (termed "subsymmetric") stacking sequence capable of producing mechanical in-plane/out-of-plane coupling; however, once again, these families are not shown to be complete or optimal.

A study of the necessary and sufficient conditions for a laminate with hygrothermal isotropy was undertaken by Chen[6]. He identifies four conditions that correspond to making the two axial non-mechanical stress resultants equal and making the remaining non-mechanical stress and moment resultants zero to yield zero non-mechanical curvatures. He was able to identify an antisymmetric five-ply laminate that is hygrothermally isotropic as well as asymmetric six- and seven-ply laminates. Hygrothermal isotropy, however, is not necessary for hygrothermal stability.

2.2 Extension-twist Coupling with Hygrothermal Stability

There have been several attempts at exploiting extension-twist coupling for use in rotor applications. Many of these simply used angle-ply stacking sequences $[\pm\theta]$, largely due to their ease of analysis and manufacture. For example, Crawley and Lazarus[7] used

$[\pm(45°_3)]$ in their study of induced strain actuation of plates. Nampy[8] used $[\theta]_6$ in a box beam configuration to investigate the feasibility of employing flexible-matrix composites.

Uses of hygrothermally isotropic sublaminates appear frequently in literature after first being proposed by Winckler[2]. Nixon[9] was one of the first to use the Winckler-type layups to produce a closed-section rotor blade that could change its twist distribution as a function of rotor speed and avoid thermal coupling, which he then demonstrated later using a $[20°]_4$ stacking sequence of [0°/90°] cloth weave graphite/epoxy. Chandra and Chopra[10] conducted a detailed study of the structural response of anisotropic blades using $[\pm\theta]$ and [20°/-70°] layups, the latter of which is hygrothermally isotropic. Hill and Winckler[11] used laminates with hygrothermally isotropic sublaminates to create extension-twist coupled composite tubes that have reduced hygrothermal coupling. Bothwell *et al.*[12] continued the induced strain study, this time using an $[11°]_2$ stacking sequence to achieve extension-twist coupling and creating a [20°/-70°] layup for comparison.

Some attempts at optimization of extension-twist coupling have been undertaken in the past. Armanios *et al.*[13] performed a constrained optimization using the Winckler-type laminate as an initialization to maximize the coupling compliance coefficient β_{16}, defined later, under the conditions of minimum non-mechanical curvatures. Improved extension-twist results were found for eight-ply laminates, but did not suggest a global maximum. Gürdal *et al.*[3] presented a method of maximizing B_{16}, the extension-twist coupling stiffness coefficient, employing genetic algorithms using the same constraints for zero non-mechanical curvature. Chen optimized 16-ply laminates to maximize

extension-twist coupling, through β_{16}, while being constrained to the conditions of hygrothermal isotropy.

2.3 Bend-twist Coupling with Hygrothermal Stability

Bend-twist coupling is achievable using symmetric layups. The simplest laminate would have a unidirectional stacking sequence, but unidirectional laminates are known to be susceptible to splitting failures and, therefore, are not practical for structural purposes. One of the most well-known applications of bend-twist coupling was the aeroelastic tailoring of the X-29A wing, which delayed the onset of aeroelastic instabilities. The wing was manufactured from 156 plies of an AS/3501/5A graphite/epoxy tape with [0°/90°/45°] ply angles rotated 9° forward of the reference structural axis. This inhibited divergence of the wing with -29.3° leading-edge sweep[14,15].

To investigate the effect of vibration coupling between bending and twisting on damping, Hwang and Gibson used unidirectional $[\theta]_{12}$ laminates[16]. Ong and Tsai investigated maximum bend-twist coupling in D-spars and found that $[20°]_{16}$ and $[25°]_{16}$ stacking sequences optimized bend-twist coupling for graphite and glass composites, respectively[17]. In both of these cases, ply orientations were restricted to common whole angles, thereby not demonstrating optimality, and in both cases unidirectional laminates were chosen based on amount of coupling. Lemanski and Weaver[18] also investigated the level of flexural-twist coupling obtainable with various unidirectional off-axis and angle-ply laminates consisting of common ply angles. Rehfield and Cheung[19] proposed a new design strategy for aeroelastic tailoring. Termed "angle ply rotation," it uses unbalanced angle plies with axis-oriented plies, e.g., $[0°_m/\theta_n]$. This method combines the coupling

ability of unidirectional off-axis plies with the practicality of common layups, such as $[0°/90°/\pm45°]_s$. Angle ply rotations, however, are typically hygrothermally unstable. The aforementioned studies have not demonstrated an optimal hygrothermally stable bend-twist coupled stacking sequence.

It is worth mentioning that in contrast to laminated strips, extension-twist and bend-twist couplings are achieved in closed sections through circumferentially uniform and circumferentially asymmetric stacking sequences, respectively.[20,21,22,23] Dancila, Armanios, and Lentz[24] investigated optimum extension-twist coupling in closed sections subject to hygrothermal and natural frequency constraints. Ozbay[25] investigated the feasibility of extension-twist coupling in closed-section rotor blades to improve propulsive efficiency in both hover and forward flight regimes while meeting aeroelastic stability constraints. To this end, he proposed a sliding mass concept to increase the centrifugal force.

This literature survey points to the need for assessing the uniqueness and optimality of current hygrothermally stable extension-twist and bend-twist coupled designs. To this end, the objective of this research work is to achieve hygrothermally stable laminate strips with optimal couplings. The approach taken in this dissertation provides a rigorous framework to perform this analysis. The necessary and sufficient conditions for hygrothermal stability are determined first, in Chapter 3. Next, families of laminates capable of maintaining hygrothermal stability are derived in Chapter 4, including a proof that at least five plies are required to obtain a hygrothermally stable laminate with extension-twist coupling. Laminates with optimal extension-twist and bend-twist couplings are developed and presented in Chapters 5 and 6, respectively,

including validation of optimal designs through finite element analysis, nonlinear models, and manufacturing and testing. In Chapter 7, other couplings are investigated briefly, followed by conclusions and recommendations for future work in Chapters 8 and 9, respectively.

CHAPTER 3

NECESSARY AND SUFFICIENT CONDITIONS FOR HYGROTHERMAL STABILITY

In contrast to prior established work where researchers were primarily concerned with achieving the desired structural response and considered hygrothermal instabilities as constraints, this work considers hygrothermal stability to be the primary requirement; then, from within this class of laminates, the maximum level of coupling is sought. Therefore, to begin, the necessary and sufficient hygrothermal stability conditions are derived. Cross *et al*.[26] provides these conditions.

The general constitutive law as set forth in Classical Lamination Theory (CLT) is given as[1]

$$\left\{\begin{array}{c} N_{xx} \\ N_{yy} \\ N_{xy} \\ \hdashline M_{xx} \\ M_{yy} \\ M_{xy} \end{array}\right\} = \left[\begin{array}{ccc:ccc} A_{11} & A_{12} & A_{16} & B_{11} & B_{12} & B_{16} \\ A_{12} & A_{22} & A_{26} & B_{12} & B_{22} & B_{26} \\ A_{16} & A_{26} & A_{66} & B_{16} & B_{26} & B_{66} \\ \hdashline B_{11} & B_{12} & B_{16} & D_{11} & D_{12} & D_{16} \\ B_{12} & B_{22} & B_{26} & D_{12} & D_{22} & D_{26} \\ B_{16} & B_{26} & B_{66} & D_{16} & D_{26} & D_{66} \end{array}\right] \left\{\begin{array}{c} \varepsilon_{xx} \\ \varepsilon_{yy} \\ \gamma_{xy} \\ \hdashline \kappa_{xx} \\ \kappa_{yy} \\ \kappa_{xy} \end{array}\right\} + \left\{\begin{array}{c} N_{xx} \\ N_{yy} \\ N_{xy} \\ \hdashline M_{xx} \\ M_{yy} \\ M_{xy} \end{array}\right\}^{(T,H)} \tag{2}$$

where N_{xx}, N_{yy}, N_{xy}, M_{xx}, M_{yy}, and M_{xy} are the stress resultants, and ε_{xx}, ε_{yy}, γ_{xy}, κ_{xx}, κ_{yy}, and κ_{xy} are the strains and curvatures. The stiffness coefficients are given as

$$
\begin{aligned}
A_{ij} &= \sum_{k=1}^{n} \overline{Q}_{ij(k)} \left(h_k - h_{k-1} \right) \\
B_{ij} &= \frac{1}{2} \sum_{k=1}^{n} \overline{Q}_{ij(k)} \left(h_k^2 - h_{k-1}^2 \right) \\
D_{ij} &= \frac{1}{3} \sum_{k=1}^{n} \overline{Q}_{ij(k)} \left(h_k^3 - h_{k-1}^3 \right)
\end{aligned}
\tag{3}
$$

where $\overline{Q}_{ij(k)}$ and h_k represent the transformed reduced stiffness coefficients and height relative to the laminate midplane for the k^{th} ply, respectively. The non-mechanical stress resultants are given as

$$
\begin{aligned}
\begin{Bmatrix} N_{xx} \\ N_{yy} \\ N_{xy} \end{Bmatrix}^{(T,H)} &= (\Delta T, \Delta H) \sum_{k=1}^{n} \left[\overline{Q} \right]_k \left\{ \overline{\alpha}, \overline{\beta} \right\}_k \left(h_k - h_{k-1} \right) \\
\begin{Bmatrix} M_{xx} \\ M_{yy} \\ M_{xy} \end{Bmatrix}^{(T,H)} &= \frac{1}{2} (\Delta T, \Delta H) \sum_{k=1}^{n} \left[\overline{Q} \right]_k \left\{ \overline{\alpha}, \overline{\beta} \right\}_k \left(h_k^2 - h_{k-1}^2 \right)
\end{aligned}
\tag{4}
$$

where $\left\{ \overline{\alpha}, \overline{\beta} \right\}_k$ are the transformed in-plane thermal and moisture expansion coefficients for the k^{th} ply. The total number of plies in the laminate is n, and T and H denote thermal and hygral quantities, respectively. For a specially orthotropic lamina, the stiffness and thermal coefficient transformations can be expressed as

$$
\begin{aligned}
\left[\overline{Q} \right] &= \left[T_\sigma \right]^{-1} \left[Q \right] \left[T_\varepsilon \right] = \left[T_\sigma \right]^{-1} \begin{bmatrix} Q_{11} & Q_{12} & 0 \\ Q_{12} & Q_{22} & 0 \\ 0 & 0 & Q_{66} \end{bmatrix} \left[T_\varepsilon \right] \\
\left\{ \overline{\alpha}, \overline{\beta} \right\} &= \left[T_\varepsilon \right]^{-1} \left\{ \alpha, \beta \right\} = \left[T_\varepsilon \right]^{-1} \begin{Bmatrix} \alpha_{11}, \beta_{11} \\ \alpha_{22}, \beta_{22} \\ 0 \end{Bmatrix}
\end{aligned}
\tag{5}
$$

where the stress and engineering strain transformation matrices are given by

$$[T_\sigma]=\begin{bmatrix} c^2 & s^2 & 2cs \\ s^2 & c^2 & -2cs \\ -cs & cs & c^2-s^2 \end{bmatrix} \qquad [T_\varepsilon]=\begin{bmatrix} c^2 & s^2 & cs \\ s^2 & c^2 & -cs \\ -2cs & 2cs & c^2-s^2 \end{bmatrix} \tag{6}$$

and $c = \cos\theta$ and $s = \sin\theta$, where θ is the fiber orientation angle.

Substituting Equations (5) and (6) into Equation (4) gives

$$\begin{Bmatrix} M_{xx} \\ M_{yy} \\ M_{xy} \end{Bmatrix}^{(T,H)} = \frac{(\Delta T, \Delta H)}{2} \sum_{k=1}^{n} \begin{bmatrix} c^2 & s^2 & -2cs \\ s^2 & c^2 & 2cs \\ cs & -cs & c^2-s^2 \end{bmatrix}_k \begin{Bmatrix} Q_{11}(\alpha_{11},\beta_{11}) + Q_{12}(\alpha_{22},\beta_{22}) \\ Q_{12}(\alpha_{11},\beta_{11}) + Q_{22}(\alpha_{22},\beta_{22}) \\ 0 \end{Bmatrix}_k \left(h_k^2 - h_{k-1}^2\right) \tag{7}$$

Assuming each ply is identical with thickness t, subscript k can be dropped from the stiffness coefficients and thermal and moisture expansion terms, and the height relative to the midplane can be expressed as

$$h_k = kt - \frac{nt}{2} \tag{8}$$

allowing the simplification

$$h_k^2 - h_{k-1}^2 = t^2(2k - n - 1) \tag{9}$$

Note that

$$\sum_{k=1}^{n} (2k - n - 1) = 0 \tag{10}$$

Simplifying Equation (7) using Equations (9) and (10) and trigonometric identities leads to the following expression for the non-mechanical moments in which the material and stacking sequence dependent terms can be separately factored as

$$\begin{Bmatrix} M_{xx} \\ M_{yy} \\ M_{xy} \end{Bmatrix}^{(T,H)} = T_1 \sum_{k=1}^{n} \begin{Bmatrix} \cos 2\theta_k \\ -\cos 2\theta_k \\ \sin 2\theta_k \end{Bmatrix} (2k - n - 1) \tag{11}$$

where

$$T_1 = \frac{t^2(\Delta T, \Delta H)}{4}\left[(\alpha_{11}, \beta_{11})(Q_{11} - Q_{12}) + (\alpha_{22}, \beta_{22})(Q_{12} - Q_{22})\right] \tag{12}$$

Similarly to Equation (11), the non-mechanical force resultants in Equation (4) can be simplified to

$$\begin{Bmatrix} N_{xx} \\ N_{yy} \\ N_{xy} \end{Bmatrix}^{(T,H)} = T_2 \begin{Bmatrix} 1 \\ 1 \\ 0 \end{Bmatrix} + T_3 \sum_{k=1}^{n} \begin{Bmatrix} \cos 2\theta_k \\ -\cos 2\theta_k \\ \sin 2\theta_k \end{Bmatrix} \tag{13}$$

where

$$\begin{aligned} T_2 &= \frac{nt(\Delta T, \Delta H)}{2}\left[(\alpha_{11}, \beta_{11})(Q_{11} + Q_{12}) + (\alpha_{22}, \beta_{22})(Q_{12} + Q_{22})\right] \\ T_3 &= \frac{t(\Delta T, \Delta H)}{2}\left[(\alpha_{11}, \beta_{11})(Q_{11} - Q_{12}) + (\alpha_{22}, \beta_{22})(Q_{12} - Q_{22})\right] = \frac{2T_1}{t} \end{aligned} \tag{14}$$

Two important assumptions made in the preceding development will be reiterated here: first, all plies must be specially orthotropic, and, second, all plies must have the same mechanical and hygrothermal properties in the principle material directions. The first observation from Equation (11) is that $M_{xx} = -M_{yy}$. Second, the material-dependent parameters can be completely factored out of the stacking sequence terms. Hence, stacking sequences that result in zero non-mechanical moments are material independent. It is also possible to eliminate non-mechanical moments by choosing a ply material that sets T_1 to zero. This is the case for an isotropic ply material, but use of such a ply material results in a homogeneous plate. In the case of fiber-reinforced orthotropic laminas, manufacturing variability and availability of material systems may make setting $T_1 = 0$ impractical.

3.1 Derivation of Hygrothermal Stability Conditions

In the absence of mechanical loads, hygrothermal stability is achieved when the curvatures, κ_{xx}, κ_{yy}, and κ_{xy} are identically zero for non-zero changes in temperature and moisture. To find the necessary conditions for hygrothermal stability, consider Equation (2) with no mechanical loads, all curvatures set to zero, and the results from Equation (11)

$$\left\{\begin{array}{c} N_{xx} \\ N_{yy} \\ N_{xy} \\ \hline M_{xx} \\ -M_{xx} \\ M_{xy} \end{array}\right\}^{(T,H)} = \left[\begin{array}{ccc} A_{11} & A_{12} & A_{16} \\ A_{12} & A_{22} & A_{26} \\ A_{16} & A_{26} & A_{66} \\ \hline B_{11} & B_{12} & B_{16} \\ B_{12} & B_{22} & B_{26} \\ B_{16} & B_{26} & B_{66} \end{array}\right] \left\{\begin{array}{c} \varepsilon_{xx} \\ \varepsilon_{yy} \\ \gamma_{xy} \end{array}\right\} \tag{15}$$

Adding the expressions for the non-mechanical bending moments in Equation (15) gives a necessary condition for hygrothermal stability

$$\left(B_{11}+B_{12}\right)\varepsilon_{xx}+\left(B_{12}+B_{22}\right)\varepsilon_{yy}+\left(B_{16}+B_{26}\right)\gamma_{xy}=0 \tag{16}$$

To simplify this expression and later developments, the transformed reduced stiffness coefficients are expressed in terms of the invariants derived by Tsai and Pagano[27]

$$\begin{aligned} \overline{Q}_{11} &= U_1 + U_2\cos 2\theta + U_3\cos 4\theta \\ \overline{Q}_{12} &= U_4 - U_3\cos 4\theta \\ \overline{Q}_{22} &= U_1 - U_2\cos 2\theta + U_3\cos 4\theta \\ \overline{Q}_{16} &= \frac{1}{2}U_2\sin 2\theta + U_3\sin 4\theta \\ \overline{Q}_{26} &= \frac{1}{2}U_2\sin 2\theta - U_3\sin 4\theta \\ \overline{Q}_{66} &= \frac{1}{2}\left(U_1 - U_4\right) - U_3\cos 4\theta \end{aligned} \tag{17}$$

where

$$U_1 = \frac{3Q_{11} + 3Q_{22} + 2Q_{12} + 4Q_{66}}{8} \qquad U_2 = \frac{Q_{11} - Q_{22}}{2}$$
$$U_3 = \frac{Q_{11} + Q_{22} - 2Q_{12} - 4Q_{66}}{8} \qquad U_4 = \frac{Q_{11} + Q_{22} + 6Q_{12} - 4Q_{66}}{8} \tag{18}$$

Using Equations (3), (9), (17), and (18), the following relationships between laminate coupling stiffness terms are obtained as

$$\begin{aligned} \left(B_{11} + B_{12}\right) &= -\left(B_{12} + B_{22}\right) = \frac{U_2 t^2}{2} B_c \\ \left(B_{16} + B_{26}\right) &= \frac{U_2 t^2}{2} B_s \end{aligned} \tag{19}$$

where the following simplifying notations are used

$$B_c = \sum_{k=1}^{n} (2k - n - 1)\cos 2\theta_k \qquad B_s = \sum_{k=1}^{n} (2k - n - 1)\sin 2\theta_k \tag{20}$$

Using Equation (19), Equation (16) is simplified to be

$$\frac{U_2 t^2}{2}\left[\left(\varepsilon_{xx} - \varepsilon_{yy}\right)B_c + \gamma_{xy} B_s\right] = 0 \tag{21}$$

Since the [A] matrix is positive definite, the in-plane non-mechanical strains can be calculated by multiplying the inverse of the [A] matrix by the non-mechanical in-plane stress resultant vector as given by Equation (15).

$$\begin{aligned} \left|A\right|\varepsilon_{xx} &= N_{xx}^{(T,H)}\left(A_{22}A_{66} - A_{26}^2\right) + N_{yy}^{(T,H)}\left(A_{16}A_{26} - A_{12}A_{66}\right) + N_{xy}^{(T,H)}\left(A_{12}A_{26} - A_{16}A_{22}\right) \\ \left|A\right|\varepsilon_{yy} &= N_{xx}^{(T,H)}\left(A_{16}A_{26} - A_{12}A_{66}\right) + N_{yy}^{(T,H)}\left(A_{11}A_{66} - A_{16}^2\right) + N_{xy}^{(T,H)}\left(A_{12}A_{16} - A_{11}A_{26}\right) \\ \left|A\right|\gamma_{xy} &= N_{xx}^{(T,H)}\left(A_{12}A_{26} - A_{16}A_{22}\right) + N_{yy}^{(T,H)}\left(A_{12}A_{16} - A_{11}A_{26}\right) + N_{xy}^{(T,H)}\left(A_{11}A_{22} - A_{12}^2\right) \end{aligned} \tag{22}$$

Next use the simplified expression for non-mechanical in-plane stress resultants, Equation (13), with Equation (22) to factor the strains in Equation (21)

$$
\begin{aligned}
|A|(\varepsilon_{xx}-\varepsilon_{yy}) = \;& T_2\left[A_{66}(A_{22}-A_{11})+(A_{16}^2-A_{26}^2)\right] \\
& +T_3\left[A_{66}(A_{11}+A_{22}+2A_{12})-(A_{16}+A_{26})^2\right]C_2 \\
& +T_3\left[A_{26}(A_{11}+A_{12})-A_{16}(A_{12}+A_{22})\right]S_2 \\
|A|\gamma_{xy} = \;& T_2\left[A_{16}(A_{12}-A_{22})+A_{26}(A_{12}-A_{11})\right] \\
& +T_3\left[A_{26}(A_{11}+A_{12})-A_{16}(A_{12}+A_{22})\right]C_2 \\
& +T_3\left[A_{11}A_{22}-A_{12}^2\right]S_2
\end{aligned}
\tag{23}
$$

where the following notations are introduced for brevity

$$
C_m=\sum_{k=1}^{n}\cos m\theta_k \qquad\qquad S_m=\sum_{k=1}^{n}\sin m\theta_k \tag{24}
$$

The expressions for the transformed reduced stiffness coefficients in Equations (17) and (18) can be used with Equation (3) to find the following relationships between in-plane laminate stiffness coefficients

$$
\begin{aligned}
A_{11}+A_{22}+2A_{12} &= 2(K_1+K_4) \\
A_{22}-A_{11} &= -2U_2tC_2 \\
A_{12}-A_{11} &= K_4-K_1-U_2tC_2-2U_3tC_4 \\
A_{12}-A_{22} &= K_4-K_1+U_2tC_2-2U_3tC_4 \\
A_{16}^2-A_{26}^2 &= 2U_2U_3t^2S_2S_4 \\
(A_{16}+A_{26})^2 &= U_2^2t^2S_2^2 \\
A_{66} &= \frac{1}{2}(K_1-K_4)-U_3tC_4
\end{aligned}
\tag{25}
$$

where

$$
K_j=ntU_j;\ (j=1\ldots4) \tag{26}
$$

With Equation (25), Equation (23) is simplified into the factored form

$$
\begin{aligned}
|A|(\varepsilon_{xx}-\varepsilon_{yy}) &= \left[U_2tT_2-(K_1+K_4)T_3\right]\left[(K_4-K_1)C_2+2U_3t(C_2C_4+S_2S_4)\right] \\
|A|\gamma_{xy} &= \left[U_2tT_2-(K_1+K_4)T_3\right]\left[(K_4-K_1)S_2+2U_3t(C_2S_4-S_2C_4)\right]
\end{aligned}
\tag{27}
$$

Inserting Equation (27) into Equation (21) gives

$$M\{[(K_4 - K_1)C_2 + 2U_3 t(C_2 C_4 + S_2 S_4)]B_c + [(K_4 - K_1)S_2 + 2U_3 t(C_2 S_4 - S_2 C_4)]B_s\} = 0 \tag{28}$$

where

$$M = \frac{U_2 t^2}{2|A|}\left[U_2 t T_2 - (K_1 + K_4)T_3\right] \tag{29}$$

Since K_1, K_4, T_2, T_3, U_2, and U_3 are non-zero independent material constants and because of the fact that hygrothermal stability conditions must be invariant under a rigid rotation of the laminate, a set of necessary material-independent conditions can be obtained from Equation (28) as either

$$C_2 = S_2 = 0 \tag{30}$$

or

$$B_c = B_s = 0 \tag{31}$$

Note that the second of these conditions is identically satisfied by symmetric stacking sequences. The following developments consider each of these necessary conditions separately to determine additional requirements for sufficiency.

Consider first the necessary condition in Equation (30) to find what additional conditions are required for hygrothermal stability. Assuming Equation (30) holds, Equation (27) implies $\gamma_{xy} = 0$ and $\varepsilon_{xx} = \varepsilon_{yy}$, and thus, the thermal strain of the laminate is equal in all global directions.

Additional requirements for sufficiency are provided by the bending and twisting moment equations in Equation (15). Under the assumption that Equation (30) holds, the bending moment equations can be simplified using Equations (10) and (19) to give

$$T_1 B_c = \frac{U_2 t^2}{2} B_c \varepsilon_{xx} \tag{32}$$

which can only be satisfied for an arbitrary material choice if $B_c = 0$.

Likewise, the equation for the non-mechanical twisting moment in Equation (15) must be considered under the assumption that Equation (30) holds. The twisting moment can be simplified using Equations (10) and (19) resulting in

$$T_1 B_s = \frac{U_2 t^2}{2} B_s \varepsilon_{xx} \tag{33}$$

which can only be satisfied for arbitrary material selection if $B_s = 0$. Thus, by the non-singularity of the matrix in Equation (2), Equations (30) and (31) taken together are sufficient conditions for hygrothermal stability. These will henceforth be termed "Condition A."

Next consider the second option in the necessary conditions, given by Equation (31), which implies that the non-mechanical moments are equal to zero. From Equations (3), (9), (17), and (19), this condition also implies $B_{11} = B_{22} = -B_{12} = -B_{66}$ and $B_{16} = -B_{26}$. Substituting into the non-mechanical bending and twisting moment equations from Equation (15) gives

$$\begin{aligned} M_{xx}^{(T,H)} &= \frac{U_3 t^2}{2}\left[\left(\varepsilon_{xx} - \varepsilon_{yy}\right)\sum_{k=1}^{n}\left(2k-n-1\right)\cos 4\theta_k + \gamma_{xy}\sum_{k=1}^{n}\left(2k-n-1\right)\sin 4\theta_k\right] = 0 \\ M_{xy}^{(T,H)} &= \frac{U_3 t^2}{2}\left[\left(\varepsilon_{xx} - \varepsilon_{yy}\right)\sum_{k=1}^{n}\left(2k-n-1\right)\sin 4\theta_k - \gamma_{xy}\sum_{k=1}^{n}\left(2k-n-1\right)\cos 4\theta_k\right] = 0 \end{aligned} \tag{34}$$

This can be satisfied for arbitrary material choice in only two ways, either

$$\sum_{k=1}^{n}\left(2k-n-1\right)\cos 4\theta_k = \sum_{k=1}^{n}\left(2k-n-1\right)\sin 4\theta_k = 0 \tag{35}$$

or

$$\varepsilon_{xx} - \varepsilon_{yy} = \gamma_{xy} = 0 \tag{36}$$

The first of these conditions with the condition $B_c = B_s = 0$ implies the coupling matrix, $[B]$ is identically zero as can be shown using Equations (3), (9), (17), (31), and (35), henceforth termed "Condition B." The second is true for an arbitrary choice of material if and only if $C_2 = S_2 = 0$, as seen in Equation (27). A summary of the necessary and sufficient conditions for hygrothermal stability is provided in Table 1.

Table 1. Necessary and Sufficient Conditions for Hygrothermal Stability

Condition A		OR	Condition B
Equal normal non-mechanical stress resultants and zero non-mechanical shear and moment resultants, i.e. $N_{xx}^{(T,H)} = N_{yy}^{(T,H)}$ $N_{xy}^{(T,H)} = M_{xx}^{(T,H)} = M_{yy}^{(T,H)} = M_{xy}^{(T,H)} = 0$			Coupling stiffness matrix is zero, i.e. B_{ij}=0
Satisfied when:	Or simplified:		Satisfied when:
$\sum_{k=1}^{n}(2k-n-1)\cos 2\theta_k = 0$	$\sum_{k=1}^{n} k\cos 2\theta_k = 0$		$\sum_{k=1}^{n}(2k-n-1)\cos 2\theta_k = 0$
$\sum_{k=1}^{n}(2k-n-1)\sin 2\theta_k = 0$	$\sum_{k=1}^{n} k\sin 2\theta_k = 0$		$\sum_{k=1}^{n}(2k-n-1)\sin 2\theta_k = 0$
$\sum_{k=1}^{n}\cos 2\theta_k = 0$	$\sum_{k=1}^{n}\cos 2\theta_k = 0$		$\sum_{k=1}^{n}(2k-n-1)\cos 4\theta_k = 0$
$\sum_{k=1}^{n}\sin 2\theta_k = 0$	$\sum_{k=1}^{n}\sin 2\theta_k = 0$		$\sum_{k=1}^{n}(2k-n-1)\sin 4\theta_k = 0$
Equivalently: $\xi_1 = \xi_3 = \xi_5 = \xi_7 = 0$			Equivalently $\xi_5 = \xi_6 = \xi_7 = \xi_8 = 0$

It warrants emphasis that the derived hygrothermal stability conditions are material independent. The material independence is advantageous for several reasons. First, were the conditions material dependent, design of a hygrothermally stable laminate could not proceed until a material system is selected and its mechanical and thermal

properties are characterized. The material independence is especially important for preliminary design before a specific material has been selected. Second, material independence provides robustness against the variability in elastic constants and coefficients of thermal and moisture expansion.

3.2 Extensions

It should be mentioned that the necessary and sufficient conditions for hygrothermal stability can be derived using lamination parameters.[28] Instead of using the reduced stiffness coefficients to arrive at the matrix components in Equation (2), the following relations are used

$$\begin{Bmatrix} A_{11} \\ A_{12} \\ A_{22} \\ A_{66} \\ A_{16} \\ A_{26} \end{Bmatrix} = nt \begin{bmatrix} 1 & \xi_1 & \xi_2 & 0 & 0 \\ 0 & 0 & -\xi_2 & 1 & 0 \\ 1 & -\xi_1 & \xi_2 & 0 & 0 \\ 0 & 0 & -\xi_2 & 0 & 1 \\ 0 & \xi_3 & \xi_4 & 0 & 0 \\ 0 & \xi_3 & -\xi_4 & 0 & 0 \end{bmatrix} \underline{W} \tag{37}$$

$$\begin{Bmatrix} B_{11} \\ B_{12} \\ B_{22} \\ B_{66} \\ B_{16} \\ B_{26} \end{Bmatrix} = \frac{(nt)^2}{4} \begin{bmatrix} 0 & \xi_5 & \xi_6 & 0 & 0 \\ 0 & 0 & -\xi_6 & 0 & 0 \\ 0 & -\xi_5 & \xi_6 & 0 & 0 \\ 0 & 0 & -\xi_6 & 0 & 0 \\ 0 & \xi_7 & \xi_8 & 0 & 0 \\ 0 & \xi_7 & -\xi_8 & 0 & 0 \end{bmatrix} \underline{W} \tag{38}$$

$$\begin{Bmatrix} D_{11} \\ D_{22} \\ D_{12} \\ D_{66} \\ D_{16} \\ D_{26} \end{Bmatrix} = \frac{(nt)^3}{12} \begin{bmatrix} 1 & \xi_9 & \xi_{10} & 0 & 0 \\ 0 & 0 & -\xi_{10} & 1 & 0 \\ 1 & -\xi_9 & \xi_{10} & 0 & 0 \\ 0 & 0 & -\xi_{10} & 0 & 1 \\ 0 & \xi_{11} & \xi_{12} & 0 & 0 \\ 0 & \xi_{11} & -\xi_{12} & 0 & 0 \end{bmatrix} \underline{W} \tag{39}$$

where the lamination parameters are

$$\begin{aligned} (\xi_1, \xi_2, \xi_3, \xi_4) &= \frac{1}{nt} \sum_{i=1}^{n} (\cos 2\theta_i, \cos 4\theta_i, \sin 2\theta_i, \sin 4\theta_i)(h_i - h_{i-1}) \\ (\xi_5, \xi_6, \xi_7, \xi_8) &= \frac{2}{(nt)^2} \sum_{i=1}^{n} (\cos 2\theta_i, \cos 4\theta_i, \sin 2\theta_i, \sin 4\theta_i)(h_i^2 - h_{i-1}^2) \\ (\xi_9, \xi_{10}, \xi_{11}, \xi_{12}) &= \frac{4}{(nt)^3} \sum_{i=1}^{n} (\cos 2\theta_i, \cos 4\theta_i, \sin 2\theta_i, \sin 4\theta_i)(h_i^3 - h_{i-1}^3) \end{aligned} \tag{40}$$

and $\underline{W}$ is given by

$$\underline{W} = \begin{Bmatrix} \frac{3Q_{11} + 3Q_{22} + 2Q_{12} + 4Q_{66}}{8} \\ \frac{Q_{11} - Q_{22}}{2} \\ \frac{Q_{11} + Q_{22} - 2Q_{12} - 4Q_{66}}{8} \\ \frac{Q_{11} + Q_{22} + 6Q_{12} - 4Q_{66}}{8} \\ \frac{Q_{11} + Q_{22} - 2Q_{12} + 4Q_{66}}{8} \end{Bmatrix} \tag{41}$$

Based on this formulation, it can be shown that the necessary and sufficient conditions for hygrothermal stability can be written in terms of the lamination parameters. Condition A is equivalent to

$$\xi_1 = \xi_3 = \xi_5 = \xi_7 = 0 \tag{42}$$

and Condition B is equivalent to

$$\xi_5 = \xi_6 = \xi_7 = \xi_8 = 0 \tag{43}$$

This alternate formulation is listed in Table 1, as well.

It was mentioned previously that Winckler developed a family of hygrothermally stable laminates, provided in Equation (1), with extension-twist coupling derived using an intuitive approach. It follows that this family must meet the hygrothermal stability conditions, specifically Condition A, so that it is capable of producing non-zero extension-twist coupling. To show this, consider insertion of Equation (1) into each of the equations that satisfy Condition A and use trigonometric identities to simplify:

$$\begin{aligned} 0 &= \sum_{k=1}^{n} (2k - n - 1)\cos 2\theta_k \\ &= -7\cos 2\theta - 5\cos 2(\theta - 90) - 3\cos 2(\theta - 90) - \cos 2\theta \\ &\quad + \cos 2(-\theta) + 3\cos 2(90 - \theta) + 5\cos 2(90 - \theta) + 7\cos 2(-\theta) \\ &= (-7 + 5 + 3 - 1 + 1 - 3 - 5 + 7)\cos 2\theta = 0 \end{aligned} \tag{44}$$

$$\begin{aligned} 0 &= \sum_{k=1}^{n} (2k - n - 1)\sin 2\theta_k \\ &= -7\sin 2\theta - 5\sin 2(\theta - 90) - 3\sin 2(\theta - 90) - \sin 2\theta \\ &\quad + \sin 2(-\theta) + 3\sin 2(90 - \theta) + 5\sin 2(90 - \theta) + 7\sin 2(-\theta) \\ &= (-7 + 5 + 3 - 1 - 1 + 3 + 5 - 7)\sin 2\theta = 0 \end{aligned} \tag{45}$$

$$\begin{aligned} 0 &= \sum_{k=1}^{n} \cos 2\theta_k \\ &= \cos 2\theta + 2\cos 2(\theta - 90) + \cos 2\theta + \cos 2(-\theta) + 2\cos 2(90 - \theta) + \cos 2(-\theta) \\ &= (1 - 2 + 1 + 1 - 2 + 1)\cos 2\theta = 0 \end{aligned} \tag{46}$$

$$
\begin{aligned}
0 &= \sum_{k=1}^{n} \sin 2\theta_k \\
&= \sin 2\theta + 2\sin 2(\theta - 90) + \sin 2\theta + \sin 2(-\theta) + 2\sin 2(90 - \theta) + \sin 2(-\theta) \\
&= (1 - 2 + 1 - 1 + 2 - 1)\sin 2\theta = 0
\end{aligned}
\tag{47}
$$

Since all four equalities that satisfy Condition A are met, the Winckler-type laminates must be hygrothermally stable.

CHAPTER 4

HYGROTHERMALLY STABLE ASYMMETRIC STACKING SEQUENCES

With the necessary and sufficient conditions for hygrothermal stability defined, the range of stacking sequences that these conditions afford can be surveyed. The results using Condition A will be evaluated, followed by the results using Condition B.

4.1 Condition A

The equations that ensure hygrothermal stability according to Condition A are provided in Table 1. Laminates consisting of two through eight plies will be considered.

4.1.1 Two- and Three-ply Laminates

Expanding the four equations that satisfy Condition A for a two-ply laminate, the result is

$$\begin{aligned} -\cos 2\theta_1 + \cos 2\theta_2 &= 0 \\ -\sin 2\theta_1 + \sin 2\theta_2 &= 0 \\ \cos 2\theta_1 + \cos 2\theta_2 &= 0 \\ \sin 2\theta_1 + \sin 2\theta_2 &= 0 \end{aligned} \tag{48}$$

The first two equations indicate that

$$\theta_1 = \theta_2 + k \cdot 180°; k = ...,-1,0,1,2,... \tag{49}$$

which, when inserted into the last two equations of Equation (48) produces no solutions. For three plies, the same set of equations reduces to

$$\begin{aligned} -\cos 2\theta_1 + \cos 2\theta_3 &= 0 \\ -\sin 2\theta_1 + \sin 2\theta_3 &= 0 \\ \cos 2\theta_1 + \cos 2\theta_2 + \cos 2\theta_3 &= 0 \\ \sin 2\theta_1 + \sin 2\theta_2 + \sin 2\theta_3 &= 0 \end{aligned} \tag{50}$$

which also produces no solutions.

4.1.2 Four-ply Laminates

Next consider the case of four-ply laminates, where the zero non-mechanical moment condition can be expressed using Equation (11) as

$$\begin{aligned} -3\cos 2\theta_1 - \cos 2\theta_2 + \cos 2\theta_3 + 3\cos 2\theta_4 &= 0 \\ -3\sin 2\theta_1 - \sin 2\theta_2 + \sin 2\theta_3 + 3\sin 2\theta_4 &= 0 \\ \cos 2\theta_1 + \cos 2\theta_2 + \cos 2\theta_3 + \cos 2\theta_4 &= 0 \\ \sin 2\theta_1 + \sin 2\theta_2 + \sin 2\theta_3 + \sin 2\theta_4 &= 0 \end{aligned} \tag{51}$$

Using arithmetic and the Pythagorean identity to eliminate θ_2 and θ_3, it can be shown that

$$\theta_4 = \theta_1 + k \cdot 180°; k = ...,-1,0,1,2,... \tag{52}$$

That is, the outer plies are symmetric. Using this fact, Equation (51) reduces to

$$\begin{aligned} -\cos 2\theta_2 + \cos 2\theta_3 &= 0 \\ -\sin 2\theta_2 + \sin 2\theta_3 &= 0 \\ 2\cos 2\theta_1 + \cos 2\theta_2 + \cos 2\theta_3 &= 0 \\ 2\sin 2\theta_1 + \sin 2\theta_2 + \sin 2\theta_3 &= 0 \end{aligned} \tag{53}$$

The first two equations reveal that

$$\theta_3 = \theta_2 + k \cdot 180°; k = ...,-1,0,1,2,... \tag{54}$$

such that the inner two plies are symmetric. Equation (53) further reduces to

$$\begin{aligned} \cos 2\theta_1 + \cos 2\theta_2 &= 0 \\ \sin 2\theta_1 + \sin 2\theta_2 &= 0 \end{aligned} \tag{55}$$

Without loss of generality, θ_1 can be set to zero, which yields only one solution unique up to a rigid rotation, namely $[0°/90°]_s$. Thus, there is only one unique four-ply stacking sequence that meets the hygrothermal stability constraint of Condition A, given by

$$[\theta / 90 - \theta]_s \tag{56}$$

4.1.3 Five-ply Laminates

Since the orientation of the middle ply of a five-ply laminate does not contribute to the non-mechanical moments, it can be shown in a manner similar to the four-ply case that there exists a rotation such that $\theta_1 = -\theta_5$ and $\theta_2 = -\theta_4$. Therefore, without loss of generality, the hygrothermal stability conditions can be expressed as

$$\begin{aligned} 2\cos 2\theta_1 + 2\cos 2\theta_2 + \cos 2\theta_3 &= 0 \\ \sin 2\theta_3 &= 0 \\ 2\sin 2\theta_1 + \sin 2\theta_2 &= 0 \end{aligned} \tag{57}$$

noting that the non-mechanical bending moments are identically zero when rotated as described. From Equation (57) it is readily observed that θ_3 equals 0° or 90°. Thus, Equation (57) can be reduced to

$$\begin{cases} \cos 2\theta_1 + \cos 2\theta_2 + \dfrac{1}{2} = 0 \\ 2\sin 2\theta_1 + \sin 2\theta_2 = 0 \end{cases} \quad for\ \theta_3 = 0°$$
$$\begin{cases} \cos 2\theta_1 + \cos 2\theta_2 - \dfrac{1}{2} = 0 \\ 2\sin 2\theta_1 + \sin 2\theta_2 = 0 \end{cases} \quad for\ \theta_3 = 90° \tag{58}$$

Again using the Pythagorean identity, a single implicit equation for θ_1 can be obtained as

$$\begin{aligned} \cos^2 2\theta_1 + \cos 2\theta_1 - \frac{3}{4} + 4\sin^2 2\theta_1 = 0 \quad & for\ \theta_3 = 0° \\ \cos^2 2\theta_1 - \cos 2\theta_1 - \frac{3}{4} + 4\sin^2 2\theta_1 = 0 \quad & for\ \theta_3 = 90° \end{aligned} \tag{59}$$

Solving Equation (59) leads to

$$\begin{aligned} \cos 2\theta_1 &= \left(\frac{1}{6} - \frac{\sqrt{10}}{3} \right) \quad for\ \theta_3 = 0° \\ \cos 2\theta_1 &= -\left(\frac{1}{6} - \frac{\sqrt{10}}{6} \right) \quad for\ \theta_3 = 90° \end{aligned} \tag{60}$$

These give two angles and, with Equation (58), stacking sequences rounded to the nearest tenth of a degree, specifically

$$\begin{aligned} &[76.3° / -33.6° / 0° / 33.6° / -76.3°] \\ &[-13.7° / 56.9° / 90° / -56.9° / 13.7°] \end{aligned} \tag{61}$$

These stacking sequences are, in fact, rigid rotations of each other and, therefore, are considered members of the same family.

4.1.4 Families of Six-, Seven-, and Eight-ply Laminates

The equations that satisfy Condition A for six-ply laminates expand to be

$$\begin{aligned} 0 &= -5\cos(2\theta_1) - 3\cos(2\theta_2) - \cos(2\theta_3) + \cos(2\theta_4) + 3\cos(2\theta_5) + 5\cos(2\theta_6) \\ 0 &= -5\sin(2\theta_1) - 3\sin(2\theta_2) - \sin(2\theta_3) + \sin(2\theta_4) + 3\sin(2\theta_5) + 5\sin(2\theta_6) \\ 0 &= \cos(2\theta_1) + \cos(2\theta_2) + \cos(2\theta_3) + \cos(2\theta_4) + \cos(2\theta_5) + \cos(2\theta_6) \\ 0 &= \sin(2\theta_1) + \sin(2\theta_2) + \sin(2\theta_3) + \sin(2\theta_4) + \sin(2\theta_5) + \sin(2\theta_6) \end{aligned} \tag{62}$$

By considering a rigid rotation of the laminate by $-0.5(\theta_1+\theta_6)$, a new stacking sequence will result, of the form $[\beta_1, \beta_2, \beta_3, \beta_4, \beta_5, -\beta_1]$. Using trigonometric identities and combining equations, six-ply laminates meeting Condition A will satisfy the equation

$$\left(\cos(2\beta_1)+2\cos(2\beta_2)+\cos(2\beta_3)\right)^2+\left(5\sin(2\beta_1)+2\sin(2\beta_2)+\sin(2\beta_3)\right)^2=1 \qquad (63)$$

This form still yields a continuum of angles and is not conducive to solving for particular stacking sequences; however, a direct search of stacking sequences with whole-number angles was performed using Equation (63). The results are presented in Table 2.

Table 2. Asymmetric Six-, Seven-, and Eight-ply Laminates, Hygrothermally Stable through Condition A

Number of Plies	Stacking Sequences
6	[θ / θ-90 / θ-60 / θ+30 / θ+60 / θ-30]
6	[θ / θ-60 / θ+60 / θ-90 / θ+30 / θ-30]
7	[θ / θ-60 / θ+60 / θ-90 / θ / θ+60 / θ-30]
7	[θ / θ-90 / θ-90 / θ-30 / θ+30 / θ+30 / θ-60]
7	[θ / θ-90 / θ-30 / θ+60/ θ+90 / θ+30 / θ-30]
7	[θ / θ-60 / θ-90 / θ+60 / θ+30 / θ / θ-60]
7	[θ / θ-90 / θ-60 / θ+60 / θ / θ+30 / θ-60]
8	[θ / (θ-90)$_2$ / θ / -θ / -(90-θ_2)$_2$ / -θ]*, $\theta_1 \neq \theta_2$
8	[θ_1 / (θ_1-90)$_2$ / θ_1 / θ_2 / (90-θ_2)$_2$ / θ_2]**, $\theta_1 \neq \theta_2$
8	[θ_1 / θ_2 / θ_1-90 / θ_2-90 / θ_1-90 / θ_2-90 / θ_1 / θ_2]*, $\theta_1 \neq \theta_2$
8	[θ_1 / θ_1-90 / θ_2 / θ_2-90 / θ_1-90 / θ_1 / θ_2-90 / θ_2]*, $\theta_1 \neq \theta_2$
8	[θ / θ-90 / θ / θ-90 / θ-60 / θ+60 / θ+30 / θ-30]
8	[θ / θ-90 / θ+60 / θ-60 / θ-30 / θ+30 / θ / θ-90]
8	[θ / θ-90 / θ-60 / θ+60 / θ+30 / θ-30 / θ / θ-90]
8	[θ / θ+60 / θ-90 / θ-60 / θ / θ-60 / θ / θ+60]
8	[θ / θ-60 / θ-90 / θ+60 / θ / θ+30 / θ-90 / θ-30]
8	[θ / θ-90 / θ-30 / θ-90 / θ+60 / θ+30 / θ / θ-60]
8	[θ / θ-90 / θ+30 / θ-90 / θ-60 / θ-30 / θ / θ+60]

*Winckler-type laminates
**A generalized form of the first Winckler-type laminate

One class of six-ply laminates meeting Condition A has antisymmetric stacking sequences. This useful simplification allows for Equation (62) to reduce to

$$\begin{aligned}\cos 2\theta_1+\cos 2\theta_2+\cos 2\theta_3&=0\\ 5\sin 2\theta_1+3\sin 2\theta_2+\sin 2\theta_3&=0\end{aligned} \qquad (64)$$

Using the Pythagorean identity to eliminate θ_3 and simplifying gives an equation relating θ_1 and θ_2 as

$$1+2\cos 2(\theta_1+\theta_2)+8(\sin 2\theta_1+\sin 2\theta_2)(3\sin 2\theta_1+\sin 2\theta_2)=0 \tag{65}$$

A contour plot showing the locus of solutions in the θ_1-θ_2 space is given in Figure 1. Note that, while θ_2 has solutions in the entire range -90° to 90°, θ_1 has no solutions in the approximate range $30° < |\theta_1| < 60°$. This could restrict the elastic properties of a laminate that needs to be hygrothermally stable.

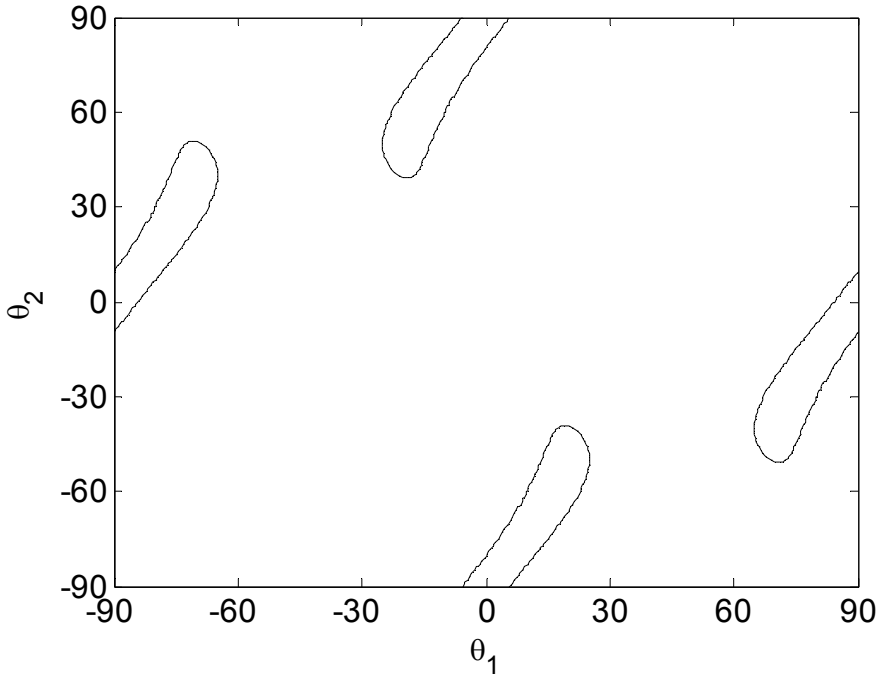

Figure 1. Locus of Six-ply Stable Antisymmetric Solutions Meeting Condition A

Using the same methods that reduced Equation (62) to Equation (63) for six-ply laminates, seven- and eight-ply laminates were reduced and evaluated to identify as many whole-angle stacking sequences as possible. Those discovered are included in Table 2. Also included are the Winckler-type laminates that have been previously published.

4.2 Condition B

The equations that ensure hygrothermal stability according to Condition B are provided in Table 1. Laminates consisting of two or more plies will be considered.

4.2.1 Two- and Three-ply Laminates

For laminates where n=(2,3), the equations that satisfy Condition B from Table 1 can be simplified to

$$\begin{aligned} 0 &= -\cos(2\theta_1) + \cos(2\theta_{(2,3)}) \\ 0 &= -\sin(2\theta_1) + \sin(2\theta_{(2,3)}) \\ 0 &= -\cos(4\theta_1) + \cos(4\theta_{(2,3)}) \\ 0 &= -\sin(4\theta_1) + \sin(4\theta_{(2,3)}) \end{aligned} \tag{66}$$

The first two equations of Equation (66) yield $\theta_1 = \theta_{2,3} + k \cdot 180°$, where k is any integer. The last two equations of Equation (66) yield $\theta_1 = \theta_{2,3} + k \cdot 90°$, where k is any integer. Since the first two equations of Equation (66) yield a more stringent relationship and since a 180° rotation yields the same fiber orientation angle, it can be said without a loss of generality that $\theta_1 = \theta_{(2,3)}$. Therefore, only symmetric two-or three-ply laminates can satisfy Condition B. Specifically, the two- and three-ply stacking sequences are given by

$$\begin{aligned} &[\theta_1]_2 \\ &[\theta_1 / \theta_2 / \theta_1] \end{aligned} \tag{67}$$

4.2.2 Four- and Five-ply Laminates

For four-ply laminates, the equations that satisfy Condition B from Table 1 can be expanded to

$$\begin{aligned} 0 &= -3\cos(2\theta_1) - \cos(2\theta_2) + \cos(2\theta_3) + 3\cos(2\theta_4) \\ 0 &= -3\sin(2\theta_1) - \sin(2\theta_2) + \sin(2\theta_3) + 3\sin(2\theta_4) \\ 0 &= -3\cos(4\theta_1) - \cos(4\theta_2) + \cos(4\theta_3) + 3\cos(4\theta_4) \\ 0 &= -3\sin(4\theta_1) - \sin(4\theta_2) + \sin(4\theta_3) + 3\sin(4\theta_4) \end{aligned} \tag{68}$$

Since rotations of hygrothermally stable laminates will be hygrothermally stable, without loss of generality, the stacking sequence can be rotated by $-0.5(\theta_1+\theta_4)$, and the following substitutions can be made

$$\begin{aligned} \beta_1 &= 0.5(\theta_1 - \theta_4) \\ \beta_2 &= \theta_2 - 0.5(\theta_1 + \theta_4) \\ \beta_3 &= \theta_3 - 0.5(\theta_1 + \theta_4) \\ \beta_4 &= -0.5(\theta_1 - \theta_4) = -\beta_1 \end{aligned} \tag{69}$$

Then Equation (68) can be simplified to

$$\begin{aligned} 0 &= -\cos(2\beta_2) + \cos(2\beta_3) \\ 0 &= -6\sin(2\beta_1) - \sin(2\beta_2) + \sin(2\beta_3) \\ 0 &= -\cos(4\beta_2) + \cos(4\beta_3) \\ 0 &= -6\sin(4\beta_1) - \sin(4\beta_2) + \sin(4\beta_3) \end{aligned} \tag{70}$$

The first and third equations of Equation (70) yield the relation that $\theta_2 = \theta_3 + k\cdot 180°$ and $\theta_2 = \theta_3 + k\cdot 90°$, where k is any integer, respectively. Since rotations by 180° produce the same fiber orientation angle, substituting $\theta_2 = \theta_3$ into the second and fourth equations of Equation (70), they dictate that $\beta_1 = k\cdot 180°$ and $\beta_1 = k\cdot 90°$, respectively. The resulting laminate, accounting for rigid rotations, is

$$[\theta_1 / \theta_2]_s \tag{71}$$

Therefore, only symmetric four-ply laminates satisfy Condition B.

A nearly identical development can be made for five-ply laminates; the only difference is that the coefficients of ±3 in Equation (68), become coefficients of ±2. This

does not affect the result that only symmetric five-ply laminates can satisfy Condition B, given by

$$\left\lfloor \theta_1 / \theta_2 / \overline{\theta_3} \right\rfloor_s \tag{72}$$

4.2.3 Six-, Seven-, and Eight-ply Laminates

The equations that satisfy Condition B for six-ply laminates expand to

$$\begin{aligned}
0 &= -5\cos(2\theta_1) - 3\cos(2\theta_2) - \cos(2\theta_3) + \cos(2\theta_4) + 3\cos(2\theta_5) + 5\cos(2\theta_6) \\
0 &= -5\sin(2\theta_1) - 3\sin(2\theta_2) - \sin(2\theta_3) + \sin(2\theta_4) + 3\sin(2\theta_5) + 5\sin(2\theta_6) \\
0 &= -5\cos(4\theta_1) - 3\cos(4\theta_2) - \cos(4\theta_3) + \cos(4\theta_4) + 3\cos(4\theta_5) + 5\cos(4\theta_6) \\
0 &= -5\sin(4\theta_1) - 3\sin(4\theta_2) - \sin(4\theta_3) + \sin(4\theta_4) + 3\sin(4\theta_5) + 5\sin(4\theta_6)
\end{aligned} \tag{73}$$

Using trigonometric identities, Equation (73) can be recast as

$$\begin{aligned}
0 &= 5\sin(\theta_6 + \theta_1)\sin(\theta_6 - \theta_1) + 3\sin(\theta_5 + \theta_2)\sin(\theta_5 - \theta_2) + \sin(\theta_4 + \theta_3)\sin(\theta_4 - \theta_3) \\
0 &= 5\cos(\theta_6 + \theta_1)\sin(\theta_6 - \theta_1) + 3\cos(\theta_5 + \theta_2)\sin(\theta_5 - \theta_2) + \cos(\theta_4 + \theta_3)\sin(\theta_4 - \theta_3) \\
0 &= 5\sin 2(\theta_6 + \theta_1)\sin 2(\theta_6 - \theta_1) + 3\sin 2(\theta_5 + \theta_2)\sin 2(\theta_5 - \theta_2) + \sin 2(\theta_4 + \theta_3)\sin 2(\theta_4 - \theta_3) \\
0 &= 5\cos 2(\theta_6 + \theta_1)\sin 2(\theta_6 - \theta_1) + 3\cos 2(\theta_5 + \theta_2)\sin 2(\theta_5 - \theta_2) + \cos 2(\theta_4 + \theta_3)\sin 2(\theta_4 - \theta_3)
\end{aligned} \tag{74}$$

Making the following substitutions

$$\begin{aligned}
\theta_6 + \theta_1 &= \beta_1 \\
\theta_6 - \theta_1 &= \beta_2 \\
\theta_5 + \theta_2 &= \beta_3 \\
\theta_5 - \theta_2 &= \beta_4 \\
\theta_4 + \theta_3 &= \beta_5 \\
\theta_4 - \theta_3 &= \beta_6
\end{aligned} \tag{75}$$

into Equation (74) yields

$$\begin{aligned} 0 &= 5\sin\beta_1 \sin\beta_2 + 3\sin\beta_3 \sin\beta_4 + \sin\beta_5 \sin\beta_6 \\ 0 &= 5\cos\beta_1 \sin\beta_2 + 3\cos\beta_3 \sin\beta_4 + \cos\beta_5 \sin\beta_6 \\ 0 &= 5\sin 2\beta_1 \sin 2\beta_2 + 3\sin 2\beta_3 \sin 2\beta_4 + \sin 2\beta_5 \sin 2\beta_6 \\ 0 &= 5\cos 2\beta_1 \sin 2\beta_2 + 3\cos 2\beta_3 \sin 2\beta_4 + \cos 2\beta_5 \sin 2\beta_6 \end{aligned} \tag{76}$$

An exhaustive survey of hygrothermally stable six-ply laminates reveals that any one of the following constitute a subset of hygrothermally stable stacking sequences which can satisfy Condition B:

$$\beta_1 + k_1 \cdot 180^\circ = \beta_3 + k_2 \cdot 180^\circ = \beta_5 + k_3 \cdot 180^\circ \tag{77}$$

where k_i is any integer. Physically, stacking sequences represented in Equation (77) are rigid rotations of antisymmetric stacking sequences. Noting that rotations of 180° do not change the fiber orientation angle, Equation (76) reduces to

$$\begin{aligned} 0 &= \sin\beta_1\left(5\sin\beta_2 + 3\sin\beta_4 + \sin\beta_6\right) \\ 0 &= \cos\beta_1\left(5\sin\beta_2 + 3\sin\beta_4 + \sin\beta_6\right) \\ 0 &= \sin 2\beta_1\left(5\sin 2\beta_2 + 3\sin 2\beta_4 + \sin 2\beta_6\right) \\ 0 &= \cos 2\beta_1\left(5\sin 2\beta_2 + 3\sin 2\beta_4 + \sin 2\beta_6\right) \end{aligned} \tag{78}$$

Since there is no angle for which $\sin\beta_1 = \cos\beta_1 = 0$, Equation (78) reduces to

$$\begin{aligned} 0 &= 5\sin\beta_2 + 3\sin\beta_4 + \sin\beta_6 \\ 0 &= 5\sin 2\beta_2 + 3\sin 2\beta_4 + \sin 2\beta_6 \end{aligned} \tag{79}$$

The Pythagorean Theorem can be used to eliminate β_6 from both Equations (77) and (78), resulting in

$$4(5\sin\beta_2 + 3\sin\beta_4)^2 - 4(5\sin\beta_2 + 3\sin\beta_4)^4 = (5\sin 2\beta_2 + 3\sin 2\beta_4)^2 \tag{80}$$

for Condition B. A contour plot of Equation (80) is given in Figure 2. β_1 is valid on the range from -180° to 180° and will yield β_3 and β_5 once chosen. Note that β_4 is only valid on the range from approximately $|\beta_4|<60°$ or $|\beta_4|>120°$. After Equation (80) is solved for β_2, either equation from Equation (79) can be used to find β_6. Finally, the entire stacking

sequence can be recovered using Equation (75). No hygrothermally stable whole-angle antisymmetric stacking sequences were found, but all symmetric stacking sequences satisfy Condition B. An example of a solution with θ=30° is provided in Table 3; recall that families defined according to Equation (77) have antisymmetric stacking sequences.

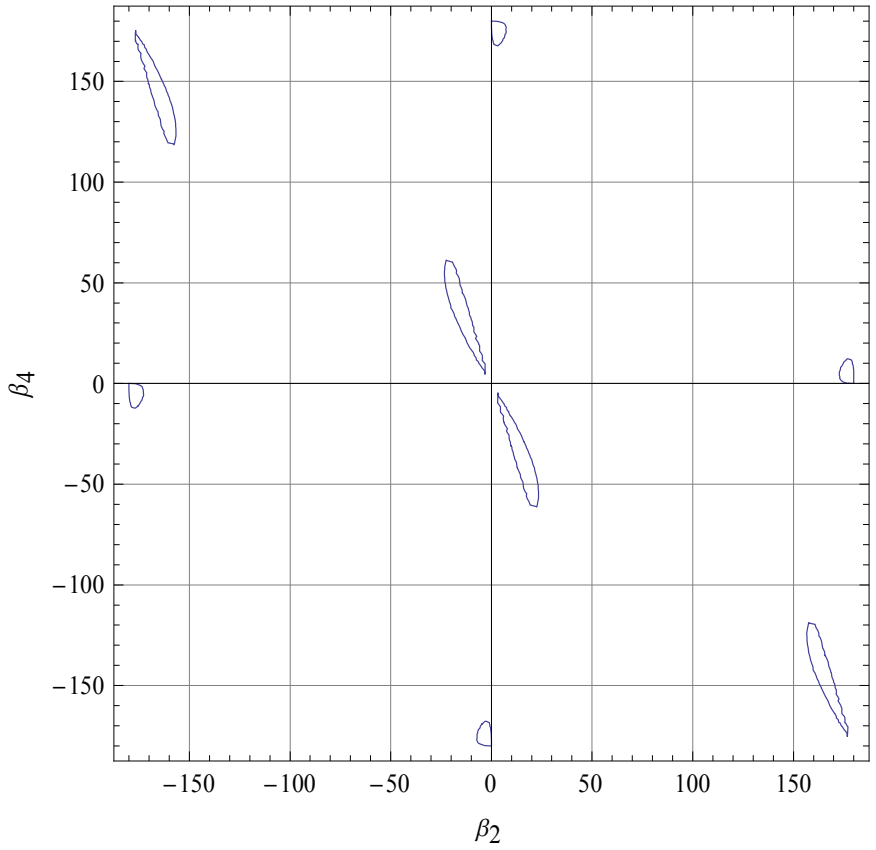

Figure 2. Locus of Six-ply Stable Antisymmetric Solutions Meeting Condition B

Using the same methods that reduced Equation (73) to Equation (80) for six-ply laminates, seven- and eight-ply laminates were reduced and evaluated to identify as many whole-angle stacking sequences as possible. An exhaustive survey returned one seven-

ply and one eight-ply asymmetric family that satisfy Condition B. They are identical to the ones discovered by Weaver[4] and are included in Table 3.

Table 3. Asymmetric Six-, Seven-, and Eight-ply Laminates, Hygrothermally Stable through Condition B

Number of Plies	Stacking Sequences
6	[6.2° / -20.1° / 30° / -30° / 20.1° / -6.2°]
7	$[\theta_1 / \theta_2 / \theta_2 / \theta_3 / \theta_1 / \theta_1 / \theta_2]$
8	$[\theta_1 / \theta_2 / \theta_2 / \theta_1 / \theta_2 / \theta_1 / \theta_1 / \theta_2]$

4.2.4 Laminates with More than Eight Plies

An analysis similar to that performed by Weaver was conducted to identify asymmetric laminates that meet Condition B. For an *n*-ply laminate, the equations that ensure hygrothermal stability expand to be

$$\begin{aligned}
0 &= (-n+1)\cos(2\theta_1) + (-n+3)\cos(2\theta_2) + \ldots + (n-3)\cos(2\theta_{n-1}) + (n-1)\cos(2\theta_n) \\
0 &= (-n+1)\sin(2\theta_1) + (-n+3)\sin(2\theta_2) + \ldots + (n-3)\sin(2\theta_{n-1}) + (n-1)\sin(2\theta_n) \\
0 &= (-n+1)\cos(4\theta_1) + (-n+3)\cos(4\theta_2) + \ldots + (n-3)\cos(4\theta_{n-1}) + (n-1)\cos(4\theta_n) \\
0 &= (-n+1)\sin(4\theta_1) + (-n+3)\sin(4\theta_2) + \ldots + (n-3)\sin(4\theta_{n-1}) + (n-1)\sin(4\theta_n)
\end{aligned} \tag{81}$$

By combining like coefficients, a pattern arises such that

$$\begin{aligned}
0 &= (n-1)\left[\cos(2\theta_n) - \cos(2\theta_1)\right] + (n-3)\left[\cos(2\theta_{n-1}) - \cos(2\theta_2)\right] + \ldots \\
0 &= (n-1)\left[\sin(2\theta_n) - \sin(2\theta_1)\right] + (n-3)\left[\sin(2\theta_{n-1}) - \sin(2\theta_2)\right] + \ldots \\
0 &= (n-1)\left[\cos(4\theta_n) - \cos(4\theta_1)\right] + (n-3)\left[\cos(4\theta_{n-1}) - \cos(4\theta_2)\right] + \ldots \\
0 &= (n-1)\left[\sin(4\theta_n) - \sin(4\theta_1)\right] + (n-3)\left[\sin(4\theta_{n-1}) - \sin(4\theta_2)\right] + \ldots
\end{aligned} \tag{82}$$

By making the following substitutions

$$\begin{aligned}
\cos(2\theta_n)-\cos(2\theta_1)=\xi_{1,1},\ \cos(2\theta_{n-1})-\cos(2\theta_2)=\xi_{1,2},\ldots\\
\sin(2\theta_n)-\sin(2\theta_1)=\xi_{2,1},\ \sin(2\theta_{n-1})-\sin(2\theta_2)=\xi_{2,2},\ldots\\
\cos(4\theta_n)-\cos(4\theta_1)=\xi_{3,1},\ \cos(4\theta_{n-1})-\cos(4\theta_2)=\xi_{3,2},\ldots\\
\sin(4\theta_n)-\sin(4\theta_1)=\xi_{4,1},\ \sin(4\theta_{n-1})-\sin(4\theta_2)=\xi_{4,2},\ldots
\end{aligned} \tag{83}$$

the conditions reduce to

$$\begin{aligned}
0&=(n-1)\xi_{1,1}+(n-3)\xi_{1,2}+\ldots\\
0&=(n-1)\xi_{2,1}+(n-3)\xi_{2,2}+\ldots\\
0&=(n-1)\xi_{3,1}+(n-3)\xi_{3,2}+\ldots\\
0&=(n-1)\xi_{4,1}+(n-3)\xi_{4,2}+\ldots
\end{aligned} \tag{84}$$

One possible solution is through judicious selection of $\xi_{i,j}$, such that $\xi_{i,j}=\pm\xi_{i,1}$, j=2,3,… This would occur if the laminate was balanced in such a way that any two plies equidistant above and below the midplane have fiber orientation angles of θ_1 and θ_n, but not necessarily respectively. To make $\xi_{i,j}=\xi_{i,1}$, $\{\theta_j,\theta_{n-j+1}\}=\{\theta_1,\theta_n\}$, and to make $\xi_{i,j}=-\xi_{i,1}$, $\{\theta_j,\theta_{n-j+1}\}=\{\theta_n,\theta_1\}$.

Take an eight-ply laminate as an example. Equation (84) becomes

$$\begin{aligned}
0&=7\xi_{1,1}+5\xi_{1,2}+3\xi_{1,3}+\xi_{1,4}\\
0&=7\xi_{2,1}+5\xi_{2,2}+3\xi_{2,3}+\xi_{2,4}\\
0&=7\xi_{3,1}+5\xi_{3,2}+3\xi_{3,3}+\xi_{3,4}\\
0&=7\xi_{4,1}+5\xi_{4,2}+3\xi_{4,3}+\xi_{4,4}
\end{aligned} \tag{85}$$

One way to satisfy these equations is if $\xi_{i,1}=-\xi_{i,2}=-\xi_{i,3}=\xi_{i,4}$. This happens if the stacking sequence is

$$[\theta_1/\theta_n/\theta_n/\theta_1/\theta_n/\theta_1/\theta_1/\theta_n] \tag{86}$$

Weaver has found and presented similar solutions for laminates ranging from seven to 13 plies[4]. By making use of repeating patterns, a general solution for a

hygrothermally stable asymmetric laminate with n>7 plies can be established in terms of ply angles $\{\alpha, \beta, \gamma\}$, given by

$$[(\alpha/\beta_2/\alpha)_x/\left\{\begin{array}{cc} \alpha/\beta_2/\alpha/\beta/\alpha_2/\beta & ,n=8,16,24,... \\ \alpha/\beta_2/\alpha/\bar{\gamma}/\beta/\alpha_2/\beta & ,n=9,17,25,... \\ \alpha/\beta_2/\alpha/0_2/\beta/\alpha_2/\beta & ,n=10,18,26,... \\ \alpha/\beta_2/\alpha/0/\bar{\gamma}/0/\beta/\alpha_2/\beta & ,n=11,19,27,... \\ \alpha/\beta/\alpha/\beta_3/\alpha_3/\beta/\alpha/\beta & ,n=12,20,28,... \\ \alpha/\beta/\alpha/\beta_2/0/\bar{\gamma}/0/\alpha_2/\beta/\alpha/\beta & ,n=13,21,29,... \\ \alpha_2/\beta_4/0_2/\beta_4/\beta_2 & ,n=14,22,30,... \\ \alpha/\beta_2/\alpha_2/\beta_2/\bar{\gamma}/\alpha_2/\beta_2/\alpha_2/\beta & ,n=15,23,31,... \end{array}\right\}/(\beta/\alpha_2/\beta)_x] \quad (87)$$

where x = n/8-1, rounded down to the next lowest integer. With the exception of n=8, these stacking sequences are not necessarily unique, but they do show the existence of solutions for n>8 laminates.

4.3 Sensitivity to Errors in Ply Angle and Verification of Hygrothermal Stability

Since asymmetric hygrothermally stable stacking sequences would not be useful if small errors in ply angle, i.e., due to manufacturing variability, can cause a significant loss of stability, a study was undertaken to compare the sensitivity of a representative antisymmetric laminate to its symmetric counterpart. To model manufacturing errors within a given laminate, the fiber orientation angle of each lamina was varied on a uniform interval of $\theta_k \pm 2°$.

The antisymmetric laminate chosen was

$$[15° / -75° / -45° / 45° / 75° / -15°] \quad (88)$$

and its symmetric counterpart was

$$[15° / -75° / -45° / -45° / -75° / 15°] \quad (89)$$

Using the material properties given in Table 4, a Monte Carlo simulation was performed wherein a set of 10^5 perturbed stacking sequences was created, and the twist curvature due to a unit temperature change was calculated. Figure 3 presents a normalized histogram of the results from both laminates. Since there is almost no discernible difference between the two distributions, the difference in sensitivity between the antisymmetric laminate and its symmetric counterpart is negligible.

The robustness of the asymmetric laminate was further confirmed using finite element models and manufacturing. For the manufacturing verification, both laminates were manufactured from the same material system. Specimens were laid up in a flat aluminum mold and cured in an autoclave with the curing cycle given in Figure 4. After curing and cooling, the specimens were trimmed to dimensions of 31.75cm by 21.6cm (12.5" by 8.5").

To measure the warping in both laminates, three corners were held against a flat surface, and the distance above the surface of the fourth corner was measured, as shown in Figure 5. Figure 6 provides close–up photographs of the raised corner displacement that was measured for both laminates. The displacement, δ, was measured with a Vernier caliper and then normalized by the average side length.

The normalized warping displacements were measured to be 0.055 and 0.049 for the antisymmetric and symmetric specimens, respectively, confirming that the warping displacements for the antisymmetric and symmetric specimens are both small and similar in magnitude. Therefore, the small post-cure deformation of the antisymmetric laminate can be attributed to small geometric imperfections and variations in ply angles as

supported by the sensitivity analysis. The fact that the antisymmetric laminate remained nearly flat after cooling from the maximum cure temperature confirms the hygrothermal stability of the stacking sequence.

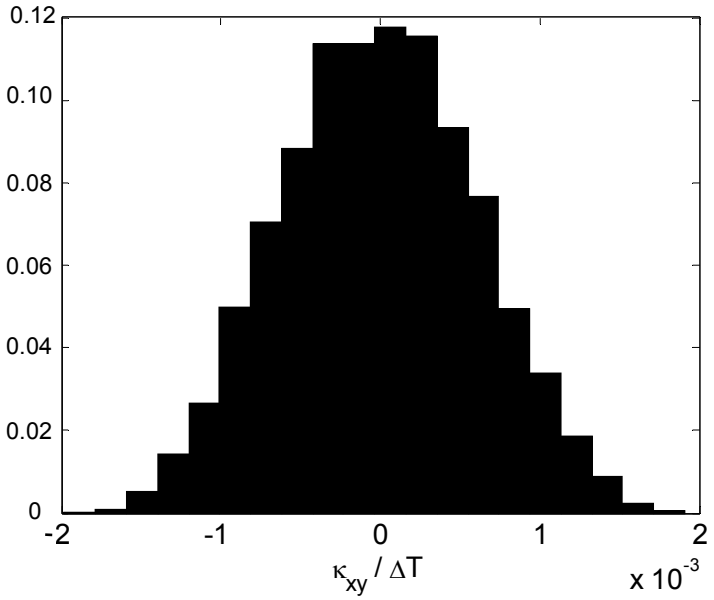

(a)

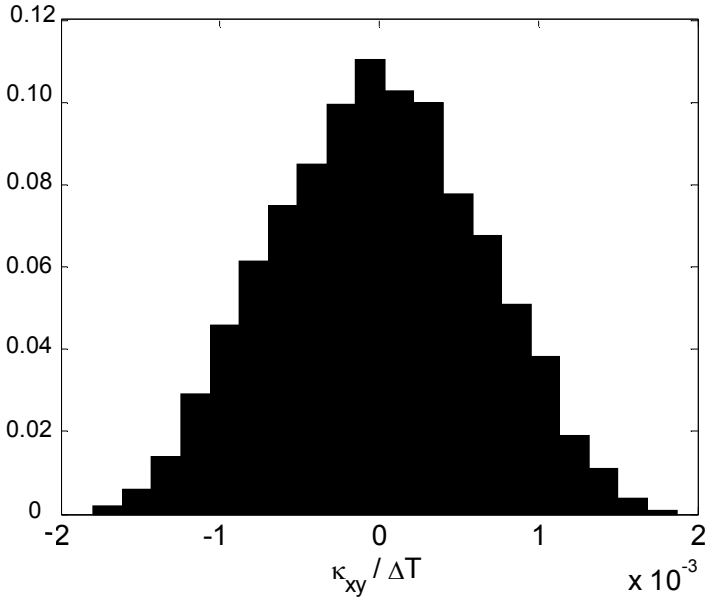

(b)

Figure 3. Normalized histograms of Twisting Curvature Due to Layup Errors in Range ±2º for the (a) Antisymmetric Layup and the (b) Corresponding Symmetric Layup; 10^5 Cases

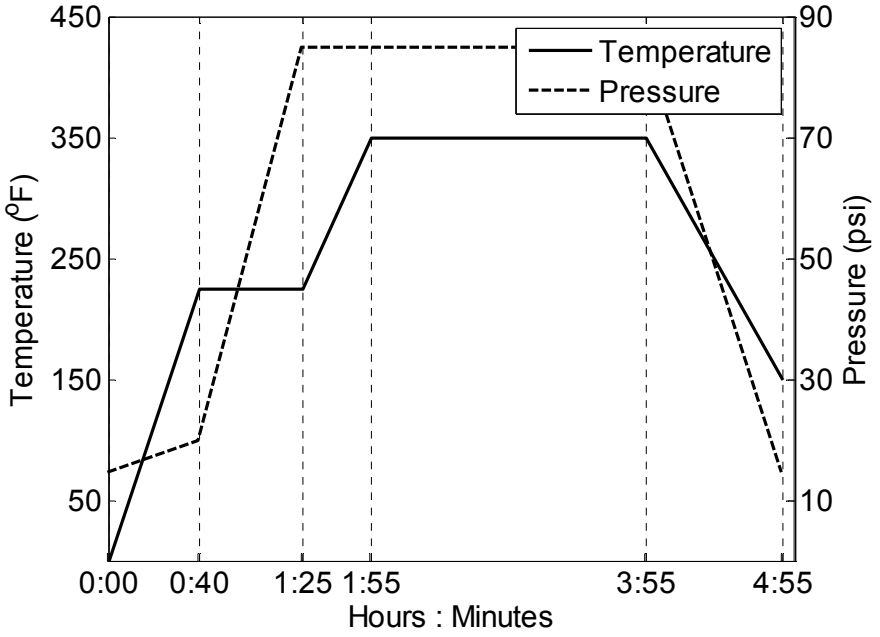

Figure 4. Curing Cycle for Graphite/Epoxy Material System

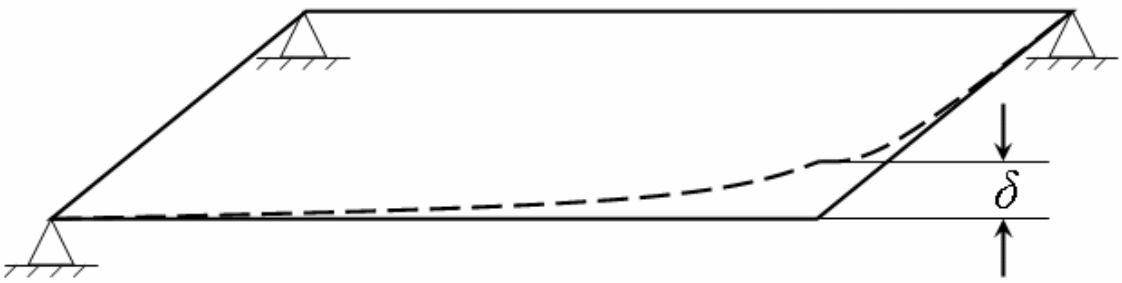

Figure 5. Warping Displacement Measurement Method

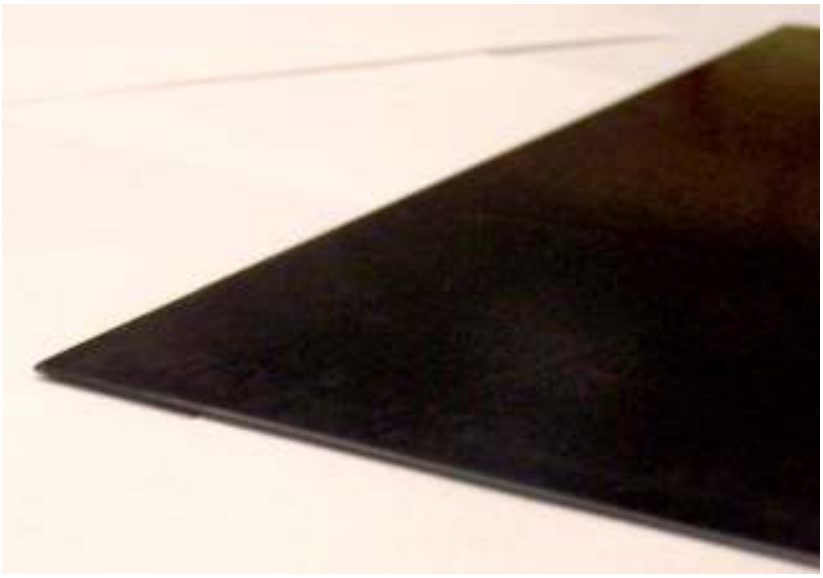

(a)

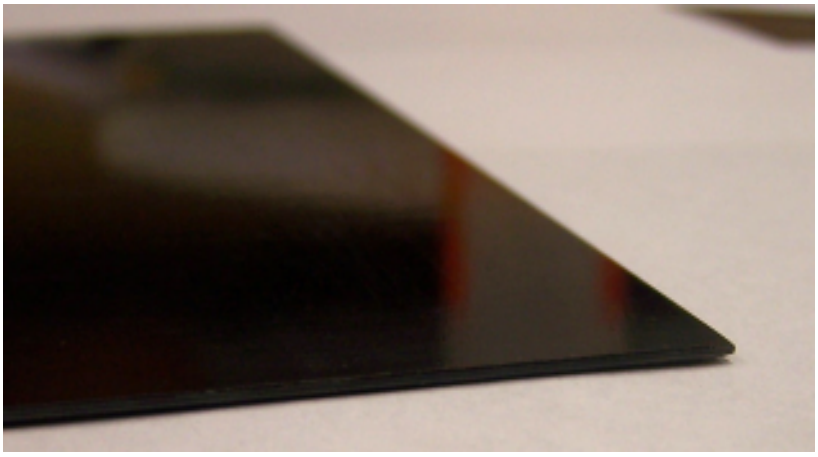

(b)

Figure 6. Detail Photographs of (a) Antisymmetric Specimen and (b) Symmetric Specimen

Finally, a finite element model (FEM) analysis was created from the stacking sequence in Equation (88) using the material properties in Table 4. A square plate model measuring 30cm on a side was constructed in ABAQUS^{TM} consisting of 100 S8R shell elements with a total of 341 nodes and 2046 degrees of freedom. For boundary

conditions, all six degrees of freedom at the center node were constrained. Simulations with imperfections were performed to confirm the stability of the flat post-cured configuration following a similar procedure to that developed by Tawfik *et al*[29].

Table 4. T300/5208 Graphite/Epoxy Pre-impregnated Lamina Elastic Properties

Property	Value
E_{11}	181 GPa
E_{22}	10.2 GPa
G_{12}	7.2 GPa
ν_{12}	0.28
α_1	$-0.1 \cdot 10^{-6}$ °C^{-1}
α_2	$25.6 \cdot 10^{-6}$ °C^{-1}
t	0.10 mm

First, small geometric perturbations consisting of a combination of the first three buckling eigenmodes of the laminated composite plate were superimposed on the model. A uniform temperature change of -150°C was then imposed on the structure. The post-cure deformed shape of the geometrically imperfect specimen appears in Figure 7. The curvature observed in the figure is due mostly to the imposed geometric perturbation, since the maximum post-cure displacement normalized by the side length is found to be $1.7 \cdot 10^{-4}$.

Next, random errors in the range of ±2° were added to each ply angle in the FEM model. A temperature change of -150°C was imposed on the model, giving the post-cure deformed shape, due to the small random ply angle errors, appearing in Figure 8. The displacements have been scaled up by a factor of five to visibly show the deformed shape. The post-cure warping is indeed small with a maximum post-cure displacement, normalized by the side length, of $4.0 \cdot 10^{-3}$. As with the geometric imperfection model, the

post-cure configuration is very close to flat, indicating that the predicted flat post-cure configuration is stable.

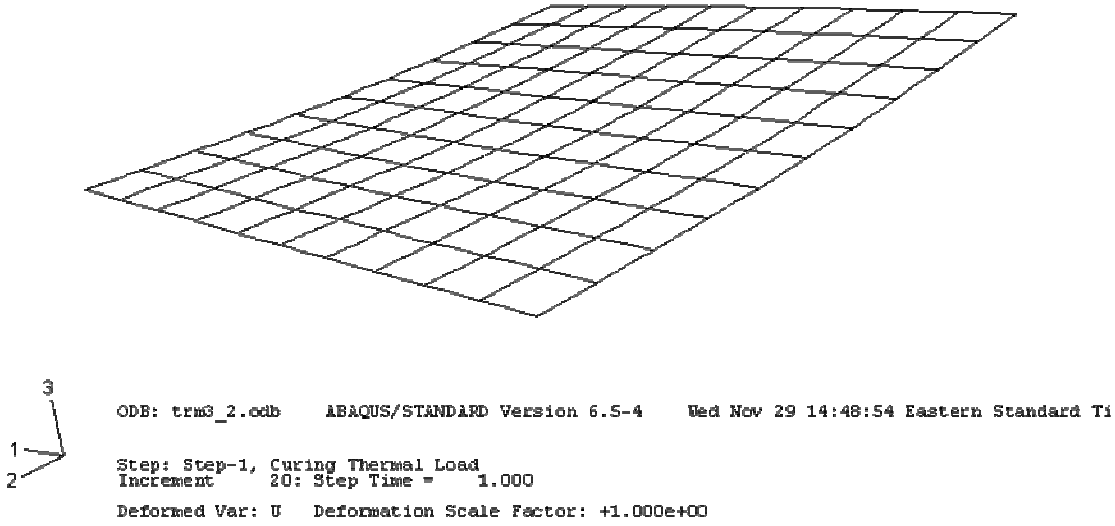

Figure 7. Post-cure Deformed Shape of Geometrically Imperfect Model

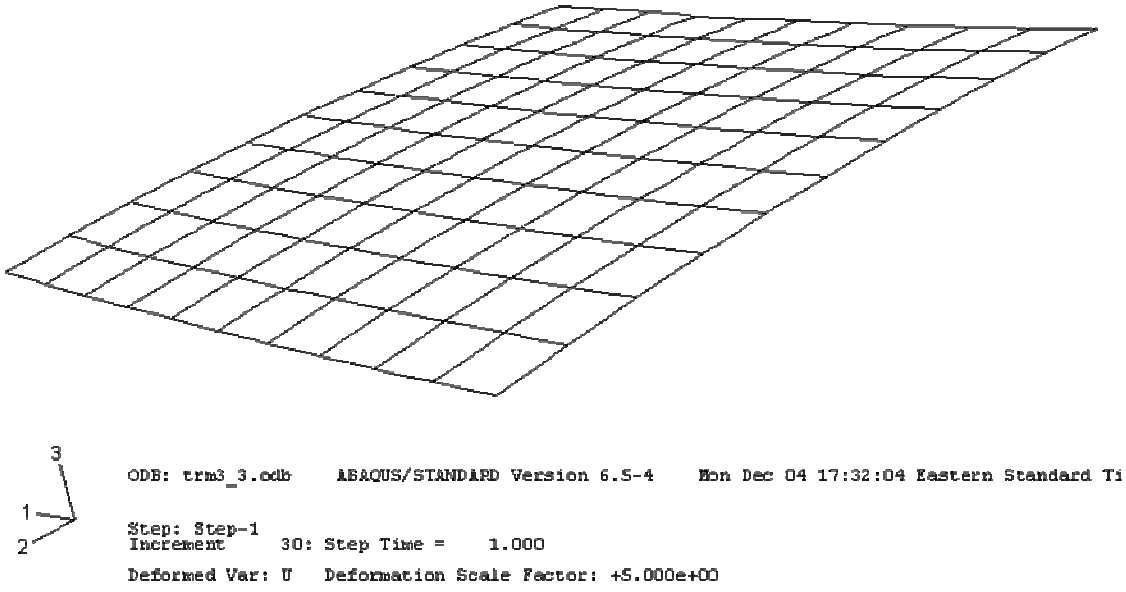

Figure 8. Post-cure Deformed Shape Due to Error in Ply Angles (Deformations Scaled by a Factor of 5)

CHAPTER 5

EXTENSION-TWIST COUPLING OF HYGROTHERMALLY STABLE LAMINATES

Extension-twist coupling is a structural phenomenon whereby an axial in-plane load induces a change in the twisting curvature of the structure. The potential for anisotropy makes it possible for flat composite laminates under axial loading to generate a non-zero twisting curvature. Physically, extension-twist coupling results from off-axis plies positioned some non-zero distance from the midplane subject to axial stress that causes shearing strains. Since these plies are constrained by bonding to the plies above and below them, shearing forces are induced. The shearing force acting through the moment arm, i.e., the distance from the midplane, causes a moment about the laminate axis, therefore, inducing a twist. For this reason, extension-twist coupling is not achievable with a symmetric stacking sequence, and many asymmetric stacking sequences warp out-of-plane with changes in temperature or moisture, i.e., cooling after curing.

In this section, extension-twist coupling is quantified; then, a constrained optimization is performed to identify the hygrothermally stable stacking sequence with the most coupling for a laminate with a set number of plies. Comparisons are made with unconstrained and intuitive optimal solutions. Confirmation of the desired level of coupling is made through manufacture and testing, nonlinear models, and FEM analysis. A study of the robustness of the optimized stacking sequences is also performed.

5.1 Optimality Parameter

Extension-twist coupling is quantified by expressing the twist rate as a function of applied nominal axial stress. Since the objective function must be evaluated repeatedly for each optimization, the twist rate is calculated using CLT rather than a more computationally expensive method. Moreover, since the optimizer searches within curvature-stable stacking sequences, the assumption that the laminate is initially flat is valid. Previous work[30,31] indicates that the axial force-twist relationship of an extension-twist coupled composite is well approximated by keeping the nonlinear term associated with the trapeze effect. Defining the coupling magnitude as the slope of the axial force-twist curve at small twist angles makes the CLT approximation acceptable.

Solving Equation (2), the midplane strains and curvatures may be calculated as

$$\begin{Bmatrix} \varepsilon_{xx} \\ \varepsilon_{yy} \\ \gamma_{xy} \\ \hdashline \kappa_{xx} \\ \kappa_{yy} \\ \kappa_{xy} \end{Bmatrix} = \left[\begin{array}{ccc:ccc} \alpha_{11} & \alpha_{12} & \alpha_{16} & \beta_{11} & \beta_{12} & \beta_{16} \\ \alpha_{12} & \alpha_{22} & \alpha_{26} & \beta_{21} & \beta_{22} & \beta_{26} \\ \alpha_{16} & \alpha_{26} & \alpha_{66} & \beta_{61} & \beta_{62} & \beta_{66} \\ \hdashline \beta_{11} & \beta_{21} & \beta_{61} & \delta_{11} & \delta_{12} & \delta_{16} \\ \beta_{12} & \beta_{22} & \beta_{62} & \delta_{12} & \delta_{22} & \delta_{26} \\ \beta_{16} & \beta_{26} & \beta_{66} & \delta_{16} & \delta_{26} & \delta_{66} \end{array}\right] \begin{Bmatrix} N_{xx} \\ N_{yy} \\ N_{xy} \\ \hdashline M_{xx} \\ M_{yy} \\ M_{xy} \end{Bmatrix} + \begin{Bmatrix} \varepsilon_{xx} \\ \varepsilon_{yy} \\ \gamma_{xy} \\ \hdashline \kappa_{xx} \\ \kappa_{yy} \\ \kappa_{xy} \end{Bmatrix}^{(T,H)} \tag{90}$$

where the non-mechanical deformations are calculated as

$$\begin{Bmatrix} \varepsilon_{xx} \\ \varepsilon_{yy} \\ \gamma_{xy} \\ \hdashline \kappa_{xx} \\ \kappa_{yy} \\ \kappa_{xy} \end{Bmatrix}^{(T,H)} = \left[\begin{array}{ccc:ccc} \alpha_{11} & \alpha_{12} & \alpha_{16} & \beta_{11} & \beta_{12} & \beta_{16} \\ \alpha_{12} & \alpha_{22} & \alpha_{26} & \beta_{21} & \beta_{22} & \beta_{26} \\ \alpha_{16} & \alpha_{26} & \alpha_{66} & \beta_{61} & \beta_{62} & \beta_{66} \\ \hdashline \beta_{11} & \beta_{21} & \beta_{61} & \delta_{11} & \delta_{12} & \delta_{16} \\ \beta_{12} & \beta_{22} & \beta_{62} & \delta_{12} & \delta_{22} & \delta_{26} \\ \beta_{16} & \beta_{26} & \beta_{66} & \delta_{16} & \delta_{26} & \delta_{66} \end{array}\right] \begin{Bmatrix} N_{xx} \\ N_{yy} \\ N_{xy} \\ \hdashline M_{xx} \\ M_{yy} \\ M_{xy} \end{Bmatrix}^{(T,H)} \tag{91}$$

The twist rate in a laminated composite strip, φ, due to a nominal axial stress, σ_0, alone may then be calculated as

$$\varphi = \frac{1}{2}\left(nt\beta_{16}\sigma_0 + \kappa_{xy}^{(T,H)}\right) \tag{92}$$

where n and t denote the number of plies and ply thickness, respectively.

Since the optimizer searches stable laminates, the non-mechanical curvature in Equation (92) is zero, suggesting the objective function to be minimized as

$$g\left(\left\{\theta_k : k = 1\ldots n\right\}\right) = -\beta_{16}^2 \tag{93}$$

5.2 Implementation

The sequential quadratic programming (SQP)[32] implementation in MATLAB 7™ was used to perform the stacking sequence optimization numerically. The equations satisfying Condition A as given in Table 1 are used to enforce hygrothermal stability, since Condition B would preclude any extension-twist coupling. The optimizer is initialized with a stacking sequence sampled from a uniform random number generator.

Early optimization runs revealed the existence of numerous suboptimal local minima satisfying the stability requirements. To find a global optimum, many optimization runs were performed starting from different random initializations. The solution yielding the highest coupling from all optimizations is taken to be the true solution. The computational efficiency of the gradient-based SQP implementation enables this repeated run approach to find the global solution in a reasonable amount of time. As implemented, an optimization run requires about 5 seconds on an Intel Pentium IV 3.2 GHz processor. Several hundred optimization runs were required to reach the global optimum.

Although the hygrothermal stability conditions are material independent, extension-twist coupling is not. Therefore, a material system is needed to complete the

numerical optimization. Since the results will be verified through manufacture and testing, the properties of a T300/976 graphite/epoxy material system that was available were used. The elastic properties of this material system were characterized in accordance with ASTM standards[33,34] and are provided in Table 5. Also included in Table 5 is the range of error from the average of the measured values for each property. All measured values were within 10% of the average.

Table 5. Elastic Properties of T300/976, First Material Characterization

Property	Value	Range
E_{xx}	125 GPa	(-1% , 1%)
E_{yy}	8.45 GPa	(-5% , 5%)
G_{xy}	4.3 GPa	(-6% , 1%)
ν_{xy}	0.328	(-2% , 1%)
t	0.152 mm	(-8% , 10%)

It should be emphasized that this optimization routine does not guarantee global convergence. Much effort was put forth to maximize confidence in the global optima of the solutions, namely through the use of many random initializations. Still, there is room for improvement in rigorously establishing the optimality of the stacking sequences established herein. Suggestions for improving the confidence in reaching a global solution are provided in Chapter 9.

5.3 Results

Optimizations were performed for laminates with five through ten plies. A Winckler-type laminate was also optimized for comparison with the previously-known optimum. The optimized stacking sequences are provided in Table 6 with ply angles

rounded to a tenth of a degree. A normalized performance parameter, η, is included for comparison between laminates with different numbers of plies, defined as

$$\eta = ntE_{xx}\beta_{16} = \frac{2\varphi E_{xx}}{\sigma_{xx}} \approx \frac{2\varphi}{\varepsilon_{xx}} \tag{94}$$

Table 6. Extension-twist Optimized Stacking Sequences for T300/976

n	Stacking Sequence (°)	η (m^{-1})	% Increase in Coupling over Winckler
5-ply	[-58.7/11.4/45/78.6/-31.3]	19767	65.2%
6-ply	[21.2/-63.8/-48.7/48.7/63.8/-21.2]	21678	81.1%
7-ply	[14.1 -76.9 -73.9 45 -16.1 -13.2 75.7]	16003	33.7%
8-ply	[-21.5/72.1/57.9/-29.6/29.6/-57.9/-72.1/21.5]	14216	18.8%
9-ply	[25.5/-79/32.5/-62.9/49.9/27.4/57/-10.6/64.9]	14102	17.8%
10-ply	[16.2/-69.0/-65.3/31.8/42.1/-42.1/-31.8/65.3/69.0/-16.2]	14001	17.0%
Winckler	$[22.5/-67.5_2/22.5/-22.5/67.5_2/-22.5]$	11969	N/A

Several results are worth noting. First, the optimal stacking sequence for laminates with an even number of plies is antisymmetric, and for laminates with an odd number of plies, the optimal stacking sequence is a rotation of an antisymmetric layup by approximately 45°. Second, all optimal stacking sequences outperform the Winckler-type laminate. The percent increase is provided in Table 6. This result is expected since Winckler-type laminates comprise a subset of hygrothermally stable eight-ply laminates and have never been shown to be optimal. Third, in general an increase in the number of plies is accompanied by a decrease in the coupling. This result can be explained by noting that the axial and torsional stiffness of these laminates increases with increasing thickness.

5.3.1 Other Constraints

For comparison, the optimization procedure was applied to extension twist coupling with no constraint on hygrothermal stability and constraint to angle-ply laminates that were considered to be an intuitive solution as mentioned previously. The results of the unconstrained optimization are provided in Table 7, and the results of the angle-ply constrained optimization are provided in Table 8.

Table 7. Globally Optimal Extension-twist Coupled Stacking Sequences

n	Unconstrained (°)	η (m^{-1})
2	[±24.7]	52381
3	[-30.1 / 90.0 / 30.1]	60185
4	[28.5 / -89.5 / 89.5 / -28.5]	50208
5	[-27.7 / 90.0 / -90.0 / -90.0 / 27.7]	41075
6	[-26.1 / -38.6 / 88.6 / -88.6 / 38.6 / 26.1]	34544
7	[-25.8 / -35.4 / 89.7 / 90 / -89.7 / 35.4 / 25.8]	30180
8	[-25.6 / -33.4 / 89.9 / 89.8 / -89.8 / -89.9 / 33.4 / 25.6]	26548
9	[24.8 / 31.3 / 42.0 / -89.2 / 90 / 89.2 / -42.0 / -31.3 / -24.8]	23696
10	[24.7 / 30.4 / 39.0 / -89.5 / -89.2 / 89.2 / 89.5 / -39.0 / 30.4 / -24.7]	21462

Table 8. Optimal Angle-ply Stacking Sequences and Comparison with Global Optima

n	Angle Ply (°)	η (m^{-1})	%Loss in Coupling between Global Optima and Angle-ply Optima	%Loss in Coupling between the Global Optima and Hygrothermally Stable Optima
2	[+/-24.7]	52381	0.0%	N/A
3	[-30.1 / 90 / 30.1]	60185	0.0%	N/A
4	$[+/-(24.7_2)]$	26191	47.8%	N/A
5	$[30.9_2 / 90.0 / -30.9_2]$	30907	24.8%	51.9%
6	$[+/-(24.7_3)]$	17460	49.5%	37.2%
7	$[30.6_3 / 90.0 / -30.6_3]$	20192	33.1%	47.0%
8	$[+/-(24.7_4)]$	13095	50.7%	46.5%
9	$[30.1_4 / 90.0 / -30.1_4]$	14844	37.4%	40.5%
10	$[+/-(24.7_5)]$	10476	51.2%	34.8%

Also included in Table 8 is the percent reduction in coupling associated with constraining to either angle ply or hygrothermal stability. Note that with odd-ply laminates, angle-ply layups offer performance closer to the global optima than the hygrothermally stable layups, but with even-ply laminates hygrothermally stable layups offer performance closer to the global optima than angle-ply layups. This suggests that odd-ply laminates are suboptimal choices for achieving extension-twist coupling with hygrothermal stability.

The same optimization with constraint to hygrothermal stability was performed again, except with constant total laminate thickness. This was done to attempt to remove the effects of thickness increase on laminates with an increasing number of plies. The stacking sequence results are identical to those in Table 6, but η is different due to t being variable between laminates. Figure 9 plots both results. A curve fit has been drawn through the points so a trend can be inferred. When the laminate is taken with a constant total ply thickness, a nearly linear trend can be seen. The six-ply laminate is the only noticeable deviation from this trend.

It is worth mentioning that in all cases the hygrothermally stable optimal laminates have significantly less coupling than the global optima, which means that the constraints must be active in preventing the hygrothermally stable solution from approaching the global optima.

5.3.2 Varying Material Properties

A computational study was performed to compare the effect of varying material properties. The same optimization was performed, but on three different material

systems and only for six-, eight-, ten-ply, and Winckler-type laminates. The material systems chosen were T300/976 graphite/epoxy, Kevlar49/CE3305 aramid/epoxy, and S2/SP250 glass/epoxy. The elastic properties of each are provided in Table 9 as taken from Cross *et al*[35].

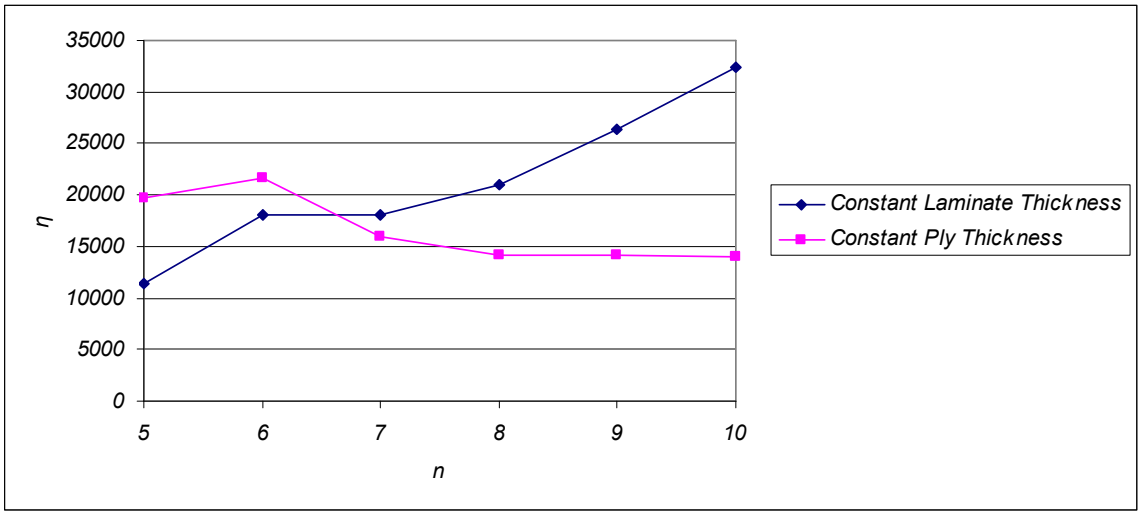

Figure 9. Comparison of η for Optimal Hygrothermally Stable Stacking Sequences

Table 9. Elastic Properties of Material Systems

Material	E_{11} (GPa)	E_{22} (GPa)	G_{12} (GPa)	ν_{12}	t (mm)
T300/976	123.7	9.73	6.3	0.322	0.1
Kev49/CE3305	82.0	4.0	2.8	0.25	0.1
S2/SP250	50.0	14.5	6.1	0.275	0.1

Each laminate was optimized for each material system. The optimal stacking sequence and η are provided in Table 10. The results show that the material system has very little influence on optimal stacking sequence. For a given laminate, the fiber orientation angle of a given ply varies by less than 3° between material systems. This

suggests that optimal stacking sequences will be robust against material property variation.

Table 10. Extension-twist Optimization Results for Various Materials

Laminate	Material	Optimal Stacking Sequence (°)	η (m^{-1})
6-ply	T300	[21.2/-63.8/-48.7/48.7/63.8/-21.2]	19997.0
	Kev49	[21.6/-62.9/-49.1/49.1/62.9/-21.6]	31906.9
	S2	[20.7/-64.8/-48.2/48.2/64.8/-20.7]	5897.4
8-ply	T300	[21.5/-72.1/-57.9/29.6/-29.6/57.9/72.1/-21.5]	13792.1
	Kev49	[21.7/-71.9/-57.0/30.4/-30.4/57.0/71.9/-21.7]	20911.5
	S2	[21.7/-71.0/-60.9/26.9/-26.9/60.9/71.0/-21.7]	4379.1
10-ply	T300	[16.2/-69.0/-65.3/31.8/42.1/-42.1/ -31.8/65.3/69.0/-16.2]	12705.9
	Kev49	[16.0/-69.2/-65.1/32.0/41.9/-41.9/ -32.0/65.1/69.2/-16.0]	20606.6
	S2	[16.4/-67.8/22.3/-61.2/-53.8/53.8/61.2/ -22.3/67.8/-16.4]	3675.7
Winckler	T300	[22.5/-67.5$_2$/22.5/-22.5/67.5$_2$/-22.5]	12270.9
	Kev49	[22.5/-67.5$_2$/22.5/-22.5/67.5$_2$/-22.5]	17588.4
	S2	[22.5/-67.5$_2$/22.5/-22.5/67.5$_2$/-22.5]	4231.0

Figure 10 and Figure 11 plot the coupling as a function of the ratios of longitudinal modulus to both transverse modulus and shear modulus, respectively, for each of the optimized laminates; the relationship suggests a linear trend for both ratios. Therefore, the ratio between fiber stiffness and matrix stiffness will be important when selecting a material system for creating an extension-twist coupled laminate. This reflects the influence of extension-shear coupling, which is governed by the difference in the stiffness coefficients, Q_{11} and Q_{22}. A greater number of material systems could add data points that help support this trend.

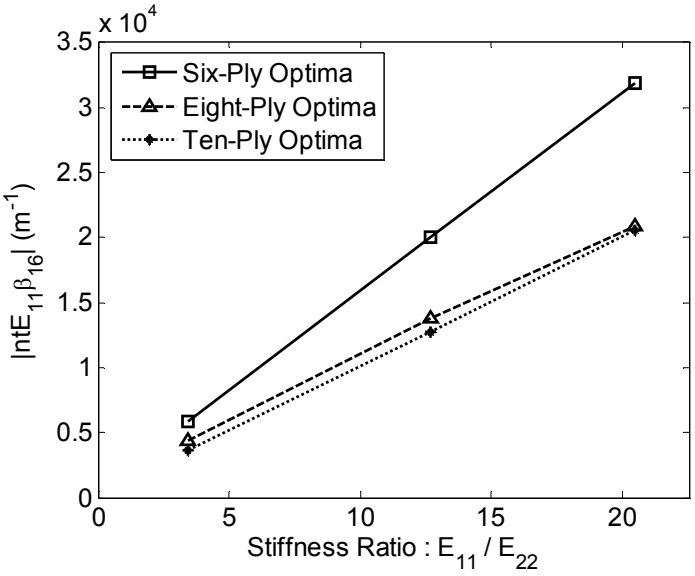

Figure 10. Coupling Strength Dependence on Longitudinal to Transverse Stiffness Ratio

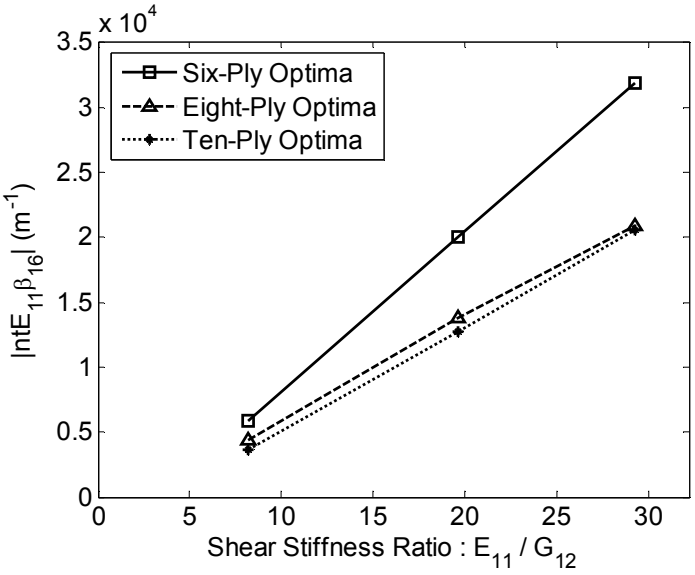

Figure 11. Coupling Strength Dependence on Longitudinal to Shear Stiffness Ratio

5.3.3 Lamination Parameters

Lamination parameters, as provided in Equation (40), were considered for use in the optimization routine since the design space would be a constant 12 variables regardless of the number of plies. However, since the lamination parameters are not independent, solutions returned by the optimizer were not necessarily physically possible, especially for lower numbers of plies.

Although the lamination parameters are not useful for optimization, they do reveal interesting trends between laminates. The non-zero lamination parameters are plotted as a function of the number of plies for the optimal hygrothermally stable laminates in Figure 12. Note that across all n, $\xi_8 \approx -0.4$. Similar plots are provided for the global optima and angle-ply optima in Figure 13 and Figure 14, respectively. Again, for the global optima $\xi_7 \approx \xi_8 \approx 0.4$, and for the angle-ply optima $\xi_7 \approx \xi_8 \approx -0.9$. These lamination parameters are associated with the coupling stiffness matrix and are expected to play an important role in determining the level of extension-twist coupling.

5.4 Validation

To confirm the expected levels of coupling determined by the optimization, manufacture and testing, a nonlinear model and FEM analysis were used. Also, a study of the sensitivity of the optimized laminates to loss of coupling was undertaken to estimate the influence of typical manufacturing errors.

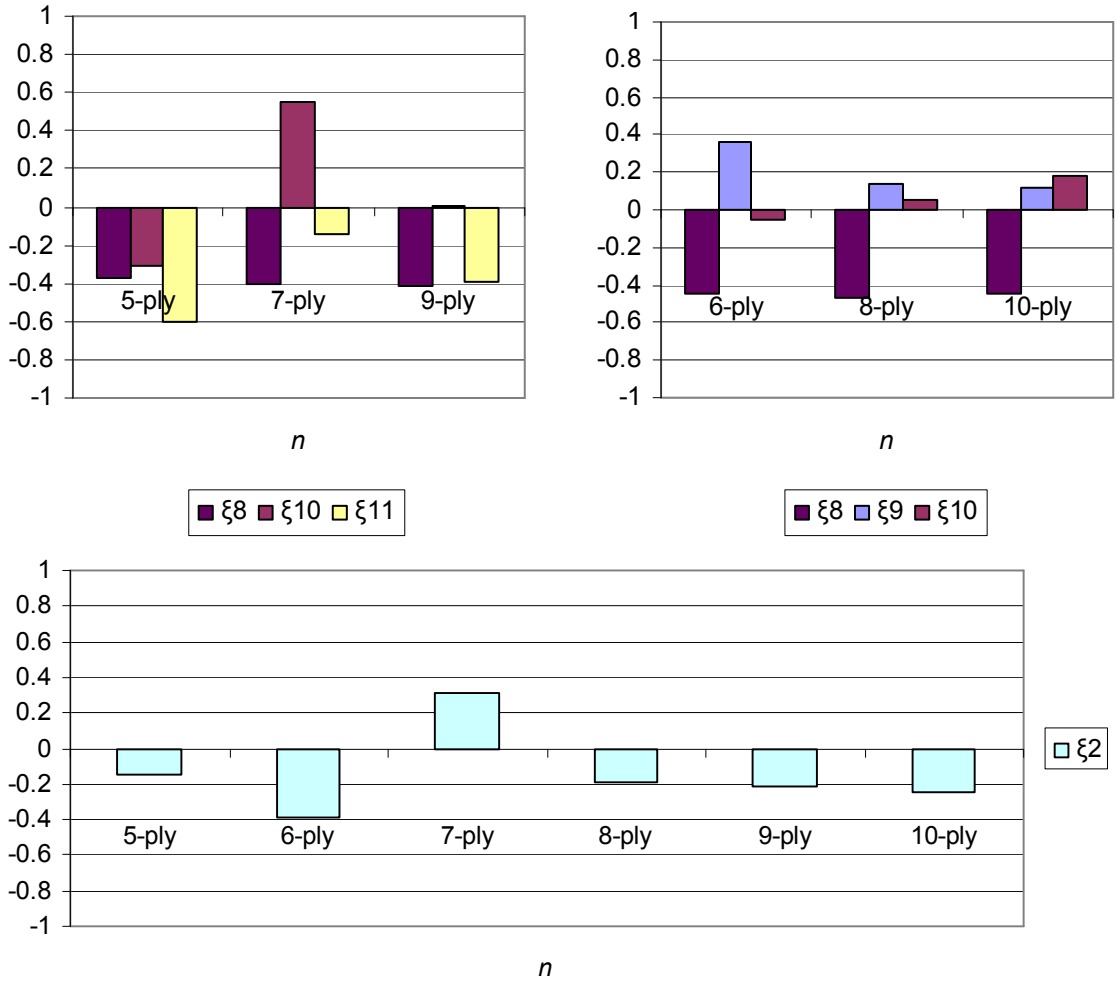

Figure 12. Non-zero Lamination Parameters for Optimal Hygrothermally Stable Laminates

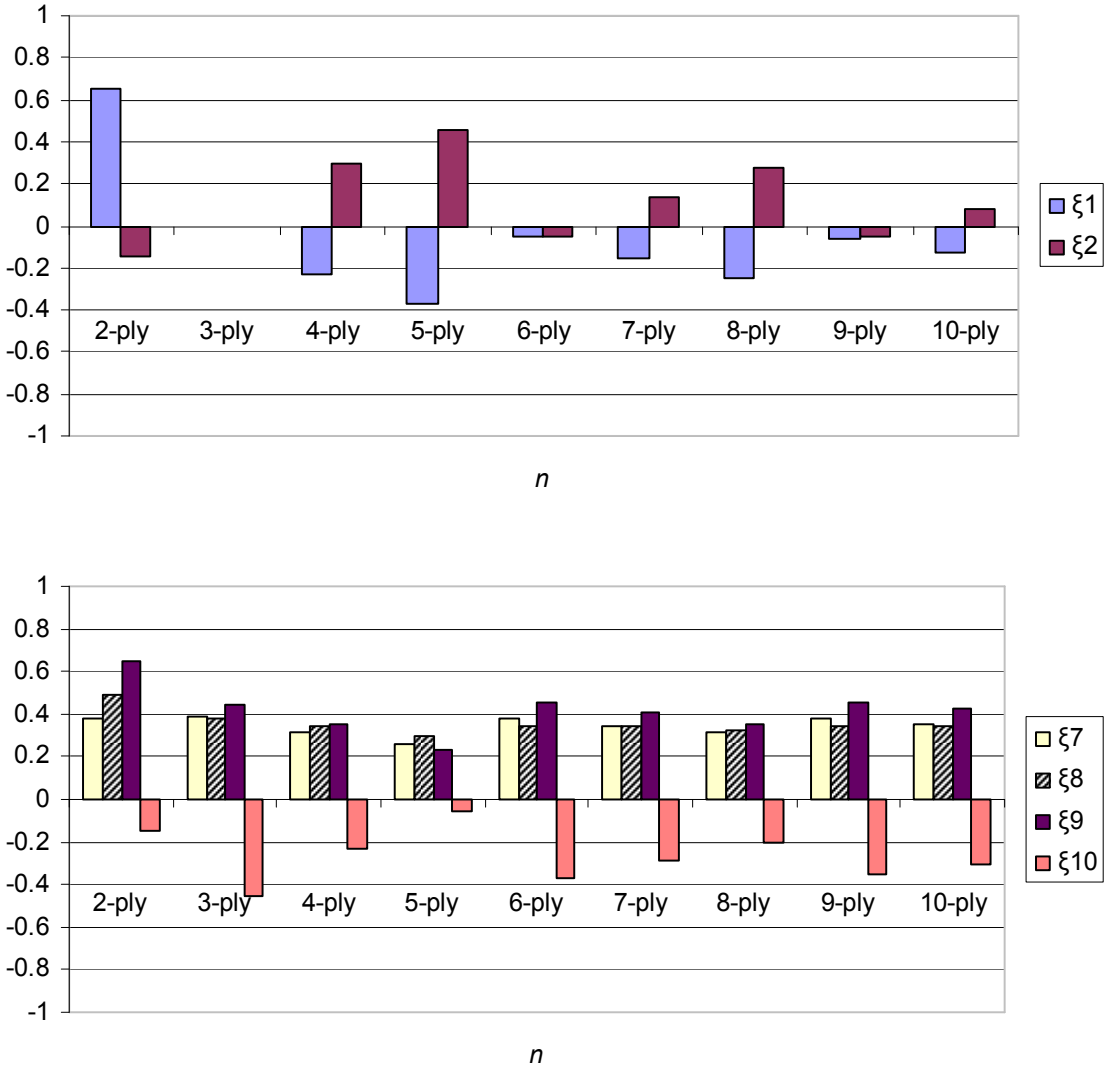

Figure 13. Non-zero Lamination Parameters for Globally Optimal Laminates

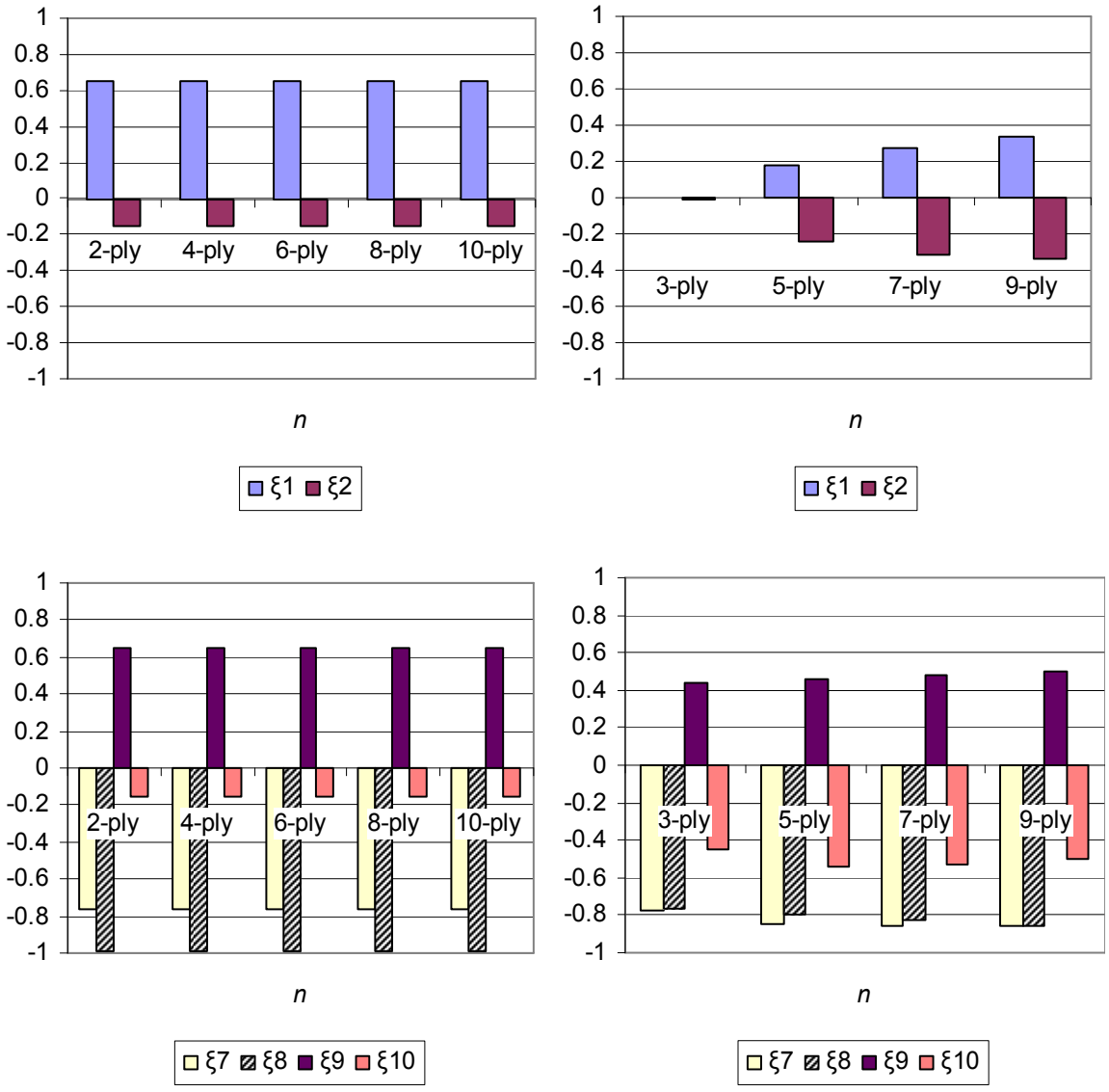

Figure 14. Non-zero Lamination Parameters for Optimal Angle-ply Laminates

5.4.1 Manufacturing and Testing

Laminates were constructed from T300/976 graphite/epoxy with elastic properties given in Table 5. Each ply was cut from a pre-impregnated roll, laid up in a flat aluminum mold, and cured in an autoclave with the curing cycle shown in Figure 4. After curing, each laminate was cut into five specimens of dimensions 2.54cm by 25.4cm (1.0" by 10.0"). Fiberglass tabs of dimensions 2.54cm by 3.81cm (1.0" by 1.5") were attached to both sides and at both ends of each specimen, leaving test sample dimensions of approximately 2.54cm by 17.78cm (1.0" by 7.0").

The specimens were tested in an Instron® 8874 biaxial tension-torsion machine. After inserting each specimen into the machine, the axial load was set to zero using the load control mode. Then the upper grip was rotated manually until the torque in the system read zero to acquire the tip pre-twist of the specimen. The low torsional stiffness of the specimens required the manual rotation of the upper grip using the displacement control mode. Once the tip pre-twist was obtained, the axial load was increased in increments of 445N (100 lb) up to 2224N (500 lb), and for each loading the upper grip was rotated until the torque in the system was zero to acquire the tip rotation angle. This process was repeated for all specimens. Figure 15 shows a specimen undergoing testing. Figure 16 through Figure 22 show all acquired data points for the five- through ten-ply and Winckler-type laminates, respectively. Also included on each plot are the nonlinear model and FEM prediction explained in the next two sections, where available.

Since the laminates are constructed using hygrothermally stable stacking sequences, there should be no curing-induced pre-twist, but the resulting laminate may have a slight initial curvature due to errors in layup during manufacturing and

nonuniform thickness. This was accounted for by measuring the pre-twist as given in the testing procedure detailed previously. In all cases, the pre-twist twist rate in each specimen was small, less than 0.20°/cm (0.5°/in).

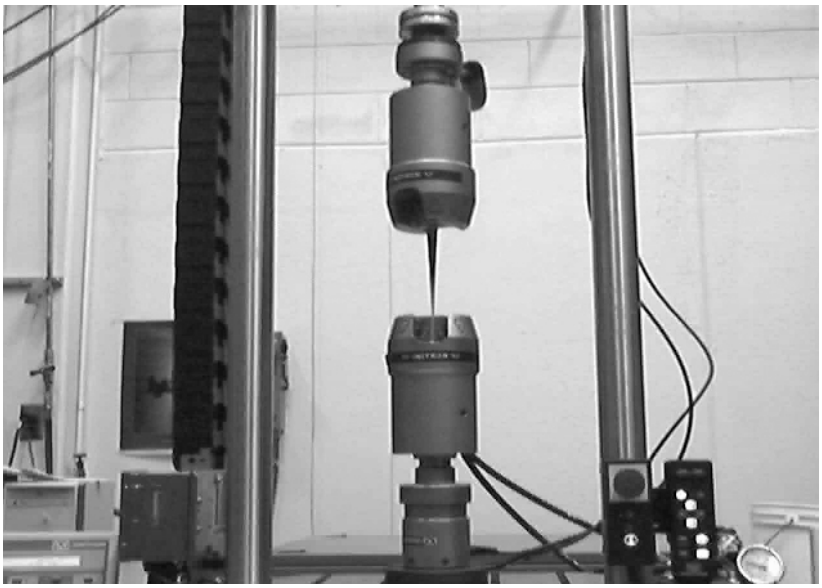

Figure 15. A Specimen Undergoing Testing in an Instron Biaxial Tension-Torsion Machine

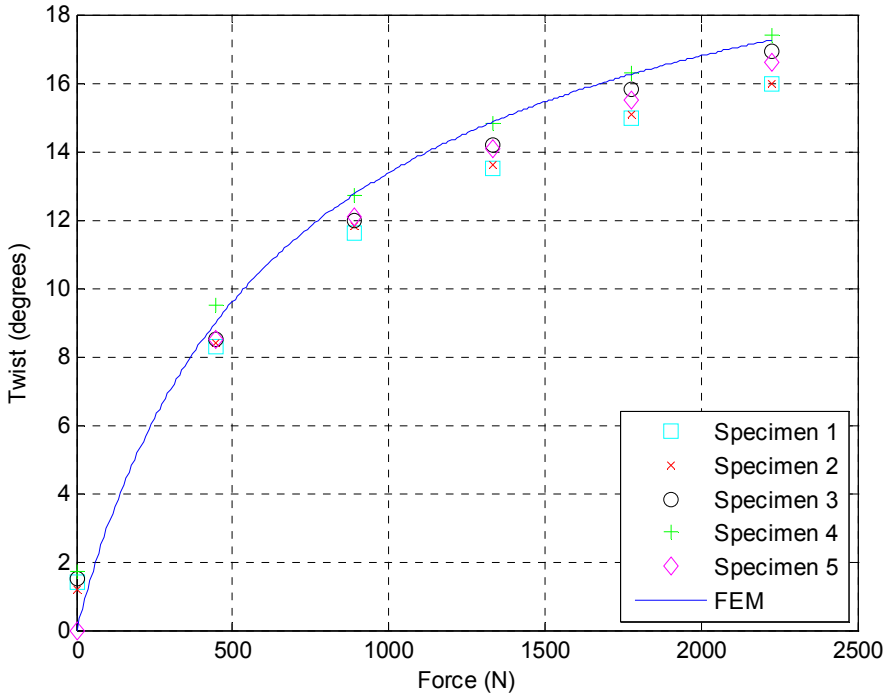

Figure 16. Response of Five-ply Maximum Extension-twist Coupled Laminate

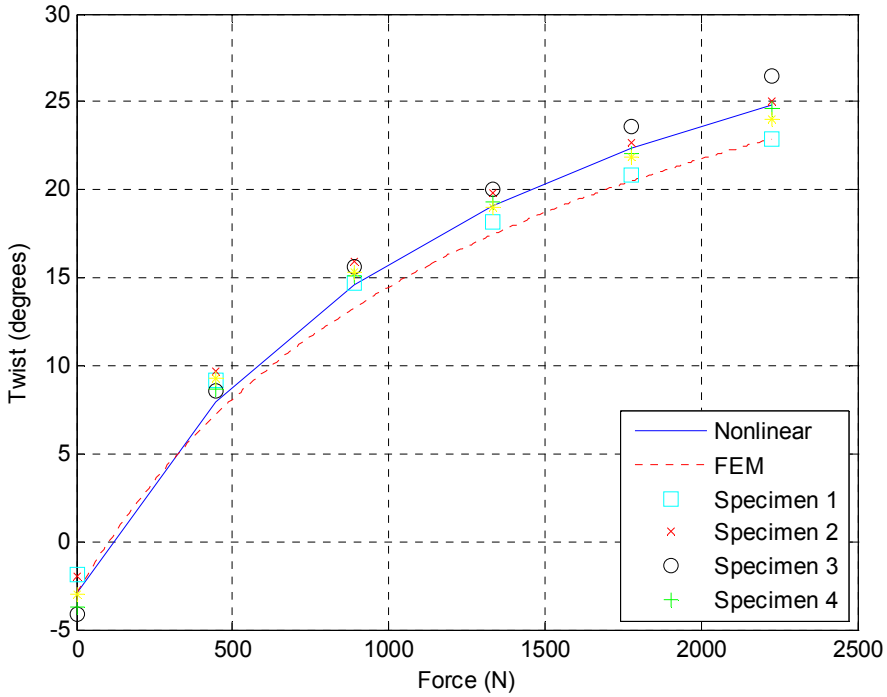

Figure 17. Response of Six-ply Maximum Extension-twist Coupled Laminate

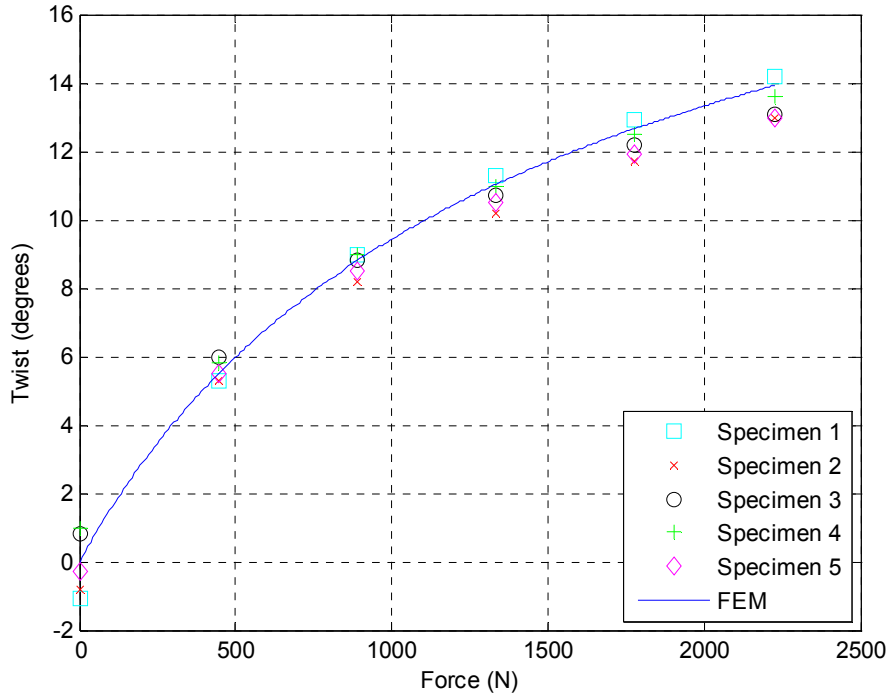

Figure 18. Response of Seven-ply Maximum Extension-twist Coupled Laminate

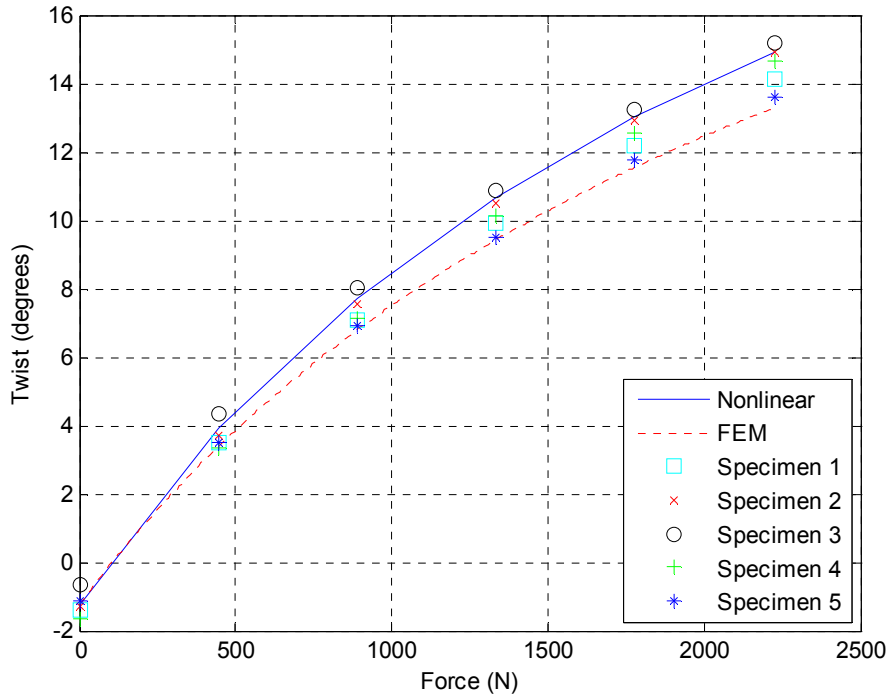

Figure 19. Response of Eight-ply Maximum Extension-twist Coupled Laminate

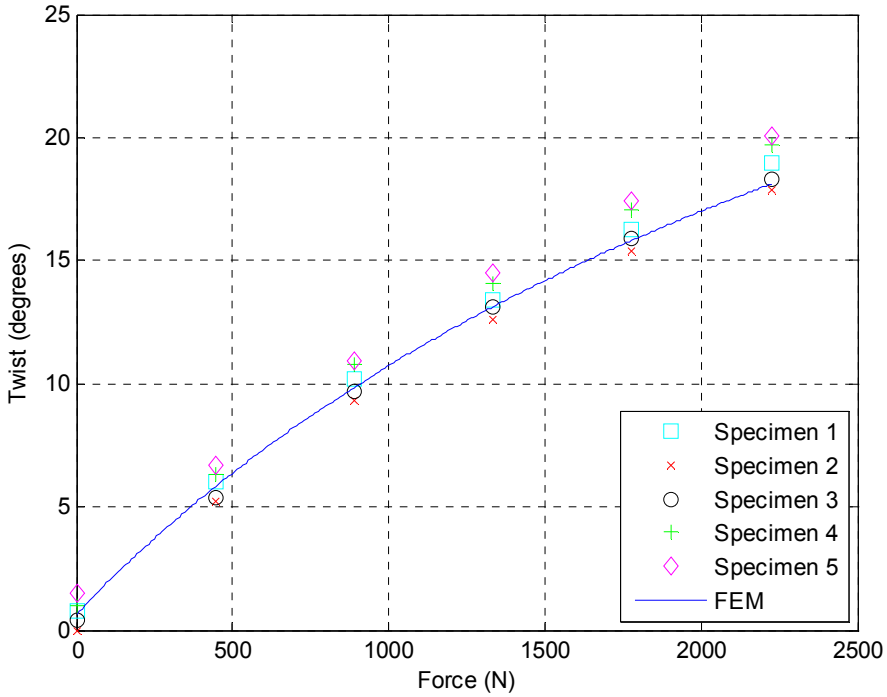

Figure 20. Response of Nine-ply Maximum Extension-twist Coupled Laminate

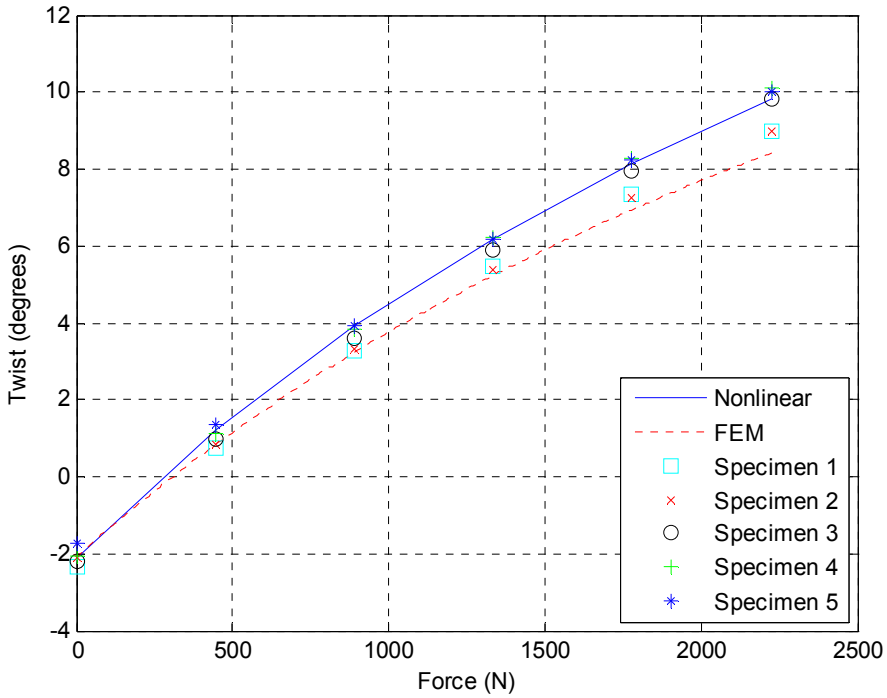

Figure 21. Response of Ten-ply Maximum Extension-twist Coupled Laminate

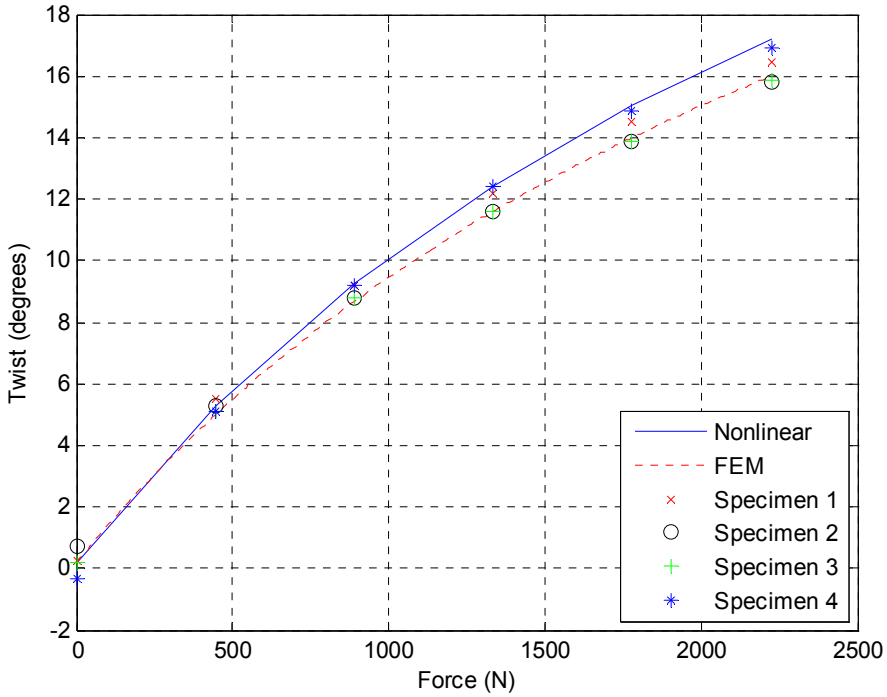

Figure 22. Response of Winckler-type Maximum Extension-twist Coupled Laminate

5.4.2 Nonlinear Model

The testing results are verified in part with a nonlinear model developed by Armanios *et al.*[30] given by

$$F_a = \frac{\left(b_1 + \frac{4}{3}b_2\theta_{oL} + 2b_3\theta_{oL}^2\right)\theta_L}{\left[b_4 - (\theta_L + \theta_{oL})\right]} \tag{95}$$

where F_a is axial force, θ_{oL} is the tip pre-twist angle, θ_L is the tip twist angle, and b_1-b_4 are functions of the geometric parameters and stiffness coefficients. Geometric nonlinearity is necessary for comparison with test data. This model was developed for antisymmetric laminates; that is, it can be used here for laminates with an even number of plies, but not for those with an odd number of plies. The model is included in Figure 17,

Figure 19, Figure 21, and Figure 22 for the six-, eight-, ten-ply, and Winckler-type laminates, respectively. Good agreement is seen between the nonlinear model and test data. The model is very sensitive to ply thickness, and variations in thickness due to uneven curing as well as measuring error are most likely responsible for any discrepancies.

The odd-ply laminates have coupling between extension and bending, which is not present in antisymmetric laminates. This additional anisotropy resulted in nontractable equations, and a nonlinear model that accurately predicts extension-twist coupling would be impractical. Therefore, these laminates were analyzed using finite element analysis.

5.4.3 FEM Analysis

Finite element models were created for each of the optimal hygrothermally stable five- through ten-ply and Winckler-type laminates using ABAQUSTM 6.8-1. The models were made to nominal dimensions of 2.54cm by 17.78cm (1.0" by 7.0") using measured thicknesses and material properties to recreate the manufactured specimens as closely as possible. An 8-node, doubly curved, thin-shell, reduced-integration element type was selected with five degrees of freedom per node (S8R5), and 222 elements were used. On one end, the specimen was clamped, and at the other end, a shell edge load was applied such that the total axial force was ramped up to 2224N (500 lb). Nonlinear geometry was selected to include trapeze effects.

Once the analysis was finished, the transverse deflection of the two corners was extracted as a function of load. Tip twist was calculated from the transverse

displacements and plotted as a function of load with the test data in Figure 16 through Figure 22 for the five- through ten-ply and Winckler-type laminates, respectively.

There is good agreement between the FEM data and test data. As with the nonlinear model, thickness variations are most likely responsible for deviations between the data and models. For all laminates there is noticeable difference between the FEM data and nonlinear model. This can be accounted for by considering that the clamped boundary condition in finite element model constrains warping.

5.4.4 Robustness in Coupling

For extension-twist coupled laminates to be useful, small errors in ply angle cannot cause significant loss of coupling. Therefore, a study was conducted to investigate the sensitivity of a representative laminate to small errors in ply angle. As with the investigation into the robustness of hygrothermal stability detailed earlier, each ply angle in a laminate was varied on a uniform interval of $\theta_k \pm 2°$, typical of hand-layup manufacturing errors. The optimal six-ply stacking sequence was chosen for this study, given by [21.2°/-63.8°/-48.7°/48.7°/63.8°/-21.2°].

A set of 10^6 samples were taken from the distribution and the error in η between the sample and optimal laminate was calculated. A normalized histogram presenting the results of the study is given in Figure 23. The error is contained to within 10% of the expected coupling. It should be noted that the error can be positive even though the stacking sequence yields maximum coupling because layups with perturbed ply angles are not subject to the hygrothermal stability conditions of the optimal laminate, and as such the resulting perturbed laminate may not be strictly hygrothermally stable.

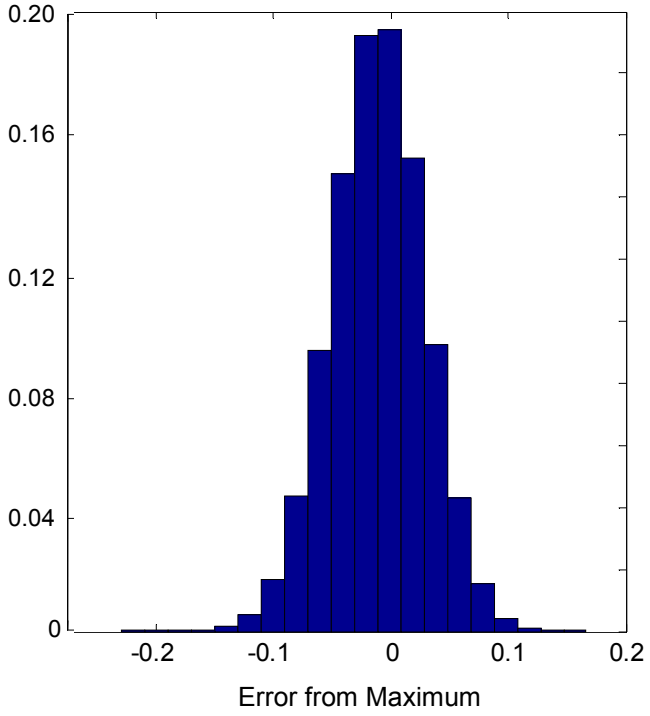

Figure 23. Robustness of Hygrothermally Stable Stacking Sequences

A similar study of robustness was performed on the six-ply unconstrained optimized and angle-ply stacking sequences, given by [-26.1°/-38.6°/88.6°/-88.6°/ 38.6°/26.1°], and $[\pm(24.7^\circ_2)]$, respectively; the results are shown in Figure 24 and Figure 25, respectively. The optimal angle-ply stacking sequences are within 10% error, but the error of the globally optimal stacking sequences is contained to within 1%.

Aside from ply angles, changes in material properties and small variations in geometric parameters should not result in significant changes in the level of coupling. Therefore, a study was conducted to investigate the sensitivity of a representative laminate to variations in material properties (E_{11}, E_{22}, G_{12}, ν_{12}) and ply thickness, t. Each of these parameters was perturbed in value on a uniform interval from 90% to 110% of its nominal value, which contains the range of measured values encountered when

performing the material characterization. The nominal values and range of measured values are given in Table 5. Using these perturbed values, η was calculated. The error in η between the perturbed and unperturbed laminates is plotted as a function of perturbation percent in Figure 26 for each of these parameters.

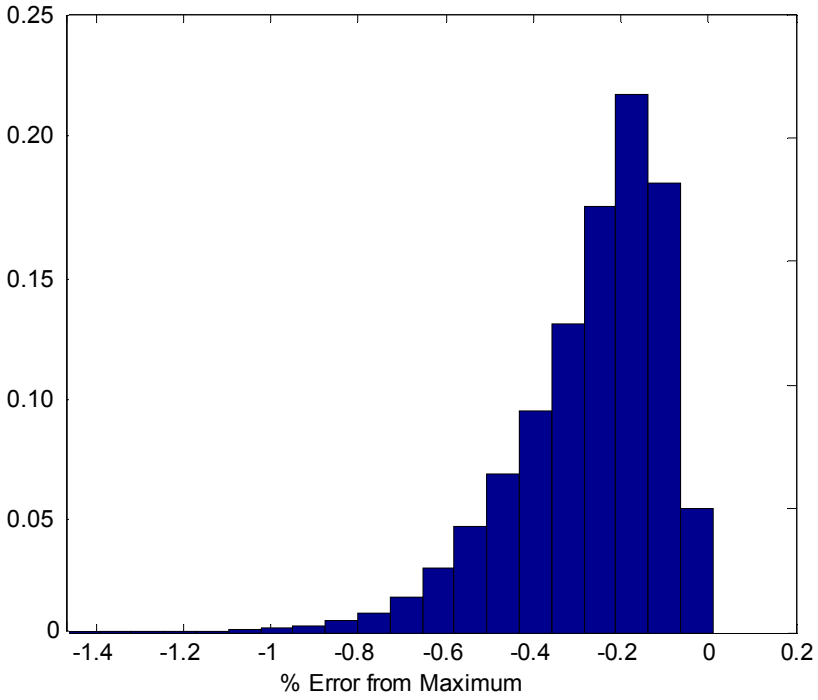

Figure 24. Robustness of Globally Optimal Stacking Sequences; 10^6 Cases

The coupling, η, has a direct relationship with E_{11}, and E_{22} and ν_{12} have a negligible effect on the coupling. The coupling, η, has an inverse relationship with G_{12} and t. This follows for t because extension-twist coupling is governed by the coupling stiffness matrix divided by the determinant of the constitutive matrix, which is proportional to a factor t^{-2}.

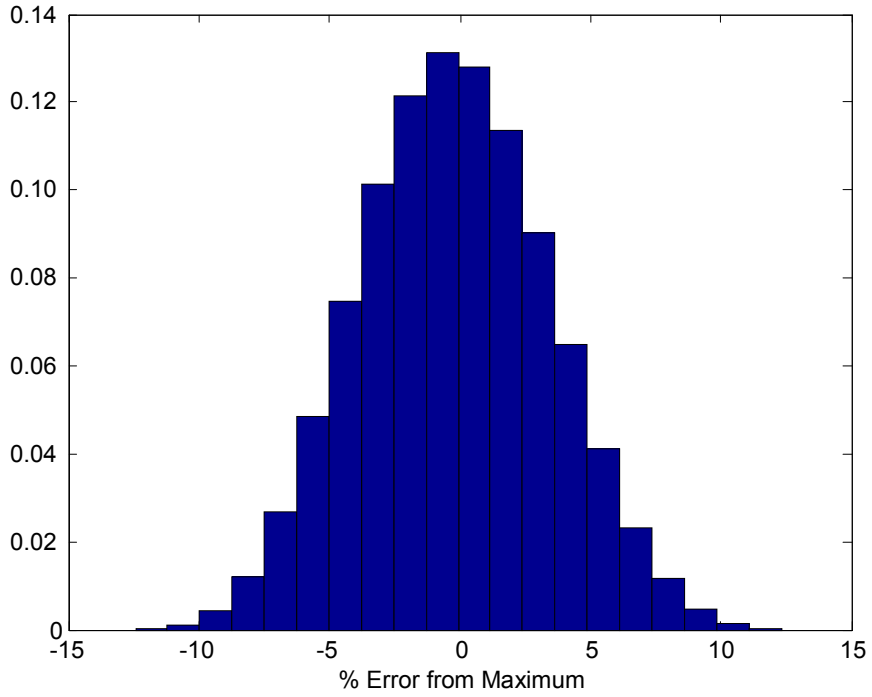

Figure 25. Robustness of Angle-ply Optimal Stacking Sequences; 10^6 Cases

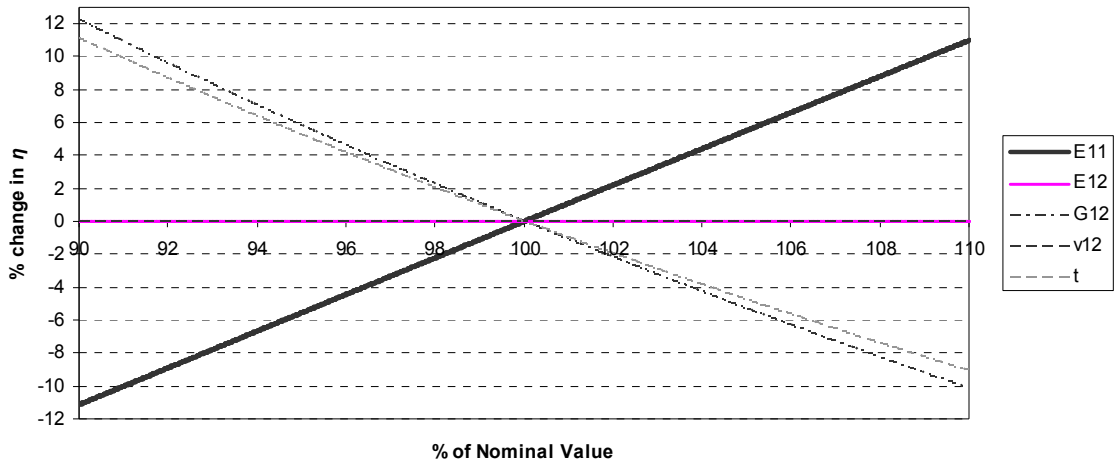

Figure 26. Robustness of Coupling to Perturbations in Material Parameters

5.4.5 Analysis

There is some scatter in the test data. This most likely can be attributed to variations in material properties and geometric parameters. Even though specimens were cut from the center of each laminate to avoid edge effects, samples taken from closer to the center of a laminate had a slightly different thickness than those further from the center in the range (-8%,10%). Care was taken to ensure that all specimens were cut to the same dimensions, but variations in specimen width and length were measured in the range (-3%, 7%) and (0%, 5%), respectively. To demonstrate that material and geometric property variations account for the scatter in the test data, the nonlinear model was plotted twice on the same graph using the highest and lowest observed values for every property. The six-ply optimal extension-twist laminate was chosen, as provided in Table 6. The two models and all test data are plotted in Figure 27. All test data is contained within the upper and lower bounds of the model, suggesting all test data scatter can be accounted for with variations in material properties and geometric parameters.

A summary of the testing data is presented in Figure 28 and Figure 29 with error bars showing one standard deviation values from all laminates along with the FEM predictions. The tip twist is divided by the specimen length to allow for comparison of twist rate between laminates. The twist rate is shown as a function of load and stress in Figure 28 and Figure 29, respectively. The stress is found by dividing the force by the average cross-sectional area of all specimens from a given laminate. The pre-twist is subtracted from all test data so that the curve for each laminate begins at the origin.

As predicted by η, nearly all laminates outperform the previously known Winckler-type laminate. For example, when compared at a load level of 2224N, the six-

ply laminate outperforms the Winckler-type laminate by 59%. This is accompanied by a 25% weight savings. Even the ten-ply laminate, which has a 25% thickness penalty, outperforms the Winckler-type laminate by 26% at the same loading.

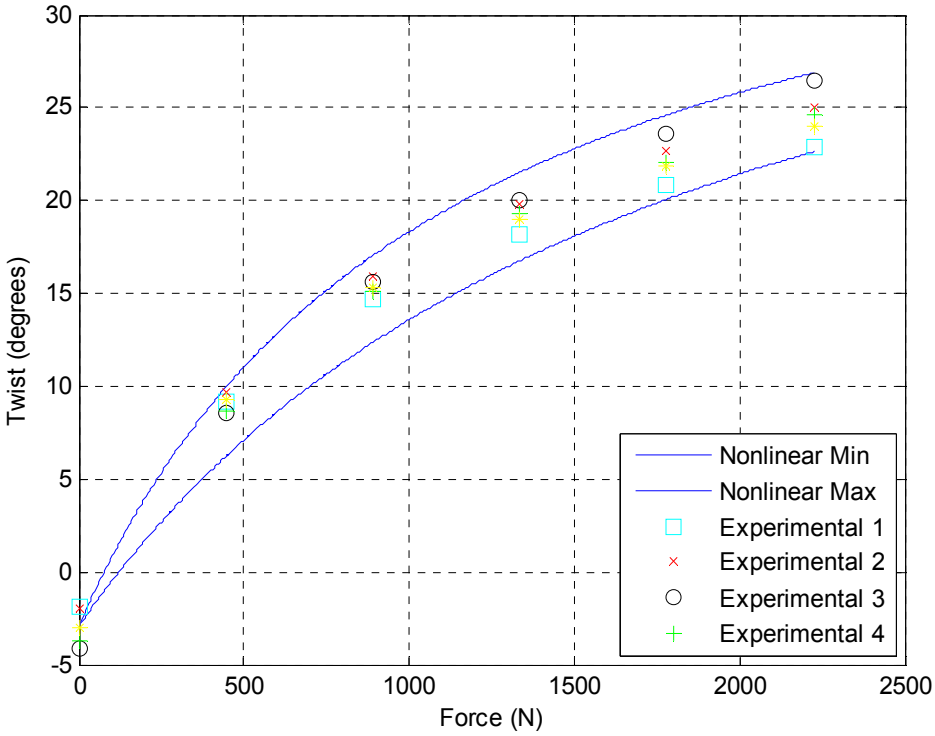

Figure 27. All Test Data Scatter Contained within Range of Material and Geometric Properties

When compared at the same axial force, as the number of plies increases, the coupling tends to decrease. This follows the same trend in η as given above, and the same reasoning applies: as the laminates become thicker, the axial and torsional stiffnesses become greater. Laminates with an even number of plies tend to outperform those with an odd number of plies. One likely explanation is that when going from an even-ply to an odd-ply laminate, the addition of a ply along the midplane increases the

torsional stiffness more than the coupling. For this reason, odd-ply laminates make suboptimal choices for extension-twist coupling.

Nonlinear effects are quite apparent in both Figure 28 and Figure 29. A general trend shows that for laminates with fewer plies, the trapeze effect is much more pronounced, while for laminates with more plies, the coupling response is closer to linear. The five-ply laminate demonstrates this effect best: at a low loading, it produces one of the highest twist rates, but by 2224N, it has the one of the lowest twist rates. This phenomenon can be explained by noting that the trapeze effect is largely governed by the twisting stiffness, D_{66}, which is very low in the five-ply laminate, while the nine- and ten-ply laminates demonstrate little trapeze effect and are nearly linear.

The coupling performance is compared at a stress level of 5.65×10^7Pa (8,194psi), which is the largest axial stress in the ten-ply laminate. Again, the six-ply laminate has the most coupling, an increase of 38.2% over the Winckler-type laminate. The laminate with the second-most coupling is the ten-ply with an increase of 29.0% over the Winckler laminate. This indicates that in this case laminates with fewer plies do not necessarily have more coupling, as suggested previously. One possible explanation for the ten-ply laminate's coupling to be so high at the same stress is because the outermost plies of the ten-ply laminate are farther from the midplane than those of the eight-ply laminate, causing the shear stress to induce a larger torsional moment. In other words, some of the effect of torsional stiffness is eliminated when dividing by the area.

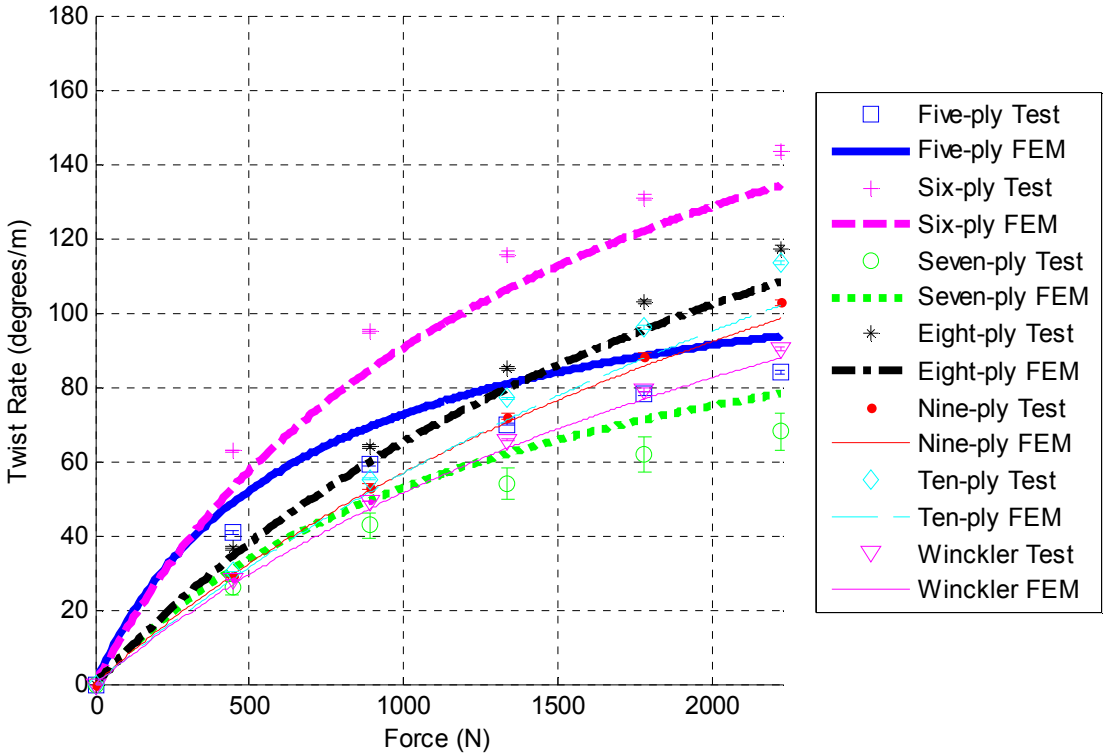

Figure 28. Comparison of Extension-twist Coupling by Force

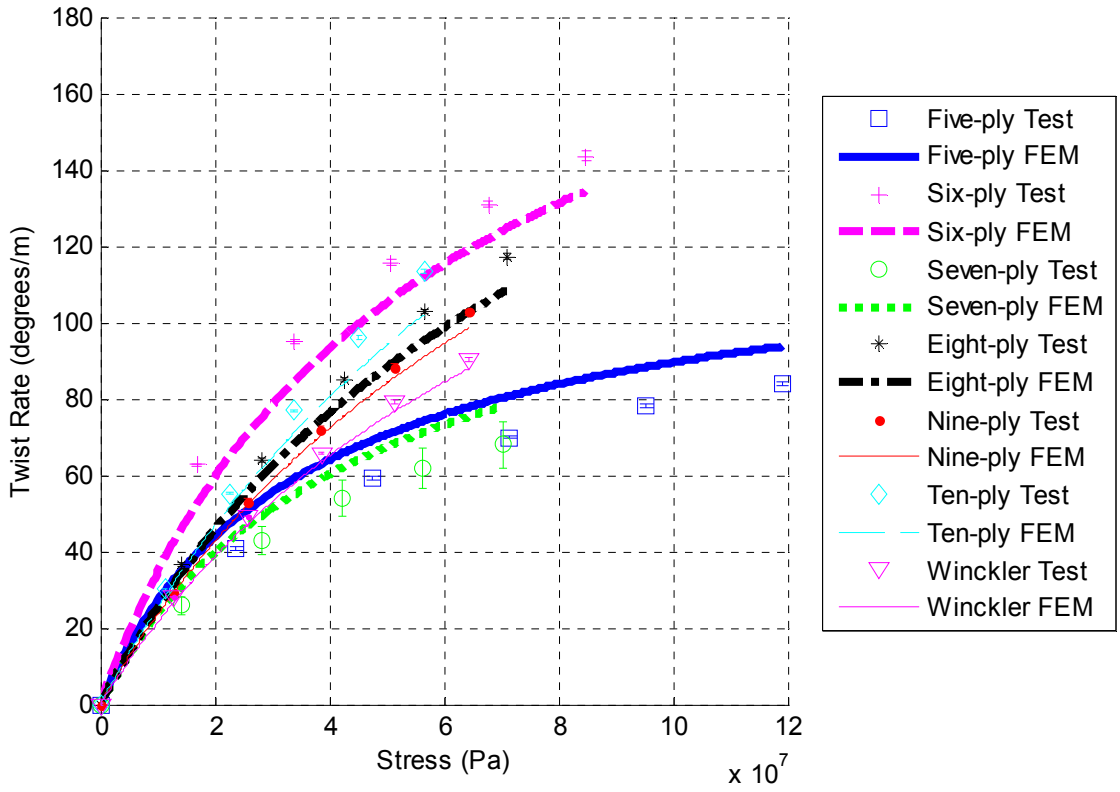

Figure 29. Comparison of Extension-twist Coupling by Stress

CHAPTER 6

BEND-TWIST COUPLING OF HYGROTHERMALLY STABLE LAMINATES

Bend-twist coupling is a phenomenon wherein a bending moment induced in a structure results in a proportional twist. Anisotropy makes it possible for flat composite laminates experiencing a bending moment loading to generate a non-zero twisting curvature. Physically, bend-twist coupling is created when the resultant moment, M_{xx}, produces an equipollent distributed axial stress through the thickness of the laminate, which in turn produces an average axial load in each lamina. An axial force applied to a generally orthotropic lamina creates a shear action, and, when a laminate is constructed from generally orthotropic laminas, the resultant shear forces in each ply at some non-zero distance from the midplane creates a twisting moment in the laminate. If the resultant moment is positive, the plies above the midplane are in compression while the plies below the midplane are in tension, meaning that a generally orthotropic lamina above the midplane will produce the opposite shear effect as if it is positioned below the midplane. Therefore, unidirectional off-axis laminates can produce a significant level of bend-twist coupling.

In this chapter, bend-twist coupling is quantified; then a constrained optimization is performed to identify the hygrothermally stable stacking sequence with the most coupling for a laminate with a set number of plies. Confirmation of the desired level of coupling is made using FEM analysis and a nonlinear model derived herein. A study of the robustness of the optimized stacking sequences is also performed. Finally, a survey

of the free vibration modes and natural frequencies of six-ply optimal bend-twist coupled laminates is conducted.

6.1 Optimality Parameter

Bend-twist coupling is quantified by expressing the twist rate as a function of an applied moment resultant. Again, CLT is used with the same assumption for extension-twist coupling that the resulting laminate will be flat and that the useful deformation range of these laminates validates using a linear theory. From Equations (90) and (91), the twist rate can be calculated as

$$\varphi = \frac{1}{2}\left(\delta_{16} M_{xx} + \kappa_{xy}^{(T,H)}\right) \tag{96}$$

Since the optimizer searches hygrothermally stable laminates, the non-mechanical curvature in Equation (96) is zero, resulting in an objective function given by

$$g\left(\{\theta_k : k = 1 \ldots n\}\right) = -\delta_{16}^2 \tag{97}$$

6.2 Implementation

The sequential quadratic programming (SQP)[32] implementation in MATLAB 7™ was used to perform the stacking sequence optimization numerically. Four sets of conditions were used consecutively during the optimization of a given laminate: 1) no constraint on hygrothermal stability, 2) the constraints of Condition A, 3) the constraints of Condition B, and 4) a constraint to a unidirectional laminate. The constraints of Conditions A and B are provided in Table 1. The optimizer was initialized with a stacking sequence sampled from a uniform random number generator. The existence of suboptimal local minima required about 75 optimization runs to reach the global

optimum. The material properties of the T300/976 graphite/epoxy material system were used as provided in Table 5.

6.3 Results

Optimizations were performed for two- through ten-ply laminates. The resulting optimal stacking sequences for the constrained optimization are presented in Table 11. Also included is a nondimensional comparison parameter for bend-twist coupling, calculated as

$$\varsigma = \frac{\delta_{16}(nt)^3 E_{11}}{12} = \delta_{16} D_{11} \approx \frac{\delta_{16} M_{xx}}{\kappa_{xx}} = \frac{2\phi}{\kappa_{xx}} \tag{98}$$

Table 11. Laminates Optimized for Bend-twist Coupling with Various Constraints

# of Plies	Condition A (°)	ζ	Condition B (°)	ζ	Unidirectional (°)	ζ
2	N/A	-	$[30.5]_2$	8.77	$[30.5]_2$	8.77
3	N/A	-	$[-31.6/\overline{87.8}]_s$	8.99	$[30.5]_3$	8.77
4	$[-24.3/65.7]_s$	7.08	$[32.8/-88.2]_s$	9.16	$[30.5]_4$	8.77
5	$[27.8/-76.7/\overline{-24.4}]_s$	7.83	$[33.3/-88.4/\overline{33.3}]_s$	9.18	$[30.5]_5$	8.77
6	[-87.0/-18.0/3.2/51.1 /72.4/-38.6]	6.61	$[33.5/-88.5/33.5]_s$	9.16	$[30.5]_6$	8.77
7	[-26.6/76.7/70.5/24.4/ -21.9/-27.8/75.4]	7.46	$[33.6/-88.5/33.6/\overline{-88.5}]_s$	9.14	$[30.5]_7$	8.77
8	[25.6/23.0/-67.0/ -64.4]$_s$	7.17	$[-32.8_2/88.2_2]_s$	9.16	$[30.5]_8$	8.77
9	[26.7/26.1/-74.6 /-66.9/$\overline{-23.2}$]$_s$	7.79	$[-33.1_2/88.4_5/-33.1_2]$	9.18	$[30.5]_9$	8.77
10	[-28.2/-27.8/78.0 /75.0/24.3]$_s$	7.74	$[-33.3_2/88.4_2/-33.3]_s$	9.18	$[30.5]_{10}$	8.77

The results of the unconstrained optimization are provided in Table 12 along with the reduction in ζ associated with each constraint. The stacking sequences optimized without

any constraints on hygrothermal stability produced symmetric laminates for two through six, nine, and ten plies; therefore, these laminates automatically meet the constraints of Condition B for hygrothermal stability. For seven- and eight-ply laminates, the optimal stacking sequences were very similar but slightly different from the laminates constrained to Condition B. There is less than a quarter of a percent difference in ζ between the global optima and the Condition B optima. There is less than 5% difference in ζ between the global optima and the unidirectional optima. Laminates constrained to Condition A have at least 15% less coupling than the global maximum.

Table 12. Global Optimal Bend-twist Coupled Laminates with Coupling Loss due to Various Constraints

# of Plies	Global Optima (°)	ζ	Coupling Loss with Condition A	Coupling Loss with Condition B	Coupling Loss with Unidirectional
2	$[30.5]_2$	8.77		0.00%	0.0%
3	$[-31.6/\overline{87.8}]_s$	8.99		0.00%	-2.4%
4	$[32.8/-88.2]_s$	9.16	-22.7%	0.00%	-4.2%
5	$[33.3/-88.4/\overline{33.3}]_s$	9.18	-14.7%	0.00%	-4.4%
6	$[33.5/-88.5/33.5]_S$	9.16	-27.9%	0.00%	-4.2%
7	[33.2/-88.4/33.4/ -88.5/-88.4/33.0_2]	9.16	-18.6%	-0.23%	-4.3%
8	[-33.3/-33.2/88.4/88.5/ -33.5/-33.4/88.4/-33.3]	9.17	-21.9%	-0.17%	-4.4%
9	$[-33.1_2/88.4_5/-33.1_2]$	9.18	-15.1%	0.00%	-4.4%
10	$[-33.3_2/88.4_2/-33.3]_s$	9.18	-15.7%	0.00%	-4.4%

Hygrothermally stable laminates with optimal bend-twist coupling have stacking sequences with two distinct groupings of ply angles: one group near the angle that

maximizes bend-twist coupling for unidirectional laminates, around ±30.5° and one group near ∓90°. This can be explained by considering the effect of a ply oriented at each angle. Plies oriented near ±30.5° maximize D_{16} and give the laminate its bend-twist coupling. These plies, however, create a large bending stiffness in the laminate, D_{11}. The outermost plies can generate the most coupling, and therefore, are consistently oriented at ±30.5°. These plies are not at ±30.5° as in the optimal unidirectional laminate; however, they are slightly closer to ±90°. This effect reduces the bending stiffness while sacrificing little coupling.

Plies oriented near ∓90° have a very low bending stiffness. This effect is also felt more strongly in plies farther from the midplane but does not contribute to the overall coupling mechanism; therefore, plies oriented near ∓90° are generally found one or two plies inside the outermost ply. These plies are not oriented at ∓90°, but are slightly closer to 0°. This allows them to produce a small amount of coupling while not increasing the bending stiffness. Also, the benefit of the plies oriented near ∓90° is the reduction in matrix-dominated splitting failure that is typically seen in unidirectional laminates.

Hygrothermally stable laminates subject to Condition B with a constant total laminate thickness were optimized. Parameter ζ is plotted in Figure 30 as a function of n for both laminates with a constant ply thickness and laminates with a constant total thickness. A curve fit has been drawn through the points so a trend can be inferred. By constraining the total laminate thickness, the effect of increasing bending and torsional stiffness with increasing number of plies is mitigated.

As for extension-twist coupling, lamination parameters are not effective in determining optimal stacking sequences, but they do reveal interesting trends between

laminates. Figure 31 plots the lamination parameters that govern the in-plane stiffness coefficients with increasing number of plies. Figure 32 plots the lamination parameters that govern the bending stiffness coefficients with increasing number of plies. Since the optimal hygrothermally stable stacking sequences are so similar in form, it follows that the lamination parameters would trend together, and indeed this is the case. For the bending stiffness, $\xi_9 \rightarrow \sim 0.1$, $\xi_{10} \rightarrow \sim -0.3$, $\xi_{11} \rightarrow \sim 0.7$, and $\xi_{12} \rightarrow \sim 0.6$. These are the lamination parameters that apparently produce optimal bend-twist coupling.

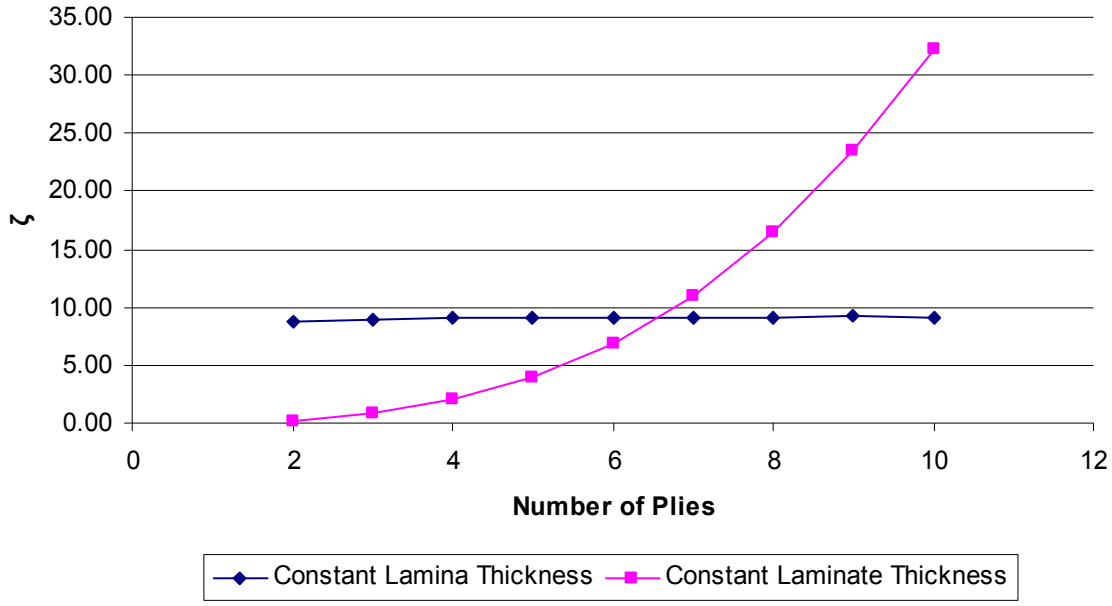

Figure 30. Comparison of Bend-twist Coupling for Laminates with Constant Ply Thickness and Constant Total Thickness

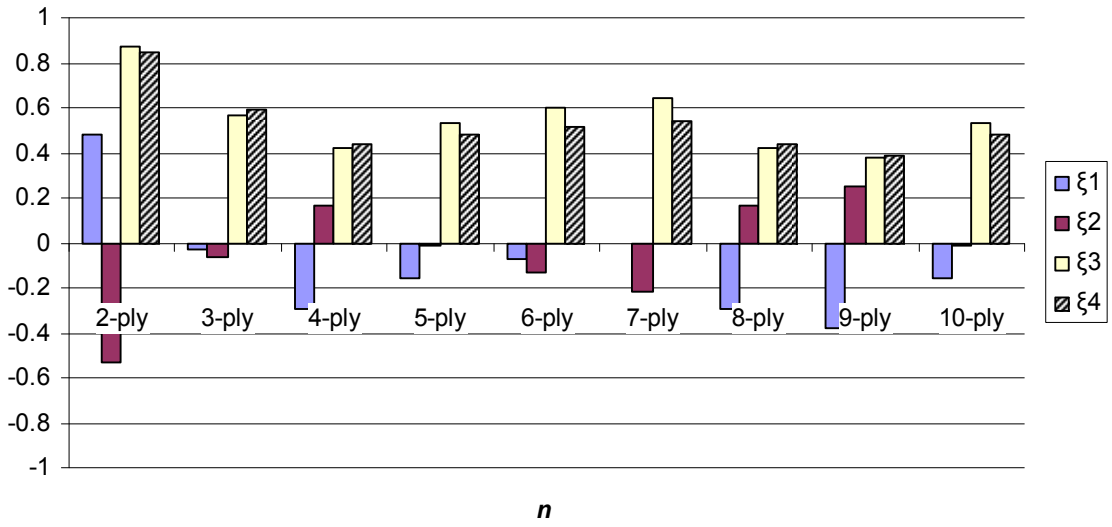

Figure 31. In-plane Stiffness Coefficient Lamination Parameters

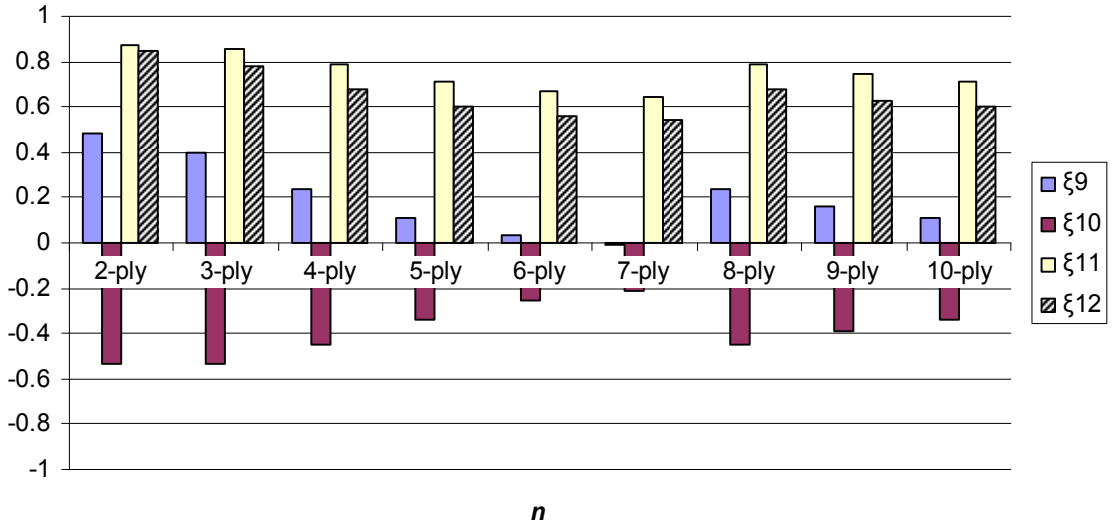

Figure 32. Bending Stiffness Coefficient Lamination Parameters

6.4 Validation

To confirm and demonstrate the expected level of bend-twist coupling, the optimal hygrothermally stable five- through ten-ply laminates were manufactured and tested. A nonlinear model was derived to predict the response of bend-twist coupled laminates to loading. Finite element models were used to verify the nonlinear model. An investigation of the robustness of optimal bend-twist coupled laminates to perturbations in material and geometric properties was conducted.

6.4.1 Manufacturing and Testing

The hygrothermally stable optimal bend-twist coupled five- through ten-ply laminates in Table 11, Condition B, were constructed from a T300/976 graphite/epoxy material system. The material properties were measured in accordance with ASTM standards and are provided in Table 13. Note that this is the same material system as characterized in Table 5, but over one year had passed since the first characterization and manufacturing of the optimal bend-twist coupled laminates, so another characterization was performed; the only difference between the two characterizations is a 9% drop in G_{12}. Each ply was cut from a pre-impregnated roll, laid up in a flat aluminum mold, and cured in an autoclave with the curing cycle shown in Figure 4. After curing, each laminate was cut into four specimens of dimensions 3.81cm by 25.4cm (1.5" by 10.0").

The specimens were tested by clamping one end and applying a transverse load to the other end. Figure 33 shows a specimen undergoing testing. A length of 2.54cm (1.0") in the specimen was clamped between a hard surface and a block of wood, leaving dimensions of 3.81cm by 22.9cm (1.5" by 9.0") for the test sample area. The wood

prevented the c-clamp from damaging the specimen. Care was taken to ensure that the hard surface was level and the specimen was cantilevered perpendicularly from its edge. A small hole, 1.6mm, (1/16") was drilled along the midline of the laminate 3.2mm (1/8") from the tip. A wire was fed through the hole and twisted on itself to form a loop. It was assumed that the hole and wire did not contribute to the response of the laminate because the dimensions of the hole were much smaller than the overall dimensions of the laminate and the wire has negligible mass.

Table 13. Elastic Properties of T300/976, Second Material Characterization

Property	Value	Range
E_{xx}	125 GPa	(-4% , 5%)
E_{yy}	8.45 GPa	(-3% , 3%)
G_{xy}	3.9 GPa	(-1% , 1%)
ν_{xy}	0.328	(-1% , 3%)
t	0.152 mm	(-8% , 10%)

Before loading, the vertical height of each tip corner from a flat level surface was measured using Vernier calipers. The pre-twist was then determined using the formula

$$\sin\theta = \frac{|d_1 - d_2|}{w} \tag{99}$$

where d_1 and d_2 are the height of the left and right tip corners, respectively, w is the specimen width, and θ is the specimen tip twist. To apply load, hooked precision weights were hung from the wire loop. The mass of the weights was confirmed using a digital balance. After the application of each load, the tip corner displacement was measured; the tip twist was then calculated using Equation (99). The five- and six-ply specimens were loaded up to 50g in increments of 10g. The seven- and eight-ply specimens were

loaded up to 100g in increments of 20g. The nine- and ten-ply specimens were loaded up to 250g in increments of 50g. It was not possible to load all specimens to the same level because the maximum loading of the five-ply laminate would induce negligible bending in the ten-ply laminate and the maximum loading of the ten-ply laminate would cause the five-ply laminate to deflect beyond where the applied load could be considered transverse.

Figure 33. Specimen Undergoing Bend-twist Coupling Testing

Figure 34 through Figure 39 plot the test data for the five- through ten-ply specimens, respectively, as a function of the average bending moment in the specimen.

Also included in each figure are the results of the nonlinear model and finite element model predictions described in later sections.

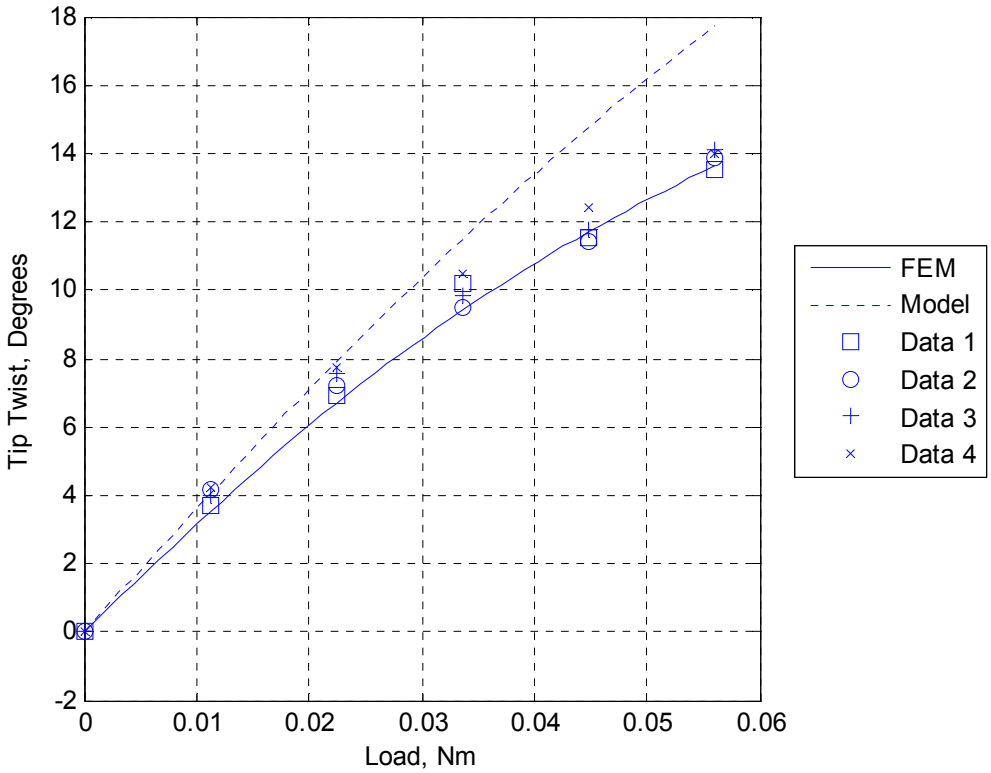

Figure 34. Test Data for Optimal Five-ply Laminate

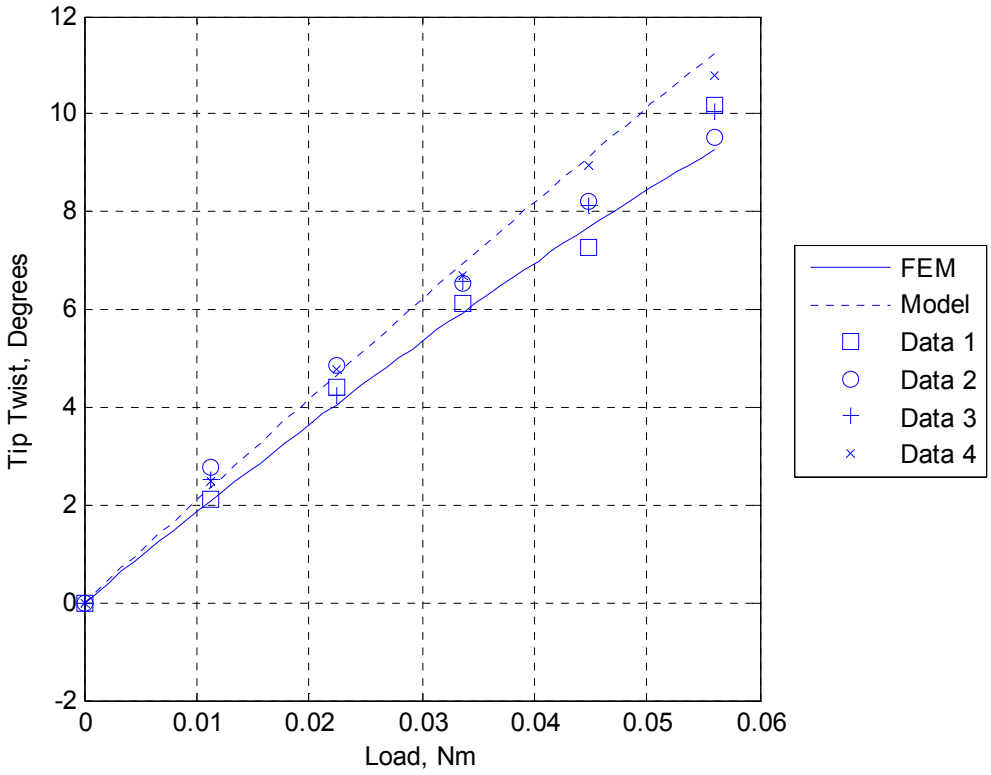

Figure 35. Test Data for Optimal Six-ply Laminate

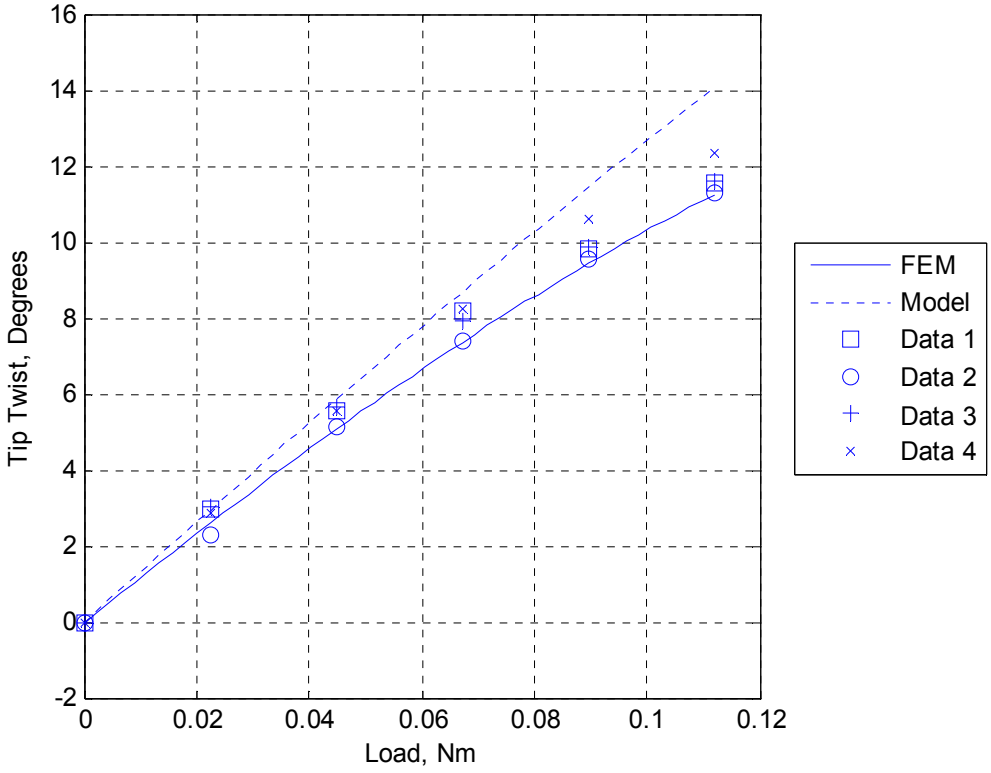

Figure 36. Test Data for Optimal Seven-ply Laminate

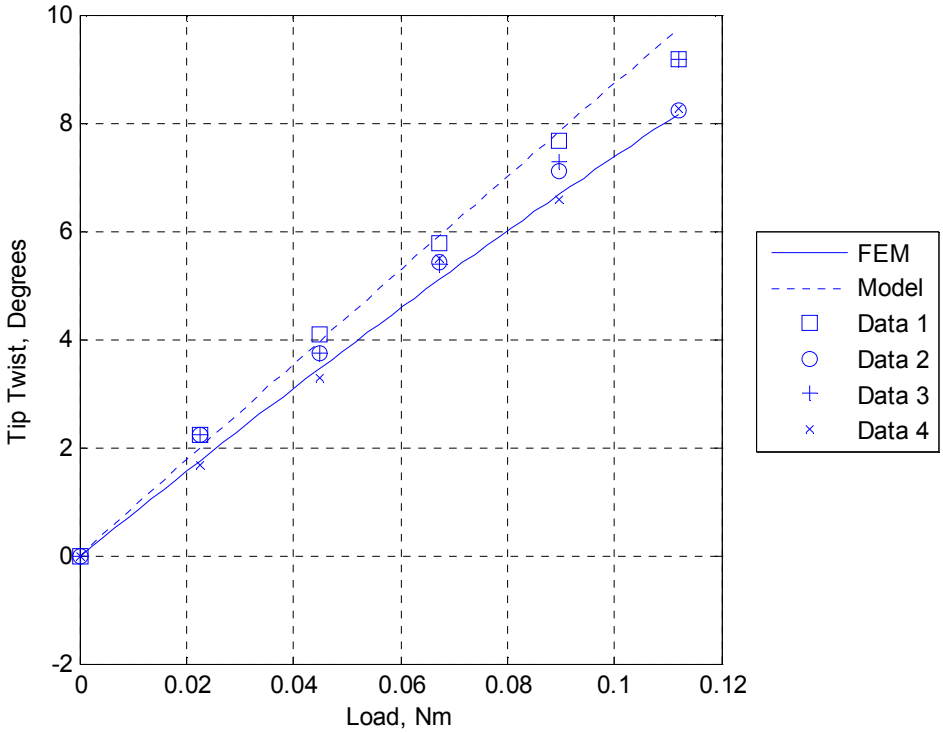

Figure 37. Test Data for Optimal Eight-ply Laminate

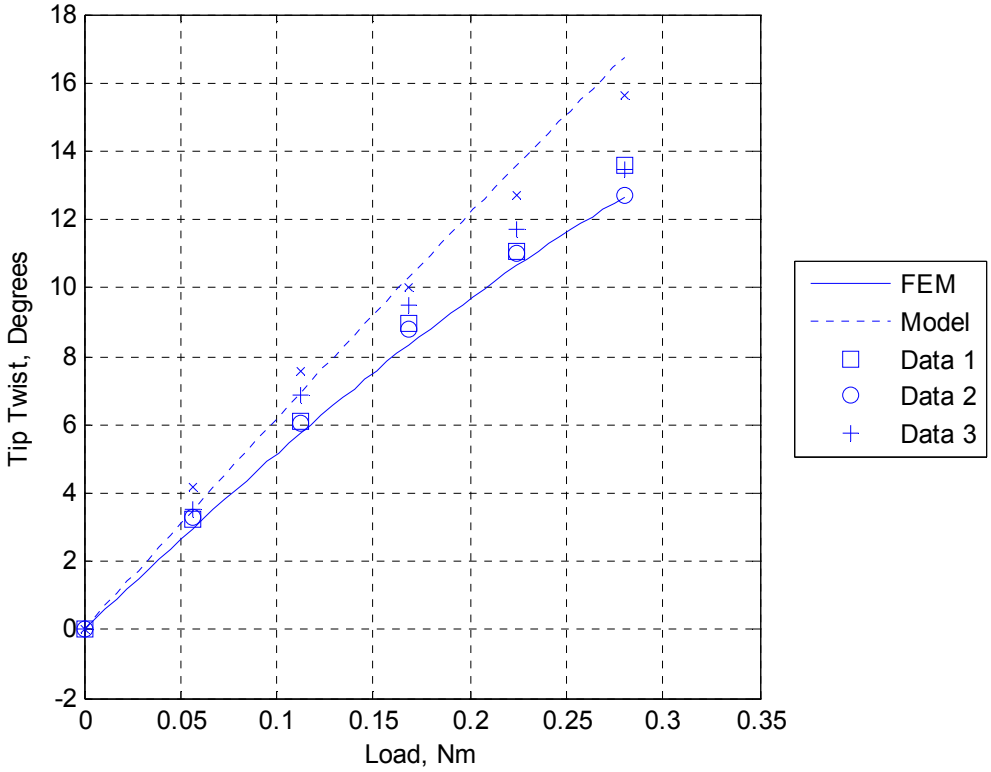

Figure 38. Test Data for Optimal Nine-ply Laminate

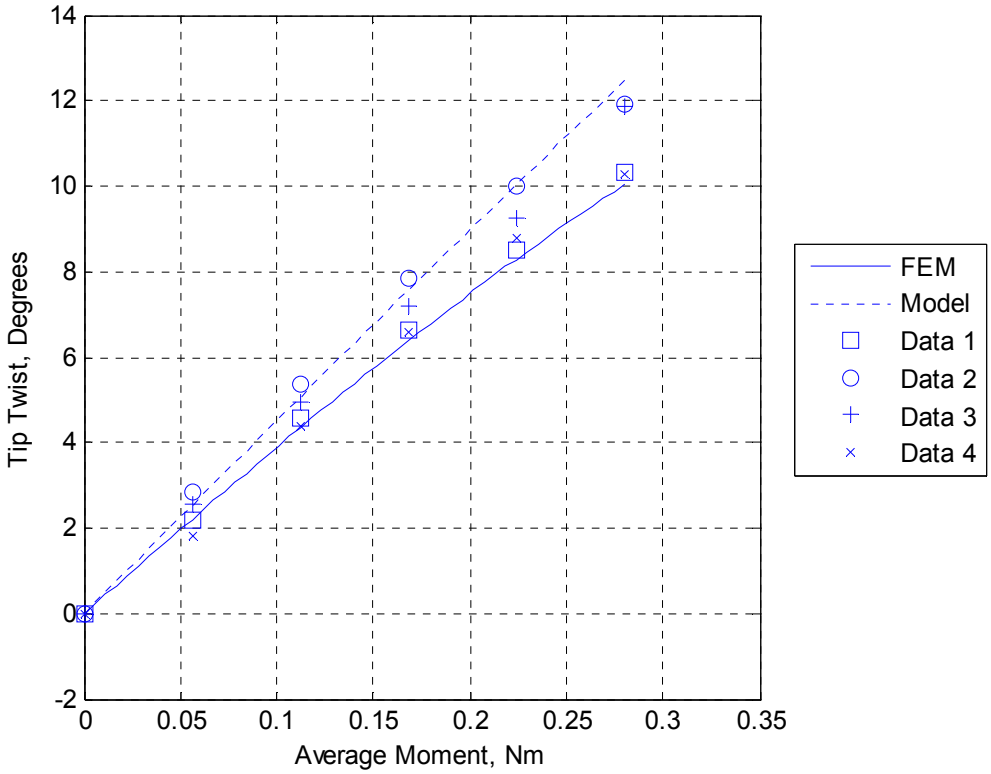

Figure 39. Test Data for Optimal Ten-ply Laminate

Since the laminates are constructed using hygrothermally stable stacking sequences, there should be no curing-induced pre-twist, but errors in layup during manufacturing likely cause the resulting laminate to have a slight initial curvature. This was accounted for by measuring the pre-twist as given in the testing procedure described previously. For all laminates, the pre-twist twist rate in each specimen was less than 0.04°/cm (0.1°/in). Also, there is some scatter in the test data. This most likely can be attributed to variations in ply thickness and sample size. Even though specimens were cut from the center of each panel to avoid edge effects, variations in thickness between samples that were closer to the center of a laminate had a slightly different thickness than those further from the center, in the range (-8%,10%). Similarly, thickness variations

caused deviations in the elastic constant data, as well. Care was taken to ensure that all specimens were cut to the same dimensions, but variations in specimen width and length were measured in the range (-3%, 7%) and (0%, 5%), respectively. As with extension-twist coupling, these variations can be shown to account for scatter in the test data.

6.4.2 Nonlinear Model

A nonlinear model was derived to predict the tip twist as a function of applied load in symmetric bend-twist coupled laminates under pure bending. Geometric nonlinearity is necessary for comparison with test data. Since the optimal hygrothermally stable bend-twist coupled laminates and the intuitive unidirectional laminates are symmetric, reductions in the constitutive law for symmetric laminates are used in this model. The derivation is similar in form to that in Armanios *et al.*[30] and begins by assuming a helical rigid deformed shape as shown in Figure 40. It is assumed that the width, w, is much larger than the thickness, h, and much smaller than the length, L, meaning

$$h<<w<<L \tag{100}$$

The laminate is assumed to deform into a helix with radius ρ and periodicity $2\pi b$. Three coordinate systems are used initially to fully express the location of every point in the deformed configuration: the original $\hat{i}\hat{j}\hat{k}$ coordinate system along the x, y, and z axes, respectively; the $\hat{i}'\hat{j}'\hat{k}'$ coordinate system which has $\hat{i}'$ in the $\hat{k}$ direction and $\hat{k}'$ aligned with the axis of the helix; and the $\hat{e}_1\hat{e}_2\hat{e}_3$ coordinate system, in which $\hat{e}_3$ points radially toward the helical axis and $\hat{e}_1$ points tangentially along the helical curve. Therefore, the position vector of point $A(x,y,z)$ in the undeformed configuration is

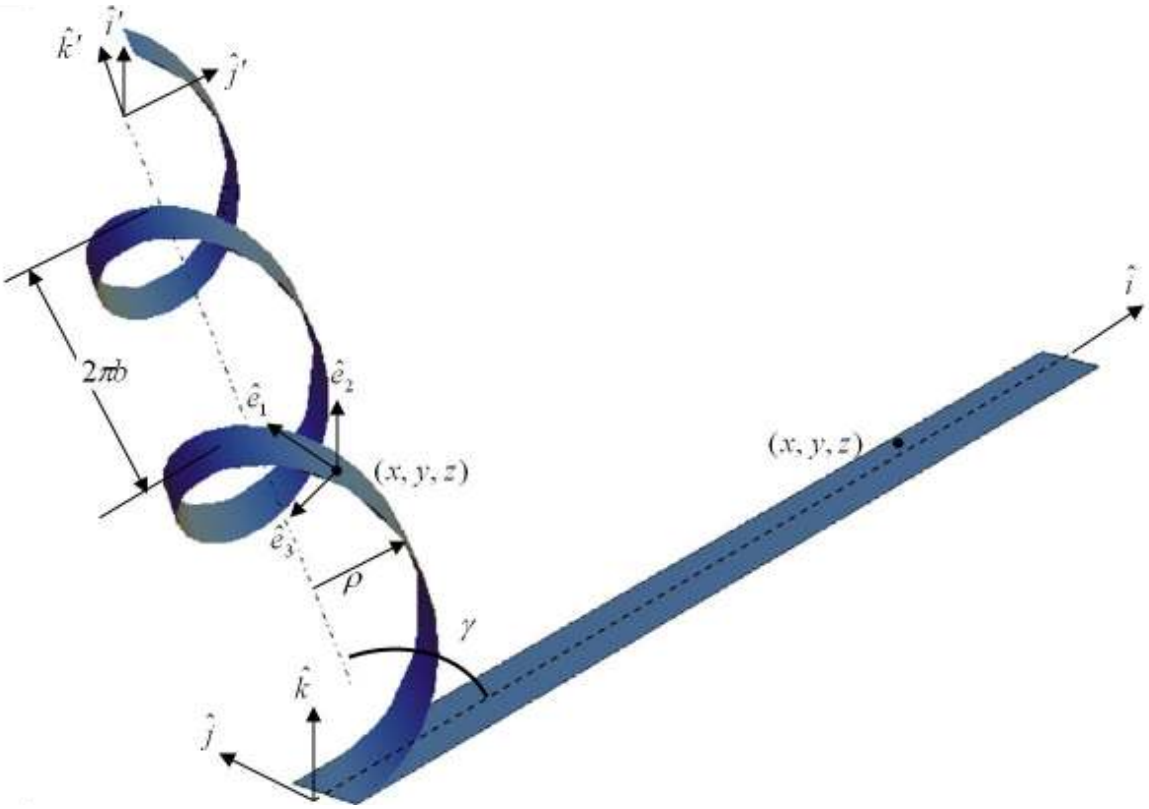

Figure 40. Bend-twist Coupled Laminate Geometry

$$\vec{r}_o = x\hat{i} + y\hat{j} + z\hat{k} \tag{101}$$

If the section undergoes a finite rigid-body rotation, point *A* has position vector

$$\vec{r}_1 = \rho(1-\cos T)\hat{k} + bT\hat{k}' + \rho \sin T\hat{j}' + y\hat{e}_2 + z\hat{e}_3 \tag{102}$$

where, $T = x/s$, and $s = (\rho^2 + b^2)^{0.5}$. The following transformations define the various coordinate systems in terms of the $\hat{i}\hat{j}\hat{k}$ system:

$$\hat{i}' = \hat{k},\ \hat{k}' = \frac{b}{s}\hat{i} + \frac{\rho}{s}\hat{j},\ \hat{j}' = \frac{\rho}{s}\hat{i} + \frac{b}{s}\hat{j} \tag{103}$$

$$\hat{e}_1 = (\overline{\rho}^2 \cos\tfrac{x}{s} + \overline{b}^2)\hat{i} + \overline{b}\,\overline{\rho}(1-\cos\tfrac{x}{s})\hat{j} + \overline{\rho}\sin\tfrac{x}{s}\hat{k};\ \overline{b}, \overline{\rho} = \frac{b, \rho}{s} \tag{104}$$

$$\hat{e}_2 = \bar{b}\,\bar{\rho}(1-\cos\tfrac{x}{s})\hat{i} + (\bar{b}^2\cos\tfrac{x}{s} + \bar{\rho}^2)\hat{j} - \bar{b}\sin\tfrac{x}{s}\hat{k} \tag{105}$$

$$\hat{e}_3 = -\bar{\rho}\sin\tfrac{x}{s}\hat{i} + \bar{b}\sin\tfrac{x}{s}\hat{j} + \cos\tfrac{x}{s}\hat{k} \tag{106}$$

In addition to the rigid-body deformation, warping in the cross section is expressed in terms of spherical coordinates with parameters α and β as defined in Figure 41, producing a deformed position vector as

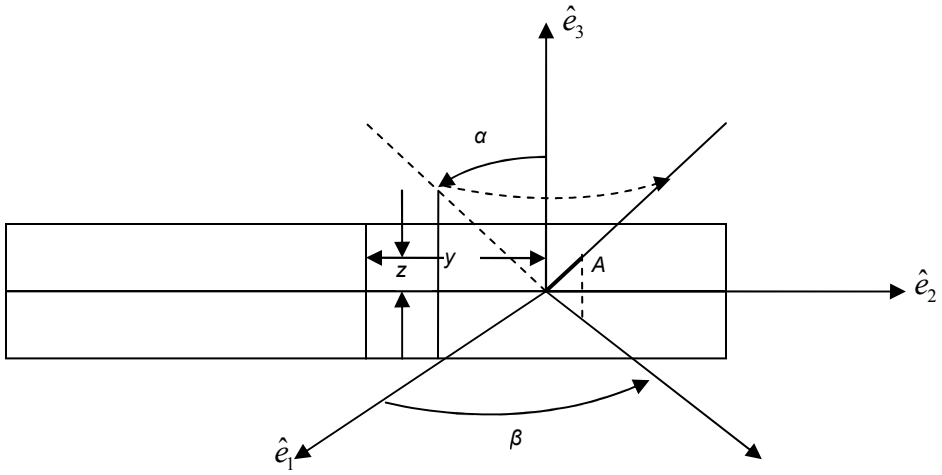

Figure 41. Warping Deformation of Cross Section

$$\begin{aligned}\vec{r}_2 = {} & (\bar{b}^2 x + s\bar{\rho}^2\sin\tfrac{x}{s})\hat{i} + \bar{b}\,\bar{\rho}(x - s\sin\tfrac{x}{s})\hat{j} + s\bar{\rho}(1-\cos\tfrac{x}{s})\hat{k} \\ & + z\sin\alpha\cos\beta\hat{e}_1 + (y + z\sin\alpha\sin\beta)\hat{e}_2 + z\cos\alpha\hat{e}_3\end{aligned} \tag{107}$$

The Lagrangian strain tensors are given by

$$2\varepsilon_{ij} = \frac{\partial r_2}{\partial x_i}\cdot\frac{\partial r_2}{\partial x_j} - \frac{\partial r_o}{\partial x_i}\cdot\frac{\partial r_o}{\partial x_j},\ (x_1 = x,\ x_2 = y,\ x_3 = z) \tag{108}$$

While undergoing a finite displacement, the cross section is assumed to have negligible transverse normal and shear strains. Substituting Equations (101) and (107) into Equation (108) yields

$$2\varepsilon_{zz} = 0 \tag{109}$$

$$2\varepsilon_{yz} = \sin\alpha\cos\beta \tag{110}$$

$$2\varepsilon_{xz} = -\frac{\bar{b}y}{s}\cos\alpha + \sin\alpha\cos\beta \tag{111}$$

and solving for α and β yields

$$\sin\beta = 0\,,\ \tan\alpha = \frac{\bar{b}y}{s} \tag{112}$$

producing a position vector of

$$\begin{aligned}\vec{r}_2 = {} & s(\bar{b}^2\tfrac{x}{s} + \bar{\rho}^2\sin\tfrac{x}{s})\hat{i} + s\bar{b}\bar{\rho}(\tfrac{x}{s} - \sin\tfrac{x}{s})\hat{j} + s\bar{\rho}(1-\cos\tfrac{x}{s})\hat{k} \\ & + \frac{\bar{b}yz/s}{\sqrt{1+(\bar{b}y/s)^2}}\hat{e}_1 + y\hat{e}_2 + \frac{z}{\sqrt{1+(\bar{b}y/s)^2}}\hat{e}_3\end{aligned} \tag{113}$$

Finally, all other extensions, shears, and curvatures are taken to be included in the vector

$$\vec{u} = U(y,z)\hat{e}_1 + V(y,z)\hat{e}_2 + W(y,z)\hat{e}_3 \tag{114}$$

which is superimposed on r_2 to make the final deformed configuration position vector

$$\begin{aligned}\vec{r} = {} & s(\bar{b}^2\tfrac{x}{s} + \bar{\rho}^2\sin\tfrac{x}{s})\hat{i} + s\bar{b}\bar{\rho}(\tfrac{x}{s} - \sin\tfrac{x}{s})\hat{j} + s\bar{\rho}(1-\cos\tfrac{x}{s})\hat{k} \\ & + \left(\frac{\bar{b}yz/s}{\sqrt{1+(\bar{b}y/s)^2}} + U\right)\hat{e}_1 + (y+V)\hat{e}_2 + \left(\frac{z}{\sqrt{1+(\bar{b}y/s)^2}} + W\right)\hat{e}_3\end{aligned} \tag{115}$$

The thin-walled assumptions of Equation (100) allow for the following bounds:

$$\begin{gathered}(h/w)^2, (w\bar{b}/s)^2, (w\bar{\rho}/s)^2, U_{,y}, U_{,z}, V_{,y}, V_{,z}, W_{,y}, W_{,z} = O(\varepsilon) \\ V\bar{b}/s, W\bar{b}/s, V\bar{\rho}/s, W\bar{\rho}/s = O(\varepsilon^{1.5})\end{gathered} \tag{116}$$

Making these reductions produces an approximate deformed configuration position vector

$$\begin{aligned}\vec{r} = s(\bar{b}^2\tfrac{x}{s} + \bar{\rho}^2\sin\tfrac{x}{s})\hat{i} + s\bar{b}\bar{\rho}(\tfrac{x}{s} - \sin\tfrac{x}{s})\hat{j} + s\bar{\rho}(1-\cos\tfrac{x}{s})\hat{k} \\ + \left(\phi yz\left(1-\tfrac{1}{2}(\phi y)^2\right)+U\right)\hat{e}_1 + \left(y+V\right)\hat{e}_2 + \left(z\left(1-\tfrac{1}{2}(\phi y)^2\right)+W\right)\hat{e}_3\end{aligned} \tag{117}$$

$$\phi = \bar{b}/s$$

The strains are assumed to have no dependency on the *x*-coordinate. This is valid under the assumption of pure bending because the state of strain in each cross section will be identical. The torsion of a helix is defined as $\bar{b}/s$, which is also the twist rate of the laminate, φ. Using Equations (101) and (117) in Equation (108) yields the strains as

$$\begin{aligned}\varepsilon_{xx} &= \tfrac{1}{2}(\phi y)^2 - z\bar{\rho}/s \\ \varepsilon_{yy} &= V_{,y} \\ \varepsilon_{zz} &= W_{,z} \\ \gamma_{xy} &= U_{,y} - 2\phi z \\ \gamma_{xz} &= U_{,z} \\ \gamma_{yz} &= V_{,z} + W_{,y}\end{aligned} \tag{118}$$

The strains will be approximated by their average through-the-thickness values as

$$(\gamma_{xz}, \gamma_{yz}, \varepsilon_{zz}) \approx \frac{1}{h}\int_{-h/2}^{h/2}\left(U_{,z}, V_{,z} + W_{,y}, W_z\right) \tag{119}$$

Integrating Equation (118) and using Equation (119) yields

$$\begin{aligned}U &= U_o(y) - zU_1(y) \\ V &= V_o(y) - zV_1(y) \\ W &= W_o(y) - zW_1\end{aligned} \tag{120}$$

Subscript *o* denotes midplane values. Strains can be expanded in terms of their midplane values and curvatures as

$$\varepsilon_{ij} = \varepsilon_{ij}^o - z\kappa_{ij} \tag{121}$$

Substituting these approximations back into Equation (118) and using Equation (121), the strains and curvatures can be expressed as

$$\begin{aligned}
\varepsilon^{o}{}_{xx} &= \tfrac{1}{2}(\phi y)^2, \quad \kappa_{xx} = K \\
\varepsilon^{o}{}_{yy} &= V_{o,y}, \qquad \kappa_{yy} = V_{1,y} \\
\varepsilon^{o}{}_{zz} &= -W_1, \qquad \kappa_{zz} = 0 \\
\gamma^{o}{}_{xy} &= U_{0,y}, \qquad \kappa_{xy} = 2\phi + U_{1,y} \\
\gamma^{o}{}_{xz} &= -U_1, \qquad \kappa_{xz} = 0 \\
\gamma^{o}{}_{yz} &= W_{0,y} - V_1, \qquad \kappa_{yz} = 0 \\
K &= \overline{\rho}/s
\end{aligned} \tag{122}$$

The curvature of a helix is defined as $\overline{\rho}/s$, which is also the curvature of the laminate, *K*. This set of strains and curvatures precludes anticlastic coupling. Anticlastic coupling is included through the $V_{1,y}$ term.

The equilibrium equations are derived from the principle of virtual work. It is assumed that a pure moment is applied to the strip. Neglecting the through-the-thickness stresses, the principle of virtual work is expanded to

$$\int_{-w/2}^{w/2}\int_{-h/2}^{h/2}\left(\sigma_{xx}\delta\varepsilon_{xx} + \sigma_{yy}\delta\varepsilon_{yy} + \sigma_{yz}\delta\gamma_{yz} + \sigma_{xz}\delta\gamma_{xz} + \sigma_{xy}\delta\gamma_{xy}\right)dxdy - P\delta K = 0 \tag{123}$$

Note that as per CLT

$$\begin{aligned}
&\left(N_{xx}, N_{yy}, Q_y, Q_x, N_{xy}, M_{xx}, M_{yy}, M_{xy}\right) \\
&\quad = \int_{-h/2}^{h/2}\left(\sigma_{xx}, \sigma_{yy}, \sigma_{yz}, \sigma_{xz}, \sigma_{xy}, z\sigma_{xx}, z\sigma_{yy}, z\sigma_{xy},\right)dz
\end{aligned} \tag{124}$$

Using Equation (121) in Equation (123) and making use of Equation (124), the following equilibrium equations are arrived at

$$N_{yy} = Q_y = N_{xy} = M_{yy} = 0 \tag{125}$$

$$M_{xy,y} - Q_x = 0 \tag{126}$$

$$\int_{-w/2}^{w/2} N_{xx} y^2 \phi - 2M_{xy} dy = 0 \tag{127}$$

$$\int_{-w/2}^{w/2} -M_{xx} dy = P \tag{128}$$

The constitutive relationship follows from Equation (2) and

$$\begin{Bmatrix} Q_y \\ Q_x \end{Bmatrix} = \begin{bmatrix} A_{44} & A_{45} \\ A_{45} & A_{55} \end{bmatrix} \begin{Bmatrix} \gamma_{yz}^o \\ \gamma_{xz}^o \end{Bmatrix} \tag{129}$$

Eliminating hygrothermal considerations, assuming a symmetric stacking sequence, i.e., B_{ij}=0, and making use of Equation (125), the constitutive law reduces to

$$\begin{Bmatrix} M_{xx} \\ M_{yy} \\ M_{xy} \end{Bmatrix} = \begin{bmatrix} D_{11} & D_{12} & D_{16} \\ D_{12} & D_{22} & D_{26} \\ D_{16} & D_{26} & D_{66} \end{bmatrix} \begin{Bmatrix} -K \\ -V_{1,y} \\ -2\phi - U_{1,y} \end{Bmatrix} \tag{130}$$

$$N_{xx} = C_1 \tfrac{1}{2} (\phi y)^2 \tag{131}$$

$$Q_x = -C_2 U_1 \tag{132}$$

where

$$C_1 = \frac{A_{11}A_{22}A_{66} - A_{11}A_{26}^2 - A_{12}^2 A_{66} - A_{16}^2 A_{22} + 2A_{12}A_{16}A_{26}}{A_{22}A_{66} - A_{26}^2}; C_2 = A_{55} - \frac{A_{45}^2}{A_{44}} \tag{133}$$

Note that

$$V_{1,y} = -\frac{D_{12}K + D_{26}(2\phi + U_{1,y})}{D_{22}} \tag{134}$$

Equation (126) with Equations (130) and (132) give that

$$k_3 U_{1,yy} + C_2 U_1 = 0\,,\ k_3 = D_{66} - \frac{D_{26}^2}{D_{22}} \tag{135}$$

Solving Equation (135) using the boundary condition that

$$M_{xy}\Big|_{y=\pm w/2} = 0 \tag{136}$$

gives the warping function as

$$U_1 = \frac{Kk_2 + 2\phi k_3}{gk_3 \cosh(gw/2)} \sinh(gy), \; g = \sqrt{\frac{C_2}{k_3}} \tag{137}$$

Equation (127) is solved using Equations (130) and (131) to give

$$K = -\frac{C_1(\frac{w}{2})^4 \phi^3 + 40k_3k_4\phi}{20k_2k_4}, \; k_2 = D_{16} - \frac{D_{12}D_{26}}{D_{22}}, \; k_4 = 1 - \frac{\tanh(gw/2)}{gw/2} \tag{138}$$

Finally, Equations (130), (137), and (138) are combined into Equation (128) to yield an equation for P in terms of the twist rate φ as

$$P = b_1\phi + b_2\phi^3, \; b_1 = 2w\left(k_2 - \frac{k_1k_3}{k_2}\right), \; b_2 = \frac{1}{640}C_1w^5\left(\frac{-k_1k_3 + k_2^2(1-k_4)}{k_2k_3k_4}\right),$$
$$k_1 = D_{11} - \frac{D_{12}^2}{D_{22}} \tag{139}$$

This model was verified using a finite element model that replicates the pure bending loading conditions. Figure 42 plots the nonlinear and FEM model predictions for all laminates that were manufactured in the loading ranges they were tested. There is less than 1% error between the two predictions.

The nonlinear model predictions are included with the test data in Figure 34 through Figure 39 for the five- through ten-ply specimens, respectively. All discrepancies can be accounted for when considering the variation in material and geometric properties and/or the difference in boundary conditions between the test setup and pure bending.

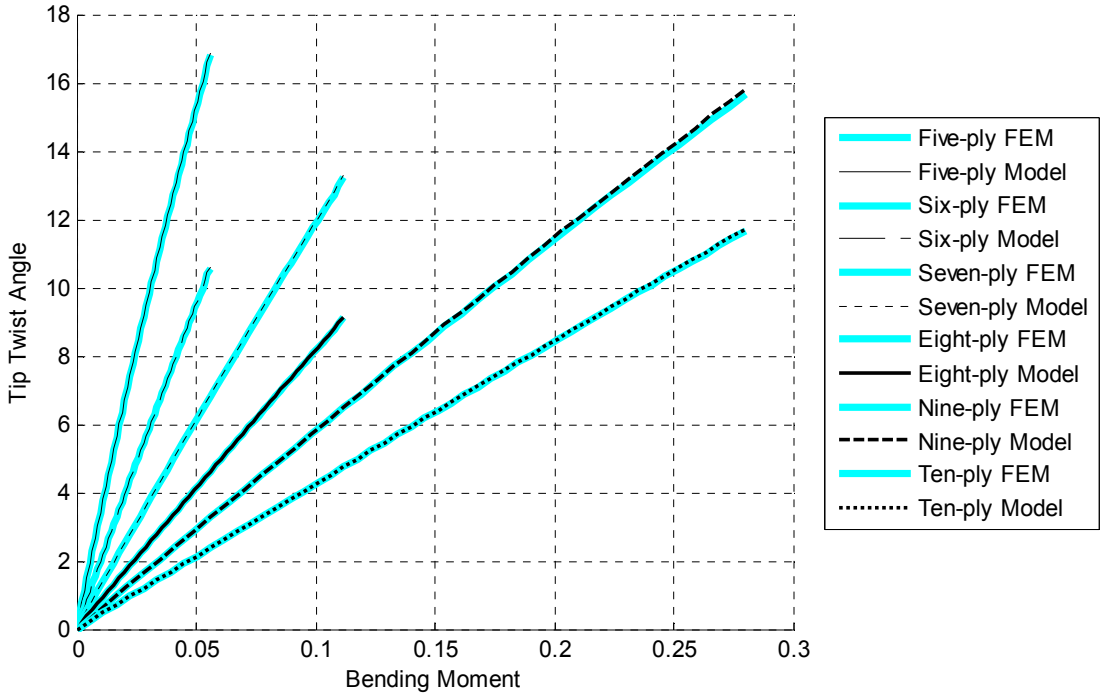

Figure 42. Comparison of Nonlinear and FEM Models

6.4.3 FEM Prediction

Finite element models were created for each of the optimal hygrothermally stable five- through ten-ply laminates in Table 11, Condition B, using ABAQUSTM 6.8-1. The specimens were made to dimensions of 2.54cm by 22.86cm (1.0" by 9.0") using measured thicknesses and material properties to recreate the manufactured specimens as closely as possible. A 9-node, doubly curved, thin-shell, reduced-integration element type was selected with six degrees of freedom per node (S8R), and 600 elements were used. One end of the modeled strip was clamped, and a transverse shell edge load was applied to the other end. Nonlinear geometry was selected.

The rotation of the midpoint along the tip edge about the x-axis was extracted as a function of time and plotted as a function of load with the test data in Figure 34 through Figure 39 for the five- through ten-ply laminates, respectively. There is good agreement between the FEM data and test data. Thickness variations are most likely responsible for deviations between the data and models.

6.4.4 Robustness of Coupling

The practicality of the stacking sequences developed herein is limited to their insensitivity to small errors in layup typically seen during the manufacturing process. To this end, a Monte Carlo simulation was performed to evaluate the loss of coupling due to small perturbations in ply angle over the uniform distribution $\theta_k \pm 2°$, assumed to be typical of hand-layup error. The optimal bend-twist coupled six-ply stacking sequence was chosen, as given in Table 11, Condition B. A set of 10^6 samples was taken from the distribution, and ζ was calculated. Figure 43 gives a normalized histogram of the error from that of the optimized stacking sequence. It is expected that 0% error is the upper bound since it has been established that the stacking sequence used also produces maximum bend-twist coupling from all six-ply laminates. The lower bound of the error is around -4%.

For comparison, the robustness of the optimal bend-twist coupled six-ply laminates under the constraints of Condition A and unidirectionality were considered. These stacking sequences are given in Table 11, columns "Condition A" and "Unidirectional," respectively. The same simulation was performed as for the optimal stacking sequence constrained to Condition B. Normalized histograms showing the

distribution of error are provided in Figure 44 and Figure 45 for Condition A- and unidirectional-constrained stacking sequences. The deviation in coupling for the stacking sequence constrained to Condition A is contained within 10% of its nominal value. It should be noted that the coupling can be higher because the perturbed stacking sequences are not constrained to hygrothermal stability. The deviation in coupling for the unidirectional stacking sequence is contained in the range [-7%, 0%]. The nonexistence of laminates with higher coupling than produced by the unperturbed stacking sequence suggests that the optimal stacking sequence corresponds to a local extremum of δ_{16}.

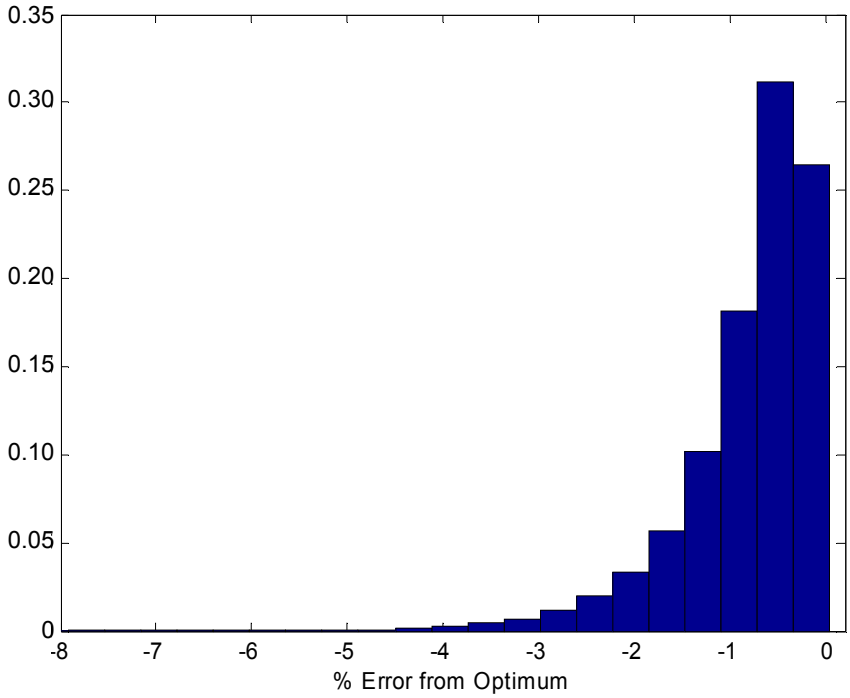

Figure 43. Distribution of Error in Coupling from Optimal Hygrothermally Stable Bend-twist Coupled Stacking Sequence; 10^6 Cases

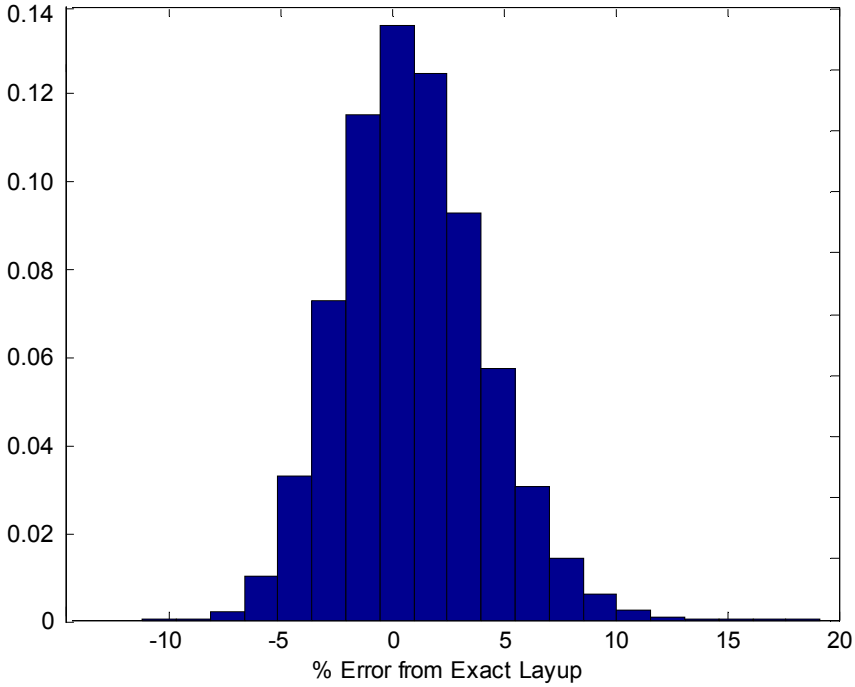

Figure 44. Distribution of Error in Coupling from Stacking Sequence Constrained to Condition A; 10^6 Cases

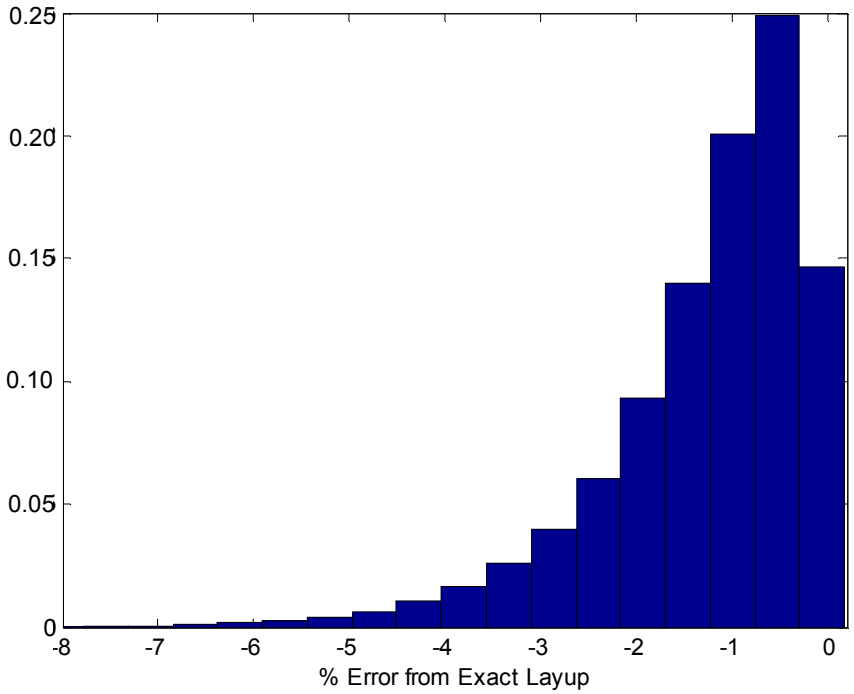

Figure 45. Distribution of Error in Coupling from Stacking Sequence Constrained to be Unidirectional; 10^6 Cases

6.4.5 Analysis

A summary of the testing data from all laminates is presented in Figure 46 with error bars showing one standard deviation and the FEM and nonlinear model predictions. As expected, the five-ply laminate produces the most coupling at a loading of 0.56N, a 39.7% increase over the six-ply laminate, which has the next-highest coupling, and a 505% increase in coupling over the 10-ply laminate, which has the least coupling.

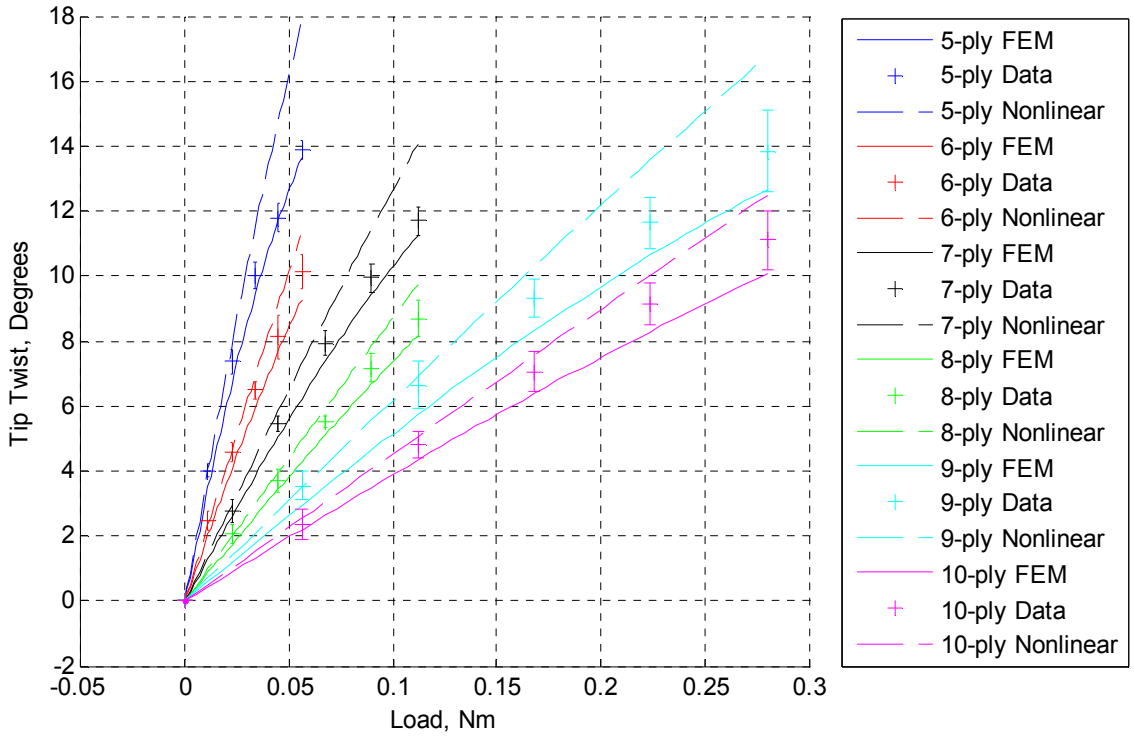

Figure 46. Summary of All Bend-twist Coupling Results

As the number of plies increases, the coupling tends to decrease. This follows the same trend as extension-twist coupling, and the same reasoning applies; as the laminates become thicker, the bending and torsional stiffnesses become greater. One explanation for nonlinear effects is that a transverse load is being used to approximate pure bending.

As the load is increased, the direction of application develops an in-plane component, and the relative magnitude of its transverse component decreases. Another explanation is that increased warping is associated with increased twisting. The warping effectively increases the stiffness of the specimen. This is accounted for in the nonlinear model by the cubic term.

6.5 Free Vibration Modes

An investigation of the natural frequencies and free vibration modes of bend-twist coupled composite laminates was conducted using a laser vibrometer. The optimal six-ply hygrothermally stable laminate that had been manufactured and tested for bend-twist coupling under static loading was chosen for this investigation, and a reflective tape with negligible stiffness was affixed to one side of all four specimens. The specimens were clamped to a vibrating table capable of producing complex waveforms. See Figure 47 for a photograph of the test setup.

For each test, the laser was focused, and a mesh of 105 data acquisition points was used, with five points across the width and 21 along the length. A random excitation was input to the vibrating table, and an accelerometer verified its motion. The test required approximately 20 minutes to run, after which a frequency response function was used to identify the first ten natural frequencies. For each frequency, the mode shape was extracted. The six-ply finite element model used to validate the bend-twist test data was analyzed for its natural frequencies.

Table 14 provides the natural frequencies from both the vibration test and FEM predictions. There is good agreement among the data and the model. The vibration test

was unable to identify the fourth mode. The error between the FEM analysis and the data is contained to within 10%. This could be explained by variations in material properties and measured geometric parameters.

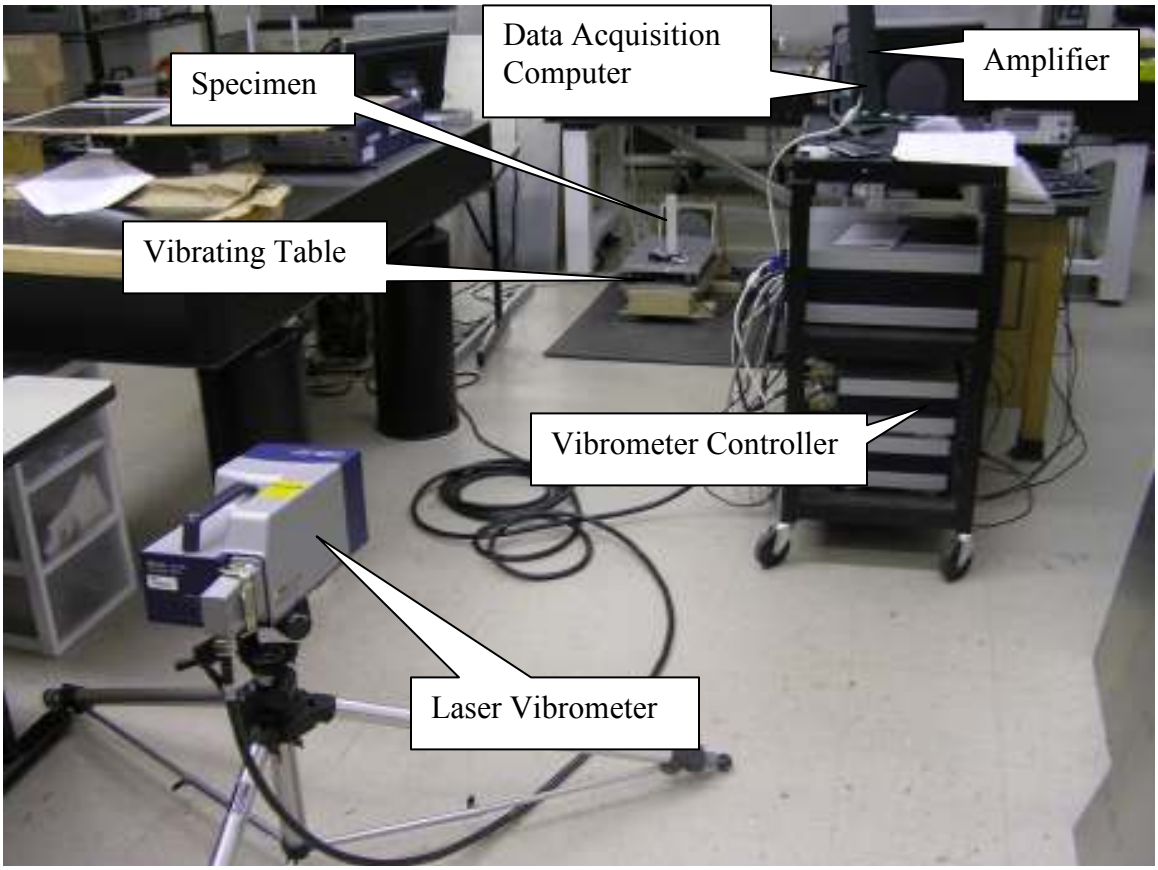

Figure 47. Laser Vibrometer Test Setup

Figure 48 shows the mode 1 to 3 and 5 to 8 shapes corresponding to the first eight natural frequencies given in Table 14 as identified from laser vibrometry. Each mode shape has been multiplied by a scaling factor to make its displacement easily identifiable. It is apparent from part (g) of the figure that five bending modes and two torsion modes are included. These modes are consistent with those expected from a cantilevered beam, but the coupling is also apparent in each mode. For example, in part (d) the axis of

bending is not perpendicular to the length of the specimen, nor is it constant along its length.

Table 14. Natural Frequencies of Six-ply Optimal Bend-twist Coupled Laminate

Mode	FEM (Hz)	Specimen 1 (Hz)	Specimen 2 (Hz)	Specimen 3 (Hz)	Specimen 4 (Hz)	Average of Specimens (Hz)
1	8.9	7.5	7.5	7.5	7.5	7.5
2	55.4	55	52.5	55	55	54.4
3	156.5	155	157.5	160	157.5	157.5
4	171.5	-	-	-	-	-
5	313.5	312.5	305	317.5	315	312.5
6	358.8	392.5	387.5	392.5	387.5	390.0
7	483.5	467.5	462.5	465	462.5	464.4
8	563.6	545	535	555	547.5	545.6

The fourth mode shape was extracted from the FEM prediction and is provided in Figure 49. This mode is a pure torsion mode which may have not been excited by the vibrating table. Good agreement was seen between the laser vibrometry and FEM predictions for all other modes except mode 6. Figure 50 shows the FEM prediction of the sixth mode shape, which is a shearing mode. One explanation for its appearance in the laser vibrometry test is coupling between the bending and shearing deformation modes. Theoretically, this coupling should not exist in a symmetric stacking sequence, but errors in manufacturing may produce a small amount of this coupling.

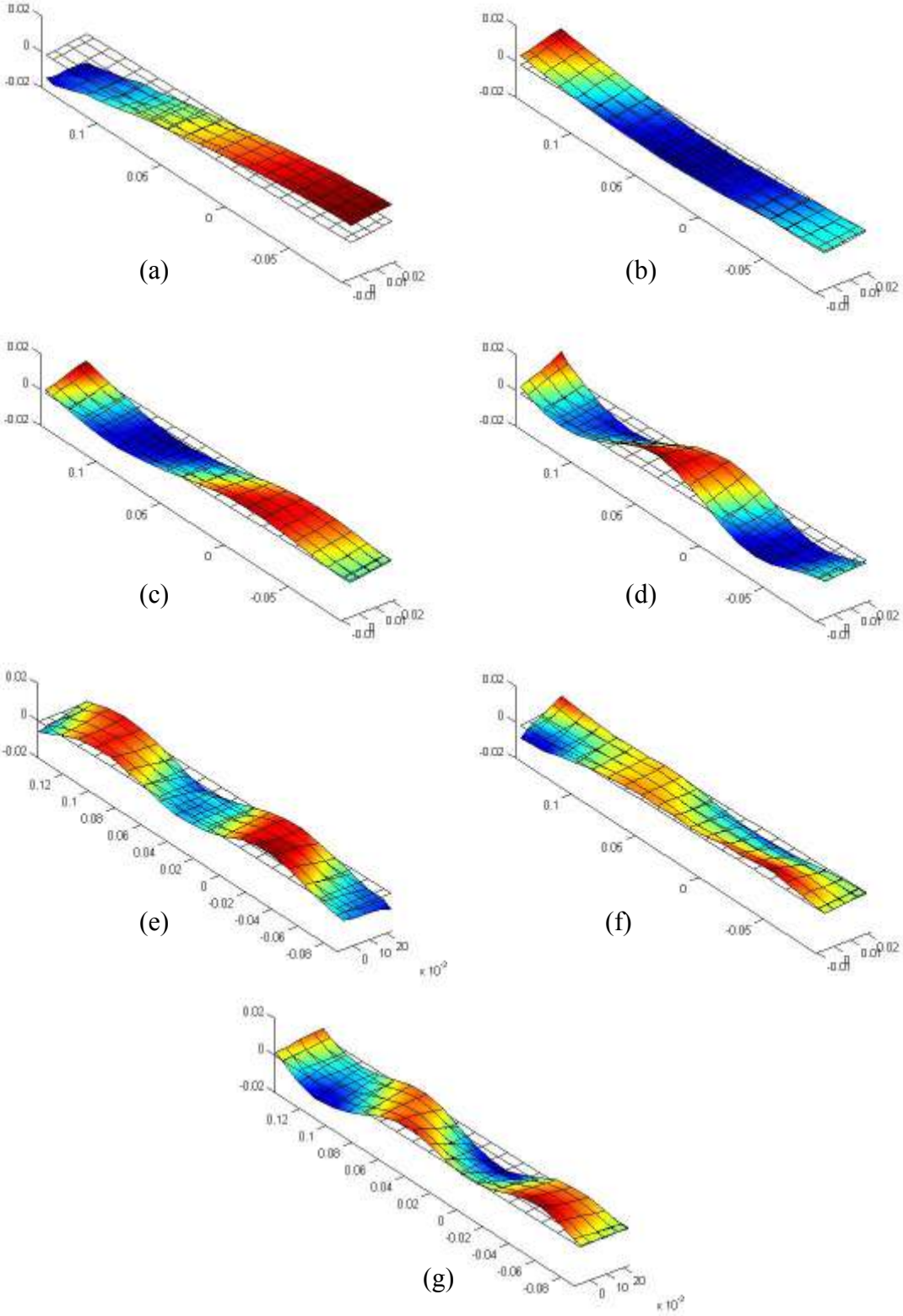

Figure 48. Mode 1 to 3 and 5 to 8 Shapes of the Optimal Six-ply Bend-twist Coupled Laminate

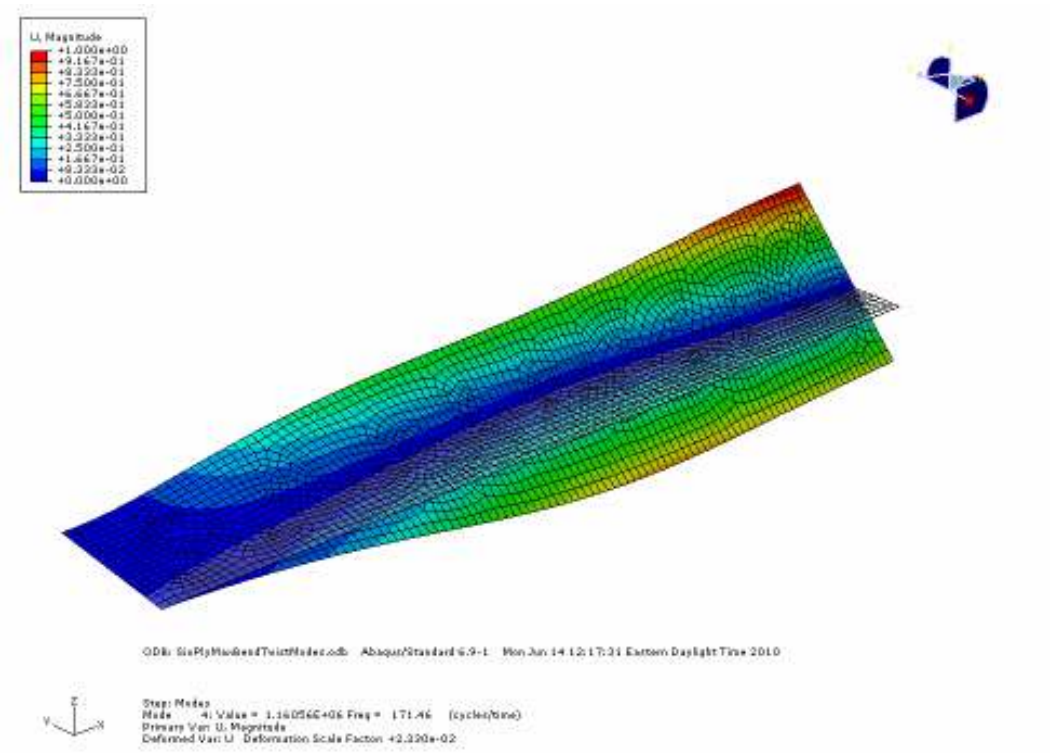

Figure 49. Mode 4 of the Optimal Six-ply Bend-twist Coupled Laminate from FEM

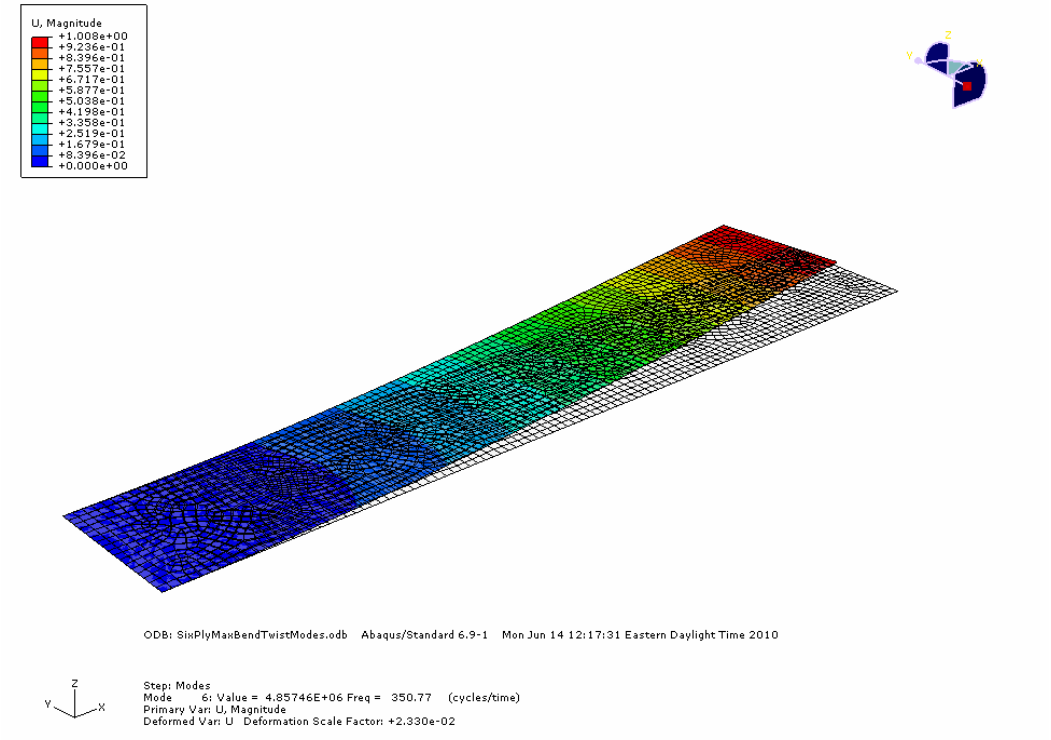

Figure 50. Mode 6 of the Optimal Six-ply Bend-twist Coupled Laminate from FEM

CHAPTER 7

OTHER COUPLINGS

Now that techniques have been established to investigate optimal couplings, a wider range of couplings can be explored, such as anticlastic, extension-bend, and shear-twist couplings. The main purpose of this chapter is to gain insight into these couplings and lay the foundation for further investigation.

There are some unique challenges in isolating a given coupling. For example, the extension-twist coupled laminates by definition have a non-zero β_{16} term, but all optimal laminates also have a non-zero β_{26} term with $\beta_{26} = -\beta_{16}$. The optimal bend-twist coupled laminates are symmetric, so there is no coupling between in-plane and out-of-plane deformation modes, but in all cases there exists anticlastic coupling. These ancillary couplings have physical significance and can have either a complementary or parasitic effect on the response of a composite structure. Therefore, it is important to examine what these couplings are and establish how to evaluate their significance in a composite laminate.

In this chapter, anticlastic, extension-bend labeled in the same direction, extension-bend labeled in orthogonal directions, and shear-twist couplings are quantified; then a constrained optimization is performed to identify the hygrothermally stable stacking sequence with the most coupling for a laminate with a set number of plies.

7.1 Optimality Parameters

For all of the subsequent objective function developments, CLT is used with the same assumption for extension-twist coupling, namely that the resulting laminate will be flat and the useful deformation range of these laminates is within a geometrically linear theory. Anticlastic coupling is quantified by expressing the bending curvature about one in-plane axis as a function of the moment resultant about its orthogonal in-plane axis. From Equation (90), the curvature about the *y*-axis can be calculated as

$$\kappa_{yy} = \delta_{12} M_{xx} + \kappa_{xx}^{(T,H)} \tag{140}$$

Since the optimizer searches hygrothermally stable laminates, the non-mechanical curvature in Equation (140) is zero, resulting in an objective function given by

$$g\left(\{\theta_k : k = 1 \ldots n\}\right) = -\delta_{12}^2 \tag{141}$$

Extension-bend coupling labeled for the same axes is quantified by expressing the bending curvature labeled for one in-plane axis as a function of the axial force resultant along the same axis, i.e., κ_{xx} from N_{xx} or κ_{yy} from N_{yy}. From Equation (90), the curvature κ_{xx} can be calculated as

$$\kappa_{xx} = \beta_{11} N_{xx} + \kappa_{xx}^{(T,H)} \tag{142}$$

Since the optimizer searches hygrothermally stable laminates, the non-mechanical curvature in Equation (142) is zero, resulting in an objective function given by

$$g\left(\{\theta_k : k = 1 \ldots n\}\right) = -\beta_{11}^2 \tag{143}$$

Extension-bend coupling labeled for orthogonal axes is quantified by expressing the bending curvature labeled for one in-plane axis as a function of the axial force resultant along the orthogonal in-plane axis, i.e., κ_{xx} from N_{yy} or κ_{yy} from N_{xx}. From Equation (90), the curvature κ_{yy} can be calculated as

$$\kappa_{yy} = \beta_{12} N_{xx} + \kappa_{xx}^{(T,H)} \tag{144}$$

Since the optimizer searches hygrothermally stable laminates, the non-mechanical curvature in Equation (144) is zero, resulting in an objective function given by

$$g\left(\{\theta_k : k = 1 \ldots n\}\right) = -\beta_{12}^2 \tag{145}$$

Shear-twist coupling is quantified by expressing the twisting curvature as a function of the in-plane shearing force resultant. From Equation (90), the curvature about the *x*-axis can be calculated as

$$\kappa_{xy} = \beta_{66} N_{xy} + \kappa_{xy}^{(T,H)} \tag{146}$$

Since the optimizer searches hygrothermally stable laminates, the non-mechanical curvature in Equation (146) is zero, resulting in an objective function given by

$$g\left(\{\theta_k : k = 1 \ldots n\}\right) = -\beta_{66}^2 \tag{147}$$

7.2 Implementation

The sequential quadratic programming (SQP)[32] implementation in MATLAB 7™ was used to perform the stacking sequence optimization numerically. For anticlastic coupling, three sets of conditions were used consecutively during the optimization of a given laminate: no constraint on hygrothermal stability, the constraints of Condition A, and the constraints of Condition B. For the two extension-bend and shear-twist couplings, optimizations were performed with the conditions of no constraint on hygrothermal stability and the constraints of Condition A only. The optimizer was initialized with a stacking sequence sampled from a uniform random number generator. The existence of suboptimal local minima required several thousand optimization runs to

reach the global optimum. The material properties of the T300/976 graphite/epoxy material system were used, and are provided in Table 5.

7.3 Results

For anticlastic coupling, optimal hygrothermally stable two- through ten-ply stacking sequences are provided in Table 15. Globally optimal two- through ten-ply stacking sequences are provided in Table 16. The globally optimal stacking sequences have only combinations of ±45°. In all cases the optimal hygrothermally stable laminates meet Condition B, and therefore, have no coupling between in-plane and out-of-plane deformation modes. There is a general trend that with increasing ply count, the level of coupling amongst hygrothermally stable laminates approaches that of the global optima. The eight-ply globally optimal stacking sequence also meets the constraints of both Condition A and Condition B, and the seven- through ten-ply stacking sequences subject to Condition B are also globally optimal.

Table 15. Optimal Anticlastic Coupled Stacking Sequences with Various Constraints

n	Condition A (°)	$\lvert\delta_{12}\rvert$	Condition B (°)	$\lvert\delta_{12}\rvert$
2	N/A		$[-45]_s$	12
3	N/A		$\left[45/-\overline{45}\right]_s$	4.7
4	$\left[\pm 45\right]_s$	2.4	$\left[\pm 45\right]_s$	2.4
5	$\left[51.3/-53.2/-\overline{1}\right]_s$	1.1	$\left[\pm 45/-\overline{45}\right]_s$	1.3
6	[-48.2 / 49.2 / 0.1 / 89.9 / 40.8 / -41.8]	0.56	$[45/-45_2]_s$	0.79
7	$\left[49.6/-48.8/-50.9/-1/50.9/48.8/-49.6\right]$	0.47	$[45/-45_2/45_3/-45]$	0.51
8	$[\pm 45/(\mp 45)_2/\pm 45]$	0.34	$[\pm 45/(\mp 45)_2/\pm 45]$	0.34
9	[47.2 / -47.8 / -48.7 / 50.6 / 0 / -50.6 / 48.7 / 47.8 / -47.2]	0.23	$\left[\mp 45/\pm 45/45/\pm 45/\mp 45\right]$	0.24
10	[44.2 / -44.0 / -43.6 / 42.7 / 89.9 / -0.1 / -47.3 / 46.4 / 46.0 / -45.8]	0.16	$\left[\pm 45/\mp 45/45_2/\mp 45/\pm 45\right]$	0.17

Table 16. Globally Optimal Anticlastic Coupled Stacking Sequences

n	Unconstrained (°)	$\lvert\delta_{12}\rvert$
2	$[\pm 45]$	18
3	$[45_2 / -45]$	5.3
4	$\left[\pm 45\right]_2$	2.7
5	$\left[\pm 45 / 45 / \pm 45\right]$	1.4
6	$[45 / -45_2 / 45_2 / -45]$	0.81
7	$[45 / -45_2 / 45_3 / -45]$	0.51
8	$[\pm 45 / (\mp 45)_2 / \pm 45]$	0.34
9	$\left[\mp 45 / \pm 45 / 45 / \pm 45 / \mp 45\right]$	0.24
10	$\left[\pm 45 / \mp 45 / 45_2 / \mp 45 / \pm 45\right]$	0.17

For extension-bend coupling about the same axis, the globally optimal and Condition A-constrained stacking sequences are provided in Table 17. All the globally optimal stacking sequences have the outermost plies on one side near 0° and the rest of the plies near 90°. This follows from a consideration that nearly all of the load will be carried by the plies near 0°, but their offset from the midplane will produce an eccentric load and subsequently a moment in the laminate. The hygrothermally stable laminates all have roughly a 50% reduction in coupling.

For extension-bend coupling about orthogonal axes, the globally optimal and Condition A-constrained stacking sequences are provided in Table 18. Generally, the globally optimal stacking sequences have the outermost plies on one side near 80° and plies oriented near ±45° on the other side. The ±45° plies rotate the extension to the orthogonal in-plane axis, and the plies near 80° offset this extension from the midplane to create an eccentric load and consequently a moment in the laminate. The hygrothermally stable laminates all have roughly a 20% reduction in coupling.

Table 17. Hygrothermally Stable and Globally Optimal Extension-bend Coupled Laminates, Same Axis

n	Unconstrained (°)	$\lvert\beta_{11}\rvert$, $\bullet 10^{-4}$	Condition A (°)	$\lvert\beta_{11}\rvert$, $\bullet 10^{-4}$
2	[0 / 90]	9.9	N/A	-
3	[0 / 90_2]	7.2	N/A	-
4	[0 / 90_3]	4.4	N/A	-
5	[0 / 90_4]	2.9	[59.6 / -34.9 / 86.2 / -29.9 / 25.6]	1.3
6	[0 / 90_5]	2.0	[89.1 / 1.1 / 30.7 / -46.5 / -54.6 / 47.8]	1.1
7	[-17.3 / 18.6 / 88.5 / 87.6 / 87.3 / -86.7 / -83.5]	1.5	[79.8 / -30.8 / 17.7 / 44.0 / -45.9 / -46.5 / 53.9]	0.73
8	[84.2 / 85.9 / -89.0 / -88.0 / -88.0 / -88.5 / -15.1 / 15.8]	1.1	[87.5 / 40.0 / -4.7 / -34.5 / -44.7 / 47.6 / -53.3 / 49.6]	0.60
9	[20.6 / -4.5 / -37.6 / -89.7 / -88.8 / -84.6 / -86.2 / 84.7 / 82.9]	0.90	[80.4 / 52.8 / 5.4 / -16.3 / -39.8 / -51.3 / -53.3 / 49.7 / 48.6]	0.48
10	[-83.0 / -84.6 / 87.7 / 86.6 / 86.5 / 88.4 / 88.9 / 27.4 / 1.3 / -22.7]	0.73	[68.0 / -71.7 / 6.6 / -10.9 / -38.9 / 44.7 / 45.0 / -50.1 / -51.8 / 50.5]	0.37

Table 18. Hygrothermally Stable and Globally Optimal Extension-bend Coupled Laminates, Orthogonal Axes

n	Unconstrained (°)	$\lvert\beta_{12}\rvert$, $\bullet 10^{-4}$	Condition A (°)	$\lvert\beta_{12}\rvert$, $\bullet 10^{-4}$
2	[85.3 / 49.7]	2.7	N/A	-
3	[44.4 / -47.8 / -14.6]	3.6	N/A	-
4	[84.0 / 18.9 / 44.3 / -45.3]	2.6	N/A	-
5	[80.7 / 21.0 / 43.5 / 45.7 / -46.5]	1.8	[74.2 / -49.1 / 14.0 / -40.4 / 46.0]	1.2
6	[80.6 / 31.7 / 5.0 / 43.1 / 44.2 / -46.2]	1.2	[89.1 / 1.5 / 29.5 / -48.0 / -54.8 / 47.1]	1.1
7	[79.7 / 32.0 / 11.9 / 42.9 / 44.2 / 44.7 / -47.3]	9.4	[79.8 / -31.1 / 17.8 / 44.1 / -44.8 / -47.1 / 54.0]	0.73
8	[81.0 / 67.9 / 19.6 / -4.4 / 41.9 / -39.9 / -45.1 / 44.7]	0.72	[87.7 / 39.4 / -4.5 / -33.9 / -47.9 / 46.3 / -52.3 / 49.8]	0.60
9	[80.3 / 69.5 / 22.4 / 5.0 / 41.2 / 43.2 / -42.0 / -46.1 / 44.9]	0.58	[77.2 / 11.8 / 59.4 / -22.8 / -40.3 / -45.5 / -48.8 / 49.2 / 47.8]	0.47
10	[80.4 / 71.6 / 28.5 / 12.9 / -9.9 / 42.6 / 43.6 / -42.5 / -46.0 / 44.8]	0.47	[69.3 / -72.9 / 0.7 / -4.1 / -33.2 / 52.4 / -44.3 / 50.5 / 51.7 / -49.5]	0.37

Finally, for shear-twist coupling about orthogonal axes, the globally optimal and Condition A-constrained stacking sequences are provided in Table 19. The globally optimal stacking sequences generally have the outermost plies on one side near 0°, the outermost plies on the other side oriented near ±45°, and plies near the midplane oriented near 90°. Twist is generated from a shear action in one direction above the midplane and in the other direction below the midplane. The shear resultant produces a shear action in one direction on the side with 0° plies, but the ±45° switch the direction of the shear action on the other side of the midplane. The 90° plies have low shear and torsional stiffness. The hygrothermally stable laminates all have roughly 10% less in coupling.

Table 19. Hygrothermally Stable and Globally Optimal Shear-twist Coupled Laminates

n	Unconstrained (°)	$\lvert\beta_{66}\rvert$, $\bullet 10^{-4}$	Condition A (°)	$\lvert\beta_{66}\rvert$, $\bullet 10^{-4}$
2	[85.3 / 49.7]	10.8	N/A	-
3	[33.2 / -12.4 / -5.5]	10.0	N/A	-
4	[-35.2 / 30.4 / 87.9 / 3.0]	7.4	N/A	-
5	[-43.5 / 46.7 / 4.6 / 88.8 / 0.2]	5.3	[-36.2 / 33.9 / 67.5 / -78.9 / -8.8]	3.4
6	[42.9 / -46.4 / -6.3 / -88.8 / 89.9 / 0.4]	3.8	[87.5 / 8.6 / 4.6 / -73.3 / -48.8 / 44.4]	3.5
7	[-42.6 / 46.8 / 10.4 / 88.7 / 89.8 / -89.6 / -0.5]	2.8	[81.9 / 0.6 / 0.7 / 86.6 / -61.6 / -16.5 / 54.9]	2.4
8	[40.8 / -48.8 / -21.2 / -89.7 / 89.9 / 89.8 / -0.1 / 0.6]	2.1	[42.2 / -15.7 / -44.2 / 86.5 / 86.4 / 2.1 / 85.7 / 1.6]	1.9
9	[41.2 / -49.9 / -32.1 / 89.9 / 89.9 / 89.8 / 89.8 / 0.3 / 0.9]	1.7	[87.6 / 2.8 / 88.6 / -0.7 / -0.8 / 85.1 / -17.9 / -65.8 / 49.6]	1.6
10	[34.4 / 46.0 / -47.6 / -23.9 / -8.9 / -89.3 / -89.7 / -1.0 / 89.9 / 0.5]	1.4	[86.8 / -0.1 / 1.3 / -88.9 / 0.6 / -88.6 / 83.7 / -8.7 / -46.1 / 43.5]	1.3

7.4 Design Space

To illustrate the nonlinearities of the design space of coupled laminates, Figure 51 plots the level of anticlastic coupling for a two-ply laminate; darker regions indicate more

coupling. Also plotted are the constraints of Condition B, indicated by the gray transparent lines. Darker lines indicate more constraints met. The darkest line follows the path $\theta_1 = \theta_2$. This is known to be the only two-ply solution to Condition B, as shown in Equation (67).

The line corresponding to meeting all constraints encounters the darkest region, i.e., highest coupling, near $\theta_1 = \theta_2 = \pm 45°$, indicating this is the optimal hygrothermally stable solution. This agrees with the two-ply stacking sequence in Table 15, Condition B. These points are also local maxima of the coupling. The global maximum is also apparent from Figure 51. By inspection, the point $\theta_1 = -\theta_2 = \pm 45°$ corresponds to the darkest region on the plot. This agrees with the two-ply stacking sequence in Table 16. While this is a convenient way to show the global and hygrothermally stable optima for a two-ply laminate, it is clear that this representation would be intractable for laminates with a greater number of plies.

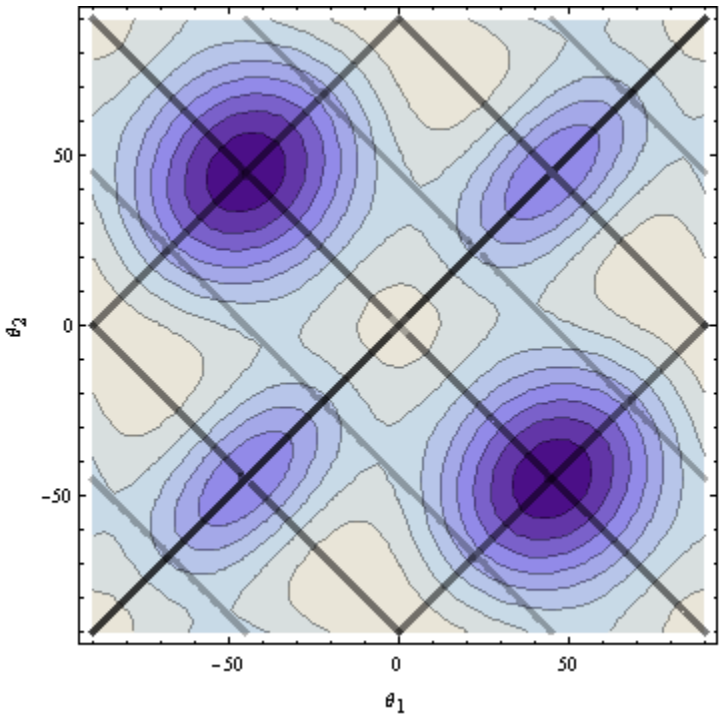

Figure 51. Design Space for Anticlastic Coupling in a Two-ply Laminate

CHAPTER 8

CONCLUSIONS

The first major discovery in this work is the necessary and sufficient conditions for hygrothermal stability. These have been classified into Condition A and Condition B. Condition A enforces equal non-mechanical axial stress resultants and zero non-mechanical shear and moment resultants. Condition B enforces the coupling stiffness matrix to be identically equal to zero. The material-independent equations that satisfy these conditions are as follows. For Condition A:

$$\sum_{k=1}^{n} k\cos 2\theta_k = \sum_{k=1}^{n} k\sin 2\theta_k = \sum_{k=1}^{n} \cos 2\theta_k = \sum_{k=1}^{n} \sin 2\theta_k = 0,$$

and for Condition B:

$$\sum_{k=1}^{n} (2k-n-1)\cos 2\theta_k = \sum_{k=1}^{n} (2k-n-1)\sin 2\theta_k$$
$$= \sum_{k=1}^{n} (2k-n-1)\cos 4\theta_k = \sum_{k=1}^{n} (2k-n-1)\sin 4\theta_k = 0$$

The second important result is the minimum number of plies necessary to satisfy hygrothermal stability. Symmetric laminates meet Condition B, so a one-ply laminate would be hygrothermally stable. For asymmetric laminates to meet Condition A, a minimum of five plies is required, and only one unique family exists, given by $[76.3 / -33.6 / 0 / 33.6 / -76.3]$ and its rigid rotations. For a given material system, this is the thinnest flat hygrothermally stable laminate that is capable of producing extension-twist coupling. The smallest asymmetric laminates meeting Condition B is a six-ply laminate, for example [6.2° / -20.1° / 30° / -30° / 20.1° / -6.2°]. If whole angles are

desired when creating an asymmetric laminate with no coupling between in-plane and out-of-plane deformation modes, then a minimum of seven plies is needed, given by the stacking sequence $[\theta_1 / \theta_2 / \theta_2 / \theta_3 / \theta_1 / \theta_1 / \theta_2]$.

The third original contribution of this work is the hygrothermally stable laminates optimized for extension-twist, bend-twist, anticlastic, both types of extension-bend, and shear-twist coupling for two- through ten-ply laminates, as possible. The five-ply through ten-ply optimal extension-twist and bend-twist coupled laminates have been manufactured and tested to demonstrate the achievable coupling. Nonlinear models and FEM analysis have verified the expected response. At a loading of 2224N, the new families of extension-twist coupled laminates produce as much as 59% more coupling than previous state-of-the-art. The optimal hygrothermally stable bend-twist coupled laminates are symmetric but not unidirectional. This should reduce their susceptibility to splitting failure.

CHAPTER 9

RECOMMENDATIONS

This work can be advanced in several directions. Further analysis that can be performed on laminates with optimal coupling involves residual stresses, multiple materials systems, and damage tolerance. Residual stresses developed during the curing process must be investigated prior to application. Classical Lamination Theory can be used to evaluate the internal stresses that develop during cooling.

The optimizations performed in this work were for laminates created from only one material system. Hybrid laminates made from several materials may provide extra design variables needed to achieve higher levels of coupling. The hygrothermal stability conditions should be expanded to account for several materials. A study of the damage tolerance of coupling-optimized stacking sequences should be performed. All optimal bend-twist coupled laminates have similar stacking sequences, but optimal extension-twist coupled laminates vary significantly, especially between even- and odd-ply laminates.

To improve upon the optimal laminates, the optimization routine can be made more robust. Currently, several thousand random initializations are needed to provide confidence in the global solution. A different optimization routine designed for global convergence would improve confidence and perhaps take less computational effort. Ant Colony Optimization (ACO) and genetic algorithms are two such global search algorithms that may streamline the optimization procedure. A current investigation is being performed into the ability of ACO to identify globally optimal hygrothermally

stable extension-twist coupled laminates.[36] Preliminary results confirmed the laminates identified in this work are indeed globally optimal. A hybrid approach has the potential to produce the best results; ACO will provide confidence in the global solution while SQP can achieve the desired tolerances on coupling and constraints.

The optimal designs achieved in this work can be used to form closed sections by wrapping them around mandrels. Composite rotor blades commonly employ closed sections to achieve the required bending and torsional stiffness. An analysis of the twist achievable with these optimal stacking sequences in a closed section would improve the applicability of this work for use on rotor blades.

This work does not consider multiple couplings acting simultaneously to achieve the same response, such as combined extension- and bend-twist coupling. A spinning rotor blade will be subject to centrifugal forces and aerodynamic bending moments, and a laminate with both couplings will have a twist response that is a function of both couplings. It is possible that a higher level of twist is achievable with stacking sequences having both couplings.

This work pursued optimizations involving coupling only, but other optimizations could be used in conjunction with hygrothermal stability constraints. For example, this work largely considers static deformations, but an analysis could extend this work to investigate the dynamic response. To this end, optimizations with respect to natural frequency are possible. Further, other stiffness and strength considerations may be useful to designers, such as requiring a minimum axial strength while maximizing coupling. Aeroelastic constraints could be optimized to determine the limits of certain performance parameters.

REFERENCES

[1] Jones, R. M., *Mechanics of Composite Materials*, 2nd ed., Taylor & Francis, Philadelphia, PA, 1999, pp. 190-203.

[2] Winckler, S. J., "Hygrothermally Curvature Stable Laminates with Tension-torsion Coupling," *Journal of the American Helicopter Society*, Vol. 31 (7), 1985.

[3] Gürdal, Z., Haftka, R.T., and Hajela, P., *Design and Optimization of Laminated Composite Materials*, John Wiley & Sons, New York, NY, 1999.

[4] Weaver, P.M., "Anisotropic Laminates that Resist Warping during Manufacture," in Proceedings of the 16th International Conference on Composite Materials, Kyoto, Japan, July 3-8, 2007.

[5] Winckler, S.J., "Tension-Torsion Coupling of Proposed Composite Rotor Blades," master's thesis, Rensselaer Polytechnic Institute, Troy, NY, 1986.

[6] Chen, H.P., "Study of Hygrothermal Isotropic Layup and Hygrothermal Curvature Stable Coupling Composite Laminates," in Proceedings of the 44th AIAA/ASME/ASCE/AHS Structures, Structural Dynamics, and Materials Conference, AIAA 2003-1506, April 7-10, 2003, Norfolk, VA, USA, 2003.

[7] Crawley, E.F. and Lazarus, K.B., "Induced Strain Actuation of Isotropic and Anisotropic Plates," *AIAA Journal*, Vol. 29 (6), 1990, pp. 944-951.

[8] Nampy, S.N., "Structural Behavior and Design of Flexible Matrix Composite Box Beams with Extension Twist Coupling," master's thesis, The Pennsylvania State University, State College, PA, 2005.

[9] Nixon, M.W., "Improvements to Tilt Rotor Performance through Passive Blade Twist Control," NASA Technical Memorandum, TM-100583, 1988.

[10] Chandra, R. and Chopra, I., "Structural Response of Composite Beams and Blades with Elastic Couplings," *Composites Engineering*, Vol. 2 (5-7), 1992, pp. 347-374.

[11] Hill, S.C. and Winckler, S.J., "The Reduction of Environmental Effects on Tension-Twist Coupled Composite Tubes," *Journal of Composite Materials*, Vol. 27 (18), 1993, pp. 762-785.

[12] Bothwell, C.M., Chandra, R., and Chopra, I., "Torsional Actuation with Extension-Torsion Composite Coupling and a Magnetostrictive Actuator," *AIAA Journal*, Vol. 33 (4), April 1995, pp. 723-729.

[13] Armanios, E. A., Hooke, D., Kamat, M., Palmer, D., and Li, J., "Design and Testing of Composite Laminates with Optimum Extension-twist Coupling," Camponeschi Jr., E. T. (Ed), *Composite Materials: Testing and Design*, Vol. 11, ASTM STP 1206, American Society for Testing and Materials, Philadelphia, PA, 1993, pp. 249-262.

[14] Hicks, J.W. and Huckabone, T., "Preliminary Flight-Determined Subsonic Lift and Drag Characteristics of the X-29A Forward-Swept Airplane," NASA Technical Memorandum, TM-100409, August, 1989.

[15] Shirk, M.H., Hertz, T.J., and Weisshaar, T.A., "Aeroelastic Tailoring–Theory, Practice, and Promise," *Journal of Aircraft*, Vol. 23 (6), 1984, pp. 6-18.

[16] Hwang, S.J. and Gibson, R.F., "Influence of Bending-twisting and Extension-bending Coupling on Damping of Laminated Composites," *Journal of Material Science*, Vol. 28, 1993, pp. 1-8.

[17] Ong, C.H. and Tsai, S.W., "Design, Manufacture and Testing of a Bend-Twist D-Spar," Sandia National Laboratories SAND99-13, June, 1999.

[18] Lemanski, S. and Weaver, P.M., "Flexural-twist Coupling of Anisotropic Beams," in Proceedings of the 17th International Conference on Composite Materials, Edinburgh, UK, July 27-31, 2009.

[19] Rehfield, L.W. and Cheung, R.H., "Some Basic Strategies for Aeroelastic Tailoring of Wings with Bend-Twist Coupling: Part One," in 44th AIAA/ASME/ASCE/AHS Structures, Structural Dynamics, and Materials Conference, Norfolk, VA, April 7-10, 2003.

[20] Rehfield, L.W., Atilgan, A.R., and Hodges, D.H., "Nonclassical Behavior of Thin-Walled Composite Beams with Closed Cross Sections," *Journal of the American Helicopter Society*, Vol. 35 (2), 1990, pp. 42-50.

[21] Berdichevsky, V., Armanios, E.A., and Badir, A., "Theory of anisotropic thin-walled closed-cross-section beams," Composites Engineering, Vol. 2 (5-7), 1992, pp. 411-432.

[22] Armanios, E.A., and Badir, A., "Free Vibration Analysis of Anisotropic Thin-Walled Closed-Section Beams," *AIAA Journal*, Vol. 33 (10), 1995, pp. 1905-1910.

[23] Dancila, D.S. and Armanios, E.A., "The Influence of Coupling on the Free Vibration of Anisotropic Thin-walled Closed-section Beams," *International Journal of Solids and Structures*, Vol. 35 (23), 1998, pp. 3105-3119.

[24] Dancila, D.S., Armanios, E.A., and Lentz, W.K., "Free Vibration of Thin-Walled Closed-Section Composite Beams with Optimum and Near-Optimum Coupling," *Journal of Thermoplastic Composite Materials*, Vol. 12 (1), 1999, pp. 2-12.

[25] Ozbay, S. "Extension-Twist Coupling Optimization in Composite Rotor Blades," Ph.D. diss., Georgia Institute of Technology, Atlanta, GA, 2005.

[26] Cross, R. J., Haynes, R. A., and Armanios, E. A., "Families of Hygrothermally Stable Asymmetric Laminated Composites," *Journal of Composite Materials*, Vol. 42 (7), 2008.

[27] Tsai, S.W. and Pagano, N.J., "Invariant Properties of Composite Materials," Technical Report AFML-TR-67-349, Air Force Materials Lab, Wright Patterson Air Force Base, 1986.

[28] Fukunaga, H., "Stiffness Optimisation of Orthotropic Laminated Composites using Lamination Parameters," *AIAA Journal*, Vol. 29 (4), 1991, pp. 641-646.

[29] Tawfik, S., Tan, X., Ozbay, S., and Armanios, E.A., "Anticlastic Stability Modeling for Cross-ply Composites," *Journal of Composite Materials*, Vol. 41 (11), 2007, pp. 1325-1338.

[30] Armanios, E. A., Makeev, A., and Hooke, D., "Finite-Displacement Analysis of Laminated Composite Strips with Extension-Twist Coupling," *Journal of Aerospace Engineering*, Vol. 9 (3), 1996.

[31] Makeev, A., Armanios, E. A., and Hooke, D., "Influence of Curing Stresses on Extension–Twist Coupling in Laminated Composite Strips," *AIAA Journal*, Vol. 36 (9), September, 1998.

[32] Gill, P.E., Murray, W., and Wright, M.H., *Practical Optimization*, Academic Press, London, UK, 1981.

[33] American Society for Testing and Materials, Standard Test Method for Tensile Properties of Polymer Matrix Composite Materials, ASTM Standard D 3039/D 3039M, ASTM International, 2006.

[34] American Society for Testing and Materials, Standard Test Method for In-Plane Shear Response of Polymer Matrix Composite Materials by Tensile Test of a ±45° Laminate, ASTM Standard D 3518/D 3518M, ASTM International, 2001.

[35] Cross, R.J., Haynes, R.A., and Armanios E.A., "Design of Hygrothermally Stable Laminated Composites for Extension-Twist Coupling," Proceedings of American Society for Composites, 22nd Annual Technical Conference, Seattle, WA, September, 2007.

[36] Apte, A.P., Haynes, R.A., Wang, B.P., and Armanios, E.A., "Design of Optimal Hygrothermally Stable Laminates with Bending-Twist Coupling by Ant Colony Optimization," *accepted*, in Proceedings of 13th AIAA/ISSMO Multidisciplinary Analysis Optimization Conference, Forth Worth, TX, September, 2010.

VITA

Robert Haynes was born in Lexington, Kentucky on May 11, 1984. He grew up in Pittsburgh, Pennsylvania, and graduated from Mount Lebanon High School in May 2002. Robert began his undergraduate studies at the Georgia Institute of Technology in August 2002 and in 2005 began working with Dr. Erian Armanios researching composite mechanics. After graduating with Highest Honor with his Bachelor of Science in Aerospace Engineering in May 2007, he enrolled in the doctoral program at the Georgia Institute of Technology. Robert received his Master of Science in Aerospace Engineering in 2008 while working toward his doctorate.

In addition to his studies, Robert attained the rank of Eagle Scout with the Boy Scouts of America. He held the position of Co-op Engineer at US Airways from May 2003 to August 2005. He participated in the NASA Academy at Ames Research Center for Space Exploration during the summer of 2007. Robert received the National Defense Science and Engineering Graduate Fellowship for his graduate studies.